UNIVERSITY OF
LINCOLN

Protein-nanoparticles interaction and assembly

Wenwei Ma

Doctor of Philosophy

2017

CERTIFICATE OF ORIGINALITY

This is to certify that I am responsible for the work submitted in this thesis, that the original work is my own, except as specified in the acknowledgements and in references, and that neither the thesis nor the original work contained therein has been previously submitted to any institution for a degree.

Signature: Wenwei Ma

Name: Wenwei Ma

Date: 11/10/2017

Abstract

Nanoparticles are increasingly important in biotechnology as they are extensively used as drug delivery carriers and in biosensors. In both these two contexts, protein-nanoparticle interactions are often involved. Proteins that are present in body fluids inevitably interact with nanoparticle based drug carriers and typically surround them forming the so called "protein corona". Biosensors that are based on nanoparticles often have proteins deliberately attached to their surface, for example antibodies that bind specific analytes. The understanding of the assembly mechanisms at the protein-nanoparticle interface and the ability to engineer proteins that interact with nanoparticles in the desired way, are therefore two essential requisites for the future development of nano-medicines and nano-biosensors.

In this work, we focused on the interaction of proteins with gold nanoparticles (GNPs). GNPs are available with a broad range of surface chemistries, suitable for the conjugation of many biomolecules. Although there are at least three decades of studies on gold colloids with different surface chemistries, there is still quite little known about what are the exact features of a protein that determine its adsorption onto gold. We developed methods to study this and applied them to characterise the adsorption on GNPs of Glutathione-S-Transerase (GST), which was reported previously as a protein that strongly binds gold. We determined its affinity and kinetics of binding and unravelled the mechanism of its thiol-mediated chemisorption. We found that GST binds to GNPs even more efficiently than other known gold-binding proteins, such as Bovine Serum Albumin (BSA). We concluded that GST could be considered a very useful gold-protein interface, especially considering that GST fusion is routinely used for affinity purification of recombinant proteins and therefore well established.

We also fused self-assembling proteins to GST or chemically cross-linked them to BSA. The scope was to explore the feasibility of hierarchical and ordered assembly of designer proteins onto GNPs, with the ultimate goal of providing a convenient tool for modular assembly of proteins onto nanomaterials. It is known that proteins tend to denature and lose their function when in contact with GNPs, which is not optimal for biosensors or in nanomedicine. We found that it is possible to use GST or BSA to form a sacrificial layer on gold, which exposes linked, self-assembling proteins that are able to bind their counterpart, unaffected by the GNP surface. We reported two proof-of-concepts: the first based on mimics of the self-assembling neuronal

SNARE proteins and the second based on the pair SpyCatcher/SpyTag, derived from *Streptococcus pyogenes* proteins and used in bio-conjugation for their ability to self-catalyse the formation of isopeptidic bonds.

We believe that the novel methods and original results presented in this thesis apply to both the understanding and the engineering of the protein-nanoparticle interface and will be beneficial for the broad nanobiotechnology community. In fact, our findings have potential applications in a broad range of fields, spanning from the improvement of the circulation life-time of nanomedicines by preventing the binding of serum protein and opsonisation, to the improvement of the manufacturing of GNPs-based immune-biosensors such as those used in lateral flow devices.

Table of Contents

List of Figures

Chapter 1

Chapter 2

Chapter 3

List of tables

List of Abbreviations

AFM……...Atomic Force Microscopy

APBS…….Adaptive Poisson-Boltzmann Solver

BCA……Bicinchoninic acid

BSA……Bovine Serum Albumin

CL……..Crosslinker

DLS…….Dynamic Light Scattering

DNA……..deoxyribonucleic acid

DMF…….Dimethylformamide

DMS……...dimethyl sulfoxide

DTT……Dithiothreitol

EDTA……Ethylenediaminetetraacetic acid

FRET…….Fluorescence resonance energy transfer

FITC……Fluorescein isothiocyanate

FPLC…….Fast Protein Liquid Chromatography

GNPs……..Gold nanoparticles

GST…….Glutathione-S-Transerase

GSH…….Gluthathione

HEPES……...4-(2-hydroxyethyl)-1-piperazineethanesulfonic acid

HSA…….Human serum albumin

IPTG……..Isopropyl β-D-1-thiogalactopyranoside

LB……...Luria-Bertani

MWCO…….……..Molecular Weight Cut-Off

NEM……*N*-Nethylmaleimide

NHS……...N-hydroxysuccininmide

NIR…….Near-infrared

NTA……...Nanoparticle Tracking Analysis

OD……Optical density

OG…….....n-Octyl-β-D-glucoside

PCR……Polymerase chain reaction

PDB……..Protein data bank

PEG……..Polyethylene glycol

PLL……...Poly-L-Lysine

QD……..Quantum dots

RNA……Ribonucleic acid

SDS……..Sodium dedocyl sulphate

SDS-PAGE……...SDS-polyacrylamide gel electrophoresis

SERS…….Surface-enhanced Raman scattering

siRNA……..Small interfering RNA

SMCC……succinimidyl *trans*-4-(maleimidylmethyl) cyclohexane-1-carboxylate

SNAP25……..Synaptosomal-associated protein 25

SNAREs……..Soluble *N*-ethylmaleimide-sensible factor attachment receptor proteins

SOB…….Super Optimal Broth

SPR……...Surface plasmon resonance

Spy……...……..*Streptococcus pyogenes*

Sulfo-SMCC……Sulfosucininidyl 4-[*N*-maleimidomethyl] cyclohexane-1-carboxylate

SWSR…….Sum of the weighted square roots

TCEP……..Tris-(2-carboxethyl) Phosphine

UV-vis…….Ultra-Violet-visible spectroscopy

β-ME……...β-mercaptoethanol

List of equations

Chapter 1. Introduction

1.1 Gold Nanoparticles

Gold nanoparticles (GNPs) are widely used and have a long history in biology, chemistry and medicine. The earliest popular application of GNPs was the use for staining glass in Roman times, based on their optical properties. The first modern synthesis of GNPs could be dated back to 150 years ago by the work of Michael Faraday(Hayat 2012). What follows was a high-yielding synthesis method of GNPs by Turkevich(Turkevich, Stevenson et al. 1951) which is still used often nowadays.

In my project, I focus on interaction between protein and GNPs to understand the adsorption mechanism and develop new systems to assemble gold nanoparticles through proteins.

In this section, the synthesis of gold nanoparticles, the functionalization of GNPs and the applications of functionalized GNPs are introduced.

1.1.1 Chemical Synthesis of Gold Nanomaterials

Gold nanoparticles (or gold nanospheres, gold colloids) of diameter from 1nm to 150nm can be synthesized by varying the ratios of gold salt ($HAuCl_4$) and reducing agents. The different synthesis methods result in various capping agents (Table1.1) (Ghosh, Han et al. 2008). Different capping agent of GNPs are used for decoration with different biological molecules.

Citrate-functionalized gold nanoparticle are most often synthesised using the method based on the work of Turkevich(Turkevich, Stevenson et al. 1951) and Frens (Frens 1973). Basically, the larger amount of sodium citrate yield smaller gold nanoparticles. The homogeneously distributed GNPs display a narrow and single absorption peak in the visible range between 505nm and 560nm. The absorption peak of GNP shifts to a longer wavelength with an increasing size.

Core size (d)	Synthetic methods	capping agents
1-2 nm	Reduction of AuCl(PPh3) with diborane or sodium borohydride	Phosphine
1.5-5 nm	Biphasic reduction of HAuCl4 by sodium borohydride in the presence of thiol capping agents	Alkanethiol
10-150 nm	Reduction of HAuCl4 with sodium citrate in water	Citrate

Table 1.1 ***Table Summary of synthetic methods and capping agents of GNPs(Ghosh, Han et al. 2008)***

In recent studies, there are plenty of gold nanomaterials with non-spherical shape such as nanorods. Gold nanorods can be used in a variety of applications, for example in biosensors(Yu and Irudayaraj 2007), imaging (Huang, El-Sayed et al. 2006) and self-assembly(Thomas, Barazzouk et al. 2004). Compared to the single absorption peak of nanoparticles, gold nanorods display two peaks(Gole and Murphy 2004) including short-axis (transverse) and long-axis (longitudinal). Typically, the peak of transverse axis is in the visible range, whereas the peak of longitudinal axis can be either in the visible or in the near-infrared (NIR) range, depending on the dimensions of the nanorods.

The research in this thesis is based on gold nanospheres only, however the principles could be applied to nanorods too.

1.1.2 Functionalization of Gold Nanoparticles

Gold nanoparticles have been widely used in biomedical applications for decades, mainly for their wide size range and biocompatibility. The surface area-to-volume ratio of spherical nanoparticles is high, which provides a high density loading of biological molecules. 2nm GNPs can covalently bind approximately 100 small ligands(Hostetler, Wingate et al. 1998). This provides a high potential for GNPs functionalization with amines and amino acids, peptides, proteins and oligonucleotides (Table 1.2).

Biological Molecule	Applications	References
Amines and amino acid	Gene delivery	(Lee, Bae et al. 2008)
	Intracellular targeting	(Ghosh, Kim et al. 2008)
Nucleic acid	Nucleic acid detection	(Seferos, Giljohann et al. 2007)
	Signal amplification	(Niazov, Pavlov et al. 2004)
Peptide	Small molecule detection	(Sener, Uzun et al. 2013)
	Antisense gene regulation	(Patel, Giljohann et al. 2008)
Protein	Labeling and imaging	(Felsenfeld, Choquet et al. 1996) (Sokolov, Follen et al. 2003) (Albrecht-Buehler 1977)
	Cancer therapy	(Cai, Gao et al. 2008)
	Drug delivery	(Weerapreeyakul, Hollenbeck et al. 2000) (Bernkop-Schnürch, Guggi et al. 2004)

Table 1.2 ***Biological applications of gold nanoparticles***

In order to improve the stability of naked GNPs solutions and prevent aggregation, amines and some small amino acid molecules have been added during the synthesis. Aslam(Aslam, Fu et al. 2004) demonstrated a novel one-step method to synthesis amine-capped gold nanoparticles by using oleyl amine as the reducing/stabilizing agent. The oleyl is added into heated gold colloidal solution with chloroauric acid, resulting in a maximum shift of the surface plasmon band from 520nm to 571nm. Studies by Japanese scientists(Niidome, Nakashima et al. 2004) found that amine-modified GNPs could form complexes with DNA plasmids and the GNPs-plasmid conjugates transfect to HeLa cells and increase the gene expression about 100 fold (Figure 1.1). The amines-capped gold nanoparticles are positively charged which could form polyelectrolyte complexes through electrostatic interactions with negatively charged small interfering Ribonucleic Acid (siRNA)-polyethylene glycol (PEG) conjugates(Lee, Bae et al. 2008). This research shows that the PEG-conjugated siRNA coated amine-GNPs are more internalized by human prostate carcinoma PC-3 cells than PEG-siRNA alone.

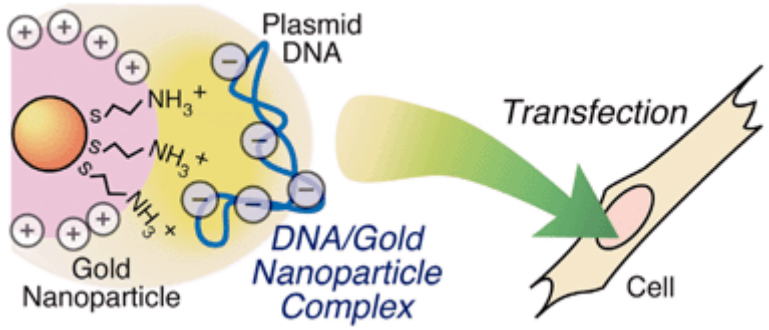

Figure 1.1 ***GNPs-plasmid conjugates transfected to cell(Niidome, Nakashima et al. 2004).***

Covalent conjugation to gold nanoparticles can be based on gold-thiol bond (Au-S). Brust reported a thiol monolayer coated gold nanoparticles in water-toluene system. $AuCl_4^-$ reduced sodium borohydride in the presence of alkanethiol, and resulted in 1-3nm gold nanoparticles with thiol coating(Brust, Walker et al. 1994). However, alkanes cannot be used to bind biological molecules. Based on this work, Majzik synthesized gold nanoparticles with cysteines. The thiol was attached to the gold surface, and carboxylate groups ($-COO^-$) and amino groups ($-NH_3^+$) were available for further binding (Majzik, Fülöp et al. 2010). Gold nanoparticles could be coated with carboxylate groups by using glutamic acid as the reducing agent. Wangoo conjugated the amino groups of BSA and anti-BSA antibody to carboxylate coated GNPs through electrostatic attraction (Figure 1.2). Circular dichroism results shown that BSA and anti-BSA undergoes a more flexible conformational state on the surface of gold nanoparticles. The substantial conformational transition from α-helix to β-sheet structure was observed after proteins conjugation to GNPs(Wangoo, Bhasin et al. 2008).

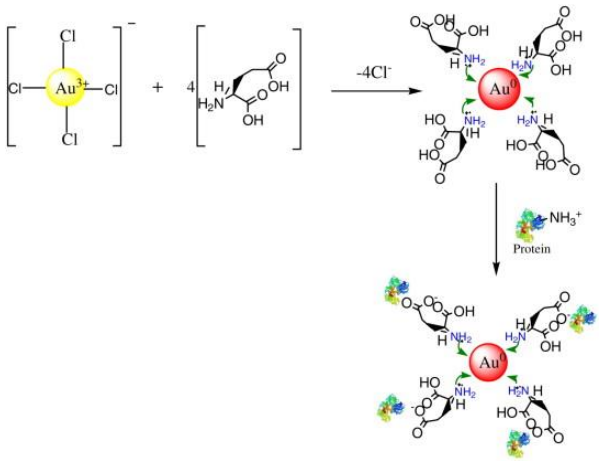

Figure 1.2 ***Amino acid functionalized GNPs. The schematic representation of glutamic acid reduced gold nanoparticles capped with the amino acid and their subsequent binding with protein through the surface lysine residues of protein molecules(Wangoo, Bhasin et al. 2008).***

Nucleic acid has been used effectively for functionalizing gold nanoparticles for many applications. Mirkin's group leads the research on attaching and controlling the amount of nucleic acid to different sizes of GNPs through thiol-gold bonds. The maximum loading of DNA coverage on GNPs was obtained by salt aging the nanoparticles to ~0.7M NaCl in the presence of DNA containing a poly-(ethylene glycol) spacer, and the 250nm GNPs have ~2 orders of magnitude higher DNA loading than smaller (13-30nm) GNPs(Hurst, Lytton-Jean et al. 2006). Chen et al. studied the kinetics and thermodynamics of DNA hybridization on gold nanoparticles and they found that, at low surface densities, ssDNA adsorbs onto the GNP first, and then diffuses on the surface until hybridizing with an immobilized DNA(Chen, Wang et al. 2009). The secondary structure of a DNA hairpin inhibits the interaction between DNPs and

DNA, therefore, the stability of the DNA hairpin adhered to GNPs was increased. The DNA functionalized GNPs were employed for transfection and mRNA detection in living cells(Seferos, Giljohann et al. 2007). GNPs functionalized with a recognition sequence were complemented with a Cy5 labelled reporter strand which was able to be displaced by target RNA (Figure 1.3).

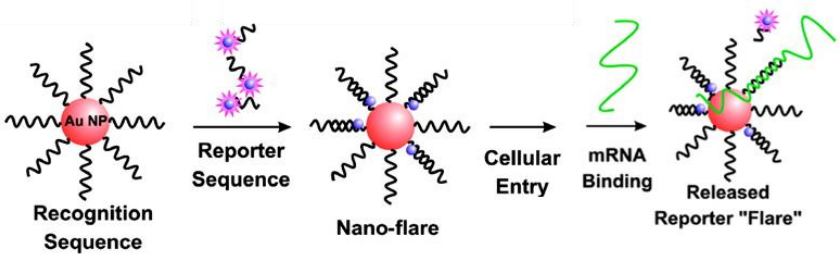

Figure 1.3 ***DNA capped GNPs. Functionalized GNPs for transfection and mRNA detection in living cells(Seferos, Giljohann et al. 2007).***

Peptides are commonly used molecules for functionalizing gold nanoparticles. Peptides normally contain positively charged amino acids such as lysine and arginine(Goldfarb, Gari épy et al. 1986) which provide an environment to combine with negatively charged GNPs. It is also known that tyrosine could be used to reduce $HAuCl_4$(Slocik, Naik et al. 2005), Slocik demonstrated a simple one-pot process for synthesizing gold nanoparticles by using A3 peptide which containing tyrosine(Slocik, Stone et al. 2005). However, the A3 peptide lost the affinity property to recognize biological molecules. CALNN (Figure 1.4) is a peptide which can remarkably stabilized gold nanoparticles. In order to understand how the sequence of peptides affects GNPs stability, Fernig's group designed 49 peptides based on CALNN, and the variation criteria were peptides length, the anchor (first amino acid), the peptide core (second and third amino acids), and the peptides carboxyl terminus (fourth and fifth amino acids).The experiment also included 9 sequences with no direct relation to CALNN for comparison(L évy, Thanh et al. 2004). It was shown that the stability of peptide-capped GNPs depends on their length, hydrophobicity and charge. The sequences containing 5 amino acids gave the highest stability to gold nanoparticles. The presence of a thiol and cohesive lateral interactions between the peptides through hydrophobic or hydrogen bonds increased the GNPs solution stability.

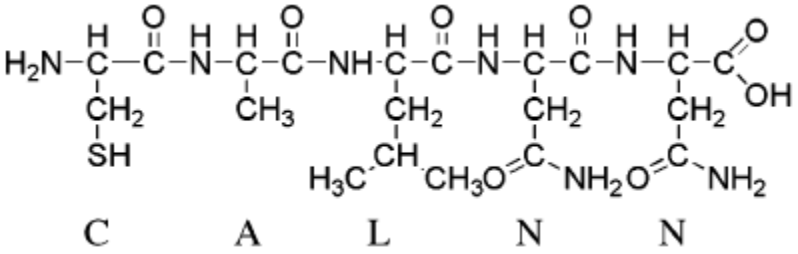

Figure 1.4 ***The CALNN structure(Slocik, Stone et al. 2005).***

Moreover, an arginine-rich peptide ($CALNNR_8$ (R is arginine)) has been derived from CALNN, and has been developed as a cell-targeting agent. Peptides mixture (90% CALNN and 10% $CALNNR_8$) were used to functionalize gold nanoparticles (30nm) for intracellular component targeting(Sun, Liu et al. 2008) because of high affinity of endoplasmic reticulum to arginine. These peptide-GNPs conjugates are now used to translocate GNPs to cells for cancer treatment. Anil and his colleagues modified 2nm GNPs with the therapeutic peptide (PMI(p12)) and a targeted peptide (CRGDK) for selective binding to neuropilin-1(Nrp-1) receptors which overexpressed on the cancer cell surfaces(Kumar, Ma et al. 2012). CRGDK-GNPs conjugates increase the binding between CRGDK peptide and targeted Nrp-1 receptor overexpressed on cancer cell surface, finally improving the delivery of the therapeutic P12 peptide inside targeted cells (Figure 1.5). This could be a promising anti-cancer system to get a good efficacy for therapeutic molecules.

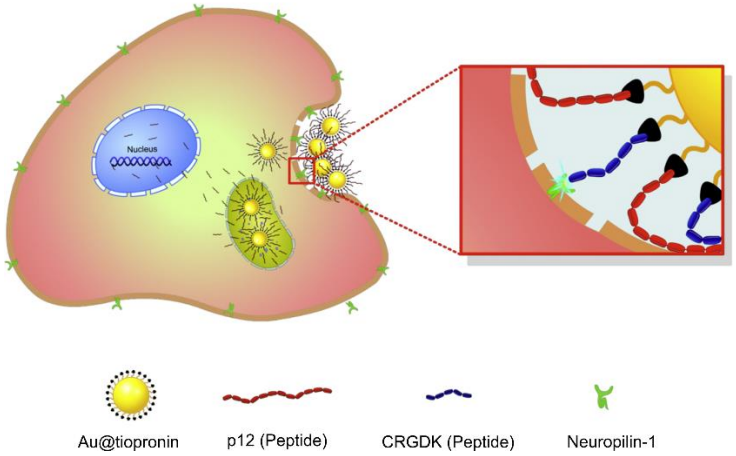

Figure 1.5 ***Peptide capped GNPs. Interaction between the receptor and targeted ligand enhances intracellular entry and increases response to intracellular release of therapeutic peptide into the cells(Kumar, Ma et al. 2012).***

Besides small molecules (amines and peptides), some proteins such as antibodies, have been also used to label gold nanoparticles for cell biology studies. El-Sayed(El-Sayed, Huang et al. 2005) and his co-workers used Surface Plasmon Resonance (SPR) and dark field microscopy to track the binding between anti-EGFR (anti-epidermal growth factor receptor) antibodies

conjugated gold nanoparticles and cells. Conjugated GNPs were able to bind specifically and homogeneously to the surface of cancer cells and non-cancerous cells with a maximum absorption at 545nm and 552nm respectively. Light scattering images showed that conjugated nanoparticles bind specifically to cancer cells and this makes the anti-body GNPs conjugates potentially usable in cancer diagnostics. They also found that benign cells, after incubation with anti-EGFR antibody conjugated GNPs, require double laser energy to be killed than malignant cells(El-Sayed, Huang et al. 2006). This finding is promising in molecularly targeted photothermal therapy.

1.1.3 Functionalized gold nanoparticles as biosensors

Gold nanoparticles biosensors are used to recognize the presence of analytes and to provide a way which indicates the analyte concentration, typically based on optical properties. Changes of GNPs optical properties can be recorded by various methods, in this section, we introduce three commonly used tools: the colour change of GNPs solution is observed by naked eyes, a fluorophore can be quenched by approaching GNPs, GNP dimers can enhance Raman scattering signal.

Colorimetric Sensors

Surface plasmon resonance (SPR) is one of the optical properties of GNPs which can be used for biosensors. The biomolecular binding to GNPs surfaces can change the SPR, resulting in a spectral shift which can be observed, for example, by dark field microscopy(Raschke, Kowarik et al. 2003). The interactions between protein/DNA-modified GNPs could form aggregates which also leads to colour change of GNPs solutions. This colour change is developed for colorimetric biosensors which can be easily read out with naked eyes.

Mirkin and co-workers are the pioneers of GNPs-based colorimetric biosensors. The earliest colorimetric sensor was used for DNA detection. GNPs were attached to oligonucleotides which were used to hybridize to target sequences. Without the target oligonucleotides, GNPs were well dispersed and the solution appeared in red colour. In the presence of target oligonucleotides, the GNPs were brought closely in contact by hybridization of complementary oligonucleotides, resulting in aggregation which lead to the colour change from red to purple or blue.

Two batches of 13nm GNPs were attached with non-complementary DNA oligonucleotides capped with thiol groups. The oligonucleotide duplex with ‘sticky ends’ that are

complementary to the two grafted sequences triggered the self-assembly of GNPs into aggregates(Mirkin, Letsinger et al. 1996). This assembly can be reversed by thermal denaturation.

It is known that Hg^{2+} leads to thymidine-thymidine mismatch in DNA hybridization (Miyake, Togashi et al. 2006). Mirkin group prepared two sets of GNPs which were conjugated with different thiolated-oligonucleotides which are complementary except for a single thymidine-thymidine mismatch(Lee, Han et al. 2007). The Hg^{2+} triggered the hybridization between thymidine and thymidine result in the aggregation of GNPs, consequently, the red GNPs solution turn into purple (Figure 1.6). This was proposed as a biosensor to detect presence of Hg^{2+}

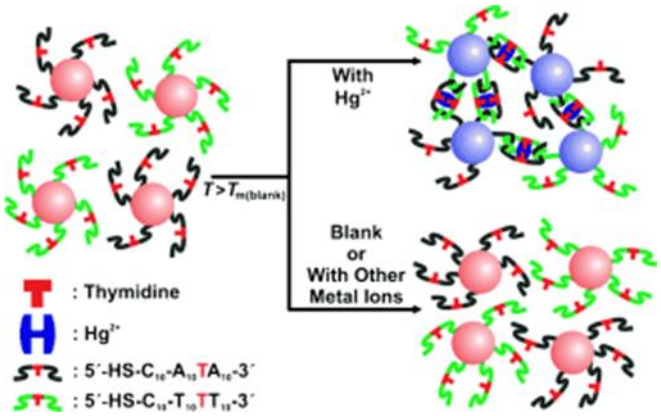

Figure 1.6 ***Colorimetric detection of mercuric ion (Hg^{2+}) using DNA–Au NPs(Lee, Han et al. 2007).***

A colorimetric sensor for multi-metal ions detection was also demonstrated. GNPs were functionalized with Flag-A3 peptide (-Asp-Tyr-Lys-Asp-Asp-Asp-Asp-Lys-Pro-Ala-Tyr-Ser-Ser-Gly-Pro-Ala-Pro-Pro-Met-Pro-Pro-Phe-)(Slocik, Zabinski et al. 2008). The A3 peptide domain (-Ala-Tyr-Ser-Ser-Gly-Pro-Ala-Pro-Pro-Met-Pro-Pro-Phe-) binds to GNPs. The Flag tag at the amino terminus of the peptide (-Asp-Tyr-Lys-Asp-Asp-Asp-Asp-Lys-) contains charged and aromatic residues that can form the complexation of metal ions(Slocik and Naik 2006). The GNPs-peptide conjugates gave different SPR peaks due to the addition of metal ions such as Co^{2+}, Hg^{2+}, Pb^{2+}, Pb^{4+} and Pt^{2+}.

Fluorescence quenching

Fluorescence is quenched when the fluorophores have a close distance to gold nanoparticles. The quenching between GNP and fluorophores is described as Fluorescence Resonance Energy Transfer (FRET), and is based on a non-radiative energy transfer between the donor (fluorophore) and the acceptor (GNP)(Clapp, Medintz et al. 2006). There are two typical

biosensor strategies based on this interesting feature. The first strategy is a competitive format for the analyte detection. GNPs are attached with ligands that could be recognized by the analyte. The binding sites of ligands are blocked by molecules which are labelled with fluorophores. In this case, the fluorophores are close to GNPs surfaces so that the fluorescence is quenched. After the addition of the analyte, the fluorophore molecules are replaced and released from GNPs into solution. Since the fluorophore is far from the GNPs, the fluorescence emission becomes visible. Basically, the more analyte is present in the solution, the higher the fluorescence will be. Quantum dots (QDs) are a new class of fluorescent materials that are efficiently quenched by GNPs. QDs FRET quenching is widely used for DNA detection (Figure 1.7). A QD tagged receptor DNA was hybridized with a short DNA sequence attached to a GNP. The fluorescence of QD was quenched by the GNP. A target DNA which complements the receptor DNA better would be able to displace the short DNA-GNP element. Consequently, the QD would be released into solution and the fluorescence could be measured (Zhao, Zhang et al. 2007). |

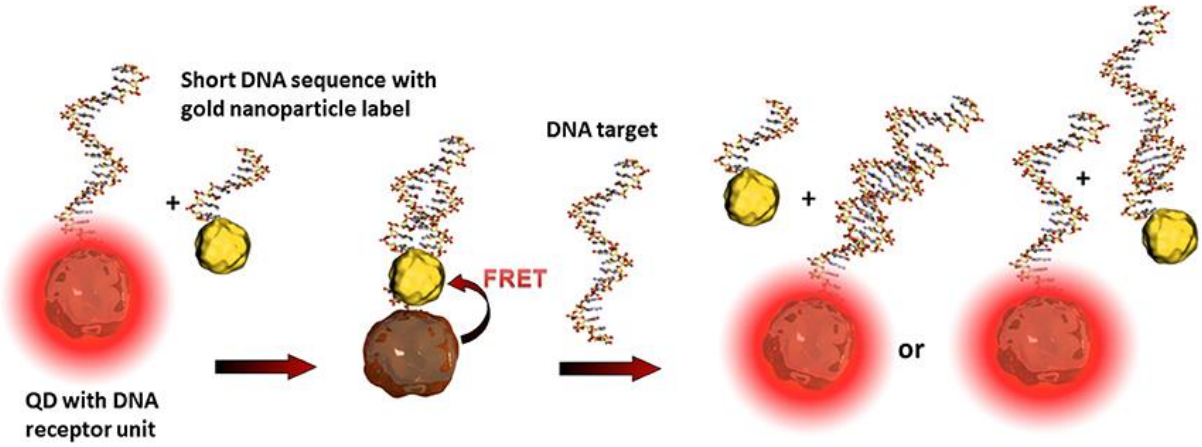

Figure 1.7 ***Illustration of FRET quenching between GNP and Quantum Dots (QD) for DNA detection(Holzinger, Le Goff et al. 2014).***

Another strategy is achieved by controlling the distance between the fluorophore and GNPs. The target analyte is used to adjust the distance. A new method for microRNA analysis based on the fluorescence quenching of GNPs integrating a hairpin-structured oligonucleotide probe was reported(Tu, Wu et al. 2012). The Fluorescein isothiocyanate (FITC) labelled probe DNA had a stem-loop which brings the fluorophore close to GNPs to quench the fluorescence. The addition of miRNA resulted in hybridization with the probe DNA and stretching of the stem-loop. This brought the FITC away from GNPs, hence the fluorescence was recovered.

Surface-enhanced Raman scattering

Raman scattering has a low energy component (Stokes, by depositing energy into the molecule) and a high energy one (anti-Stokes, by gaining energy from the molecule). The energy shift depends on the chemical structure where the scattering occurred and complex molecules have therefore a characteristic Raman spectrum that allows for detection and identification(Sperling, Gil et al. 2008). However, the Raman signal is very weak, so the sensitivity of detection is low. It was found that molecules which decorate rough noble metal surfaces provide enhanced Raman scattering signal(Campion and Kambhampati 1998). This phenomenon is known as Surface-enhanced Raman scattering (SERS).

In SERS the laser-generated Raman spectrum of a substance, which can be used to determine the identity of the analyte, is enormously amplified by the proximity of gold or silver nanoparticles(Nie and Emory 1997). The gap between two gold nanoparticles which form a dimer was also discovered to generate SERS signals(Alexander, Hampton et al. 2009). In certain circumstances, the signal intensity was increased over 1 billion times, making the detection of single molecules possible. The dimers that can be considered the closest to a practical use where manufactured and characterised by Korean scientists(Lim, Jeon et al. 2010). These objects are called nano-dumbbells: two gold nanoparticles were assembled together simply using complementary strands of DNA on each particle; a Raman-active Cy3 dye molecule was chemically bound to the DNA linker for single-molecule SERS generation. This study reported the first evidence of single molecule SERS detection from a single Cy3 molecule trapped in the gap between two gold nanoparticles.

1.1.4 Functionalized gold nanoparticles for delivery

Gold nanoparticles have been playing an important role in biological delivery for decades. Because of conjugated molecules, such as amino acids, peptides or antibodies, functionalized GNPs are able to recognize specific targets in cells, such as cancer cells and nucleus. The interaction between functionalized GNPs and human cells are regarded as biocompatible and non-toxic(Connor, Mwamuka et al. 2005). GNPs are used as carriers into cells either for gene delivery or drug delivery.

Gene delivery

Amine labelled GNPs provide a way to deliver DNA into cells. Gold nanoparticles are functionalized with lysine and lysine dendron formed particularly compact complexes and

provided highly efficient gene delivery without any observed cytotoxicity(Ghosh, Kim et al. 2008). Lysine coated GNPs could form salt bridges with the phosphate backbone of DNA(Voet and Voet 1995) which was referred as to nanoplex (Figure 1.8). The nanoplex transfected into mammalian cells while the naked DNA could not. Moreover, the conjugation of lysines on gold nanoparticles in a dendritic fashion yielded efficient vectors which are about 28-fold more efficient than polylysine for in vitro transfections.

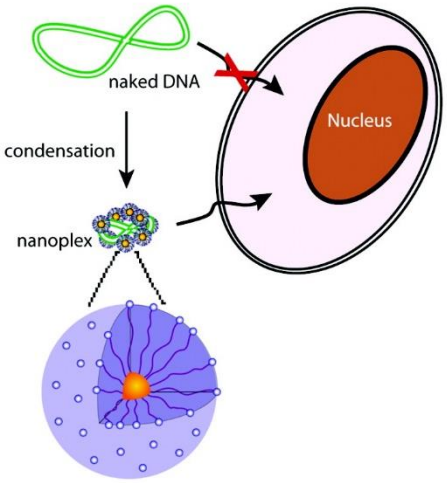

Figure 1.8 ***GNP biosensor for gene delivery. Schematic illustration of the monolayer protected gold nanoparticles used as transfection vectors in this study. DNA is condensed by lysine-coated GNPs and able to be transfected into mammalian cells.***

To achieve targeted gene delivery in human cells, the carried gene should be stable in blood and released at the target site. Niidome's study shows that PEG-modified nanoparticles maintained DNA more stably in the blood than the naked DNA, and DNA was released and passed through cellular membranes via the control of electrical pulses in a restricted area of liver(Kawano, Yamagata et al. 2006). Mirkin's group demonstrated that antisense DNA functionalized GNPs can down-regulate EGFP expression in C166, a mouse endothelial cell line(Rosi, Giljohann et al. 2006). For this purpose, GNPs were conjugated to either tetrathiol-modified or monothiol-modified antisense oligonucleotides and the latter modification had a ~35-fold higher binding affinity to gold, which resulted into better delivery of DNA into cells.

Drug delivery

The biocompatibility of gold nanoparticles has been exploited for drug delivery. GNPs can be synthesized to minimize non-specific binding to biomacromolecules. In a recent study, GNPs were produced with a *n*-alkyl disulphide layer which is a zwitterion (Rouhana, Jaber et al. 2007) or additional groups to the zwitterion layer: a hydrophobic interior layer of alkanethiol and a hydrophilic shell composed of a tetraethylene glycol unit (Kim, Ghosh et al. 2009). These

modified GNPs were reacted with three different hydrophobic compounds: a fluorescent probe, Bodipy, the therapeutic tamoxifen and the drug β-lapachone (Figure 1.9). The Bodipy was initially quenched by GNPs, while the fluorescence was switched on after the dyes/drugs were released into cells by membrane-mediated diffusion without uptake of the carrier GNPs.

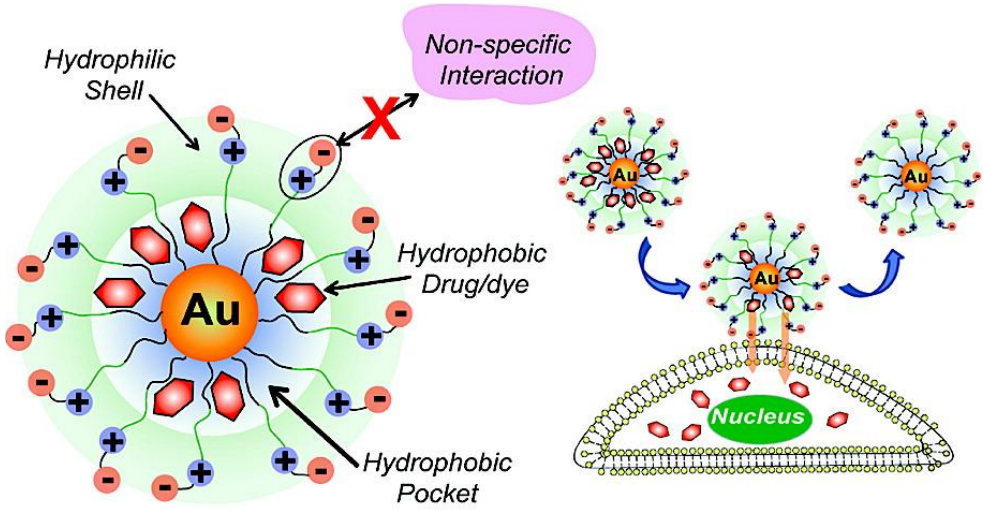

Figure 1.9 ***GNP biosensor for drug delivery.*** ***Delivery of drugs to cells through monolayer-membrane interactions(Kim, Ghosh et al. 2009).***

The above strategy is based on non-covalent binding which allows the easy release of drugs, however, premature release is an issue. Covalent binding to GNPs, for example through sulphur or sulphydric groups, provides a stable delivery vehicles for drugs.

Covalent binding has been also applied to vaccine delivery. Chitosans were covalently combined to GNPs (Chito-GNPs), and the Chito-GNPs conjugates were used as vectors for the delivery of plasmid DNA vaccine in vitro and in vivo(Zhou, Zhang et al. 2008). Chito-GNPs conjugates were delivered by intramuscular immunization into BALB/c mice resulting in 10-fold enhancement of serum antibody response compared to naked DNA vaccine.

1.2 Modular Protein Assembly

Proteins are structurally complex molecules that makes it difficult to find a unique and proven crosslinking method which consistently and efficiently produces functional NPs conjugates, regardless of the specific protein. Hence, immobilization has to be optimized according to specific conditions. For instance, proteins containing cysteine residues can be chemically bound to GNPs through Au-S bond, unfortunately, the adsorbed proteins are in a high risk to be denatured(Laera, Ceccone et al. 2011). In this project, we propose the use of "sacrificial" intermediates that bind efficiently to GNPs and carry a domain, either chemically cross-linked

or recombinantly fused, which is able to bind another protein. This protein will not be affected by the NP surface, which is passivated by the sacrificail intermediate, and can be used as an affinity tag for easy binding of potentially any protein of interest, without any need of protein-surface optimization steps. In this project, we used Glutathione-S-Transferase (GST) and Bovine Serum Albumin (BSA)as the intermediate proteins to adsorb on the GNP surfaces and form the protein corona (sacrificial layer). We used two pairs of proteins, SNARE proteins and SpyTag/SpyCatcher as affinity systems. We investigated the ability of affinity systems to form complexes while adsorbed on GNPs through GST or BSA.

1.2.1 SNARE Proteins

Neuronal SNAREs (soluble *N*-ethylmaleimide-sensible factor attachment receptor proteins) are the main proteins involved in synaptic vesicle exocytosis. SNAREs exist in many isoforms involved in trafficking, and the neuronal SNAREs are the most studied and they are the system from which the SNAREs in this study are derived from. Neuronal SNAREs are namely Syntaxin 1, SNAP25 (Synaptosomal-associated protein 25) and Synaptobrevin 2 (Figure 1.10A) and their function is to mediate the fusion of synaptic vesicles to the cell membrane at the synapses, with subsequent release of neurotransmitter in the synaptic cleft (Figure 1.10C). Part of the sequences of Syntaxin 1 and Synaptobrevin 2 anchor them to the cell membrane and the vesicle membrane respectively (transmembrane domains). SNAP25 is linked to the cell membrane through 4 palmitic acids bound to 4 cysteine residues on the loop that separates two SNARE domains. The fast interaction between the SNAREs bound to the plasma membrane and the Synaptobrevin bound to the synaptic vesicle triggers the fusion of the membranes (Figure 1.10B).

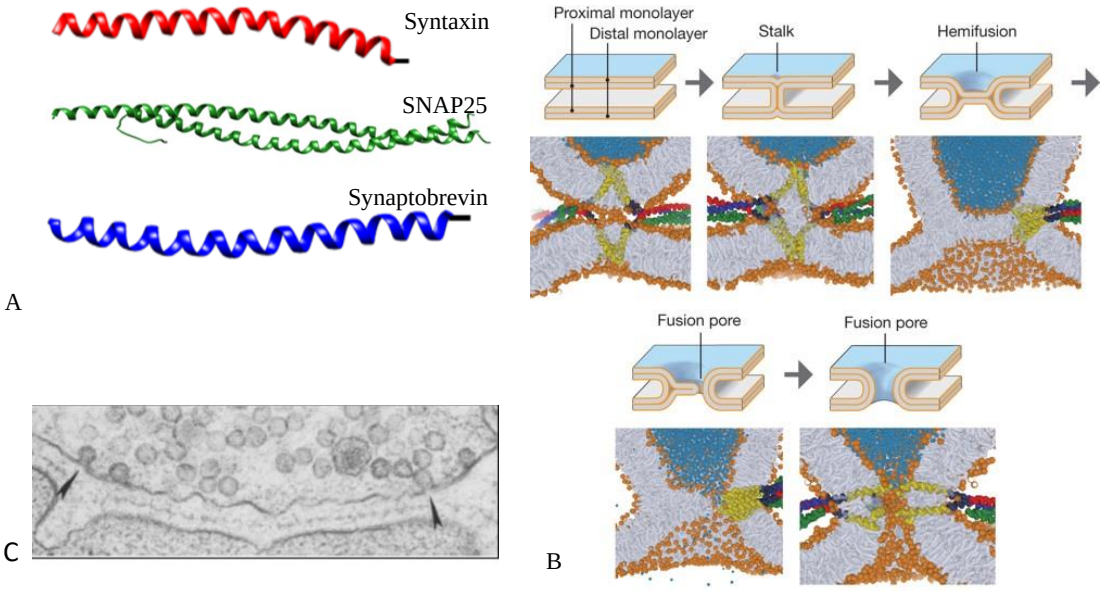

Figure 1.10 ***SNARE proteins (A) their mechanism of action (B) and an electron micrograph of a synapse (C). The two arrows indicate vesicles undergoing fusion. Figures rehashed from(Jahn and Scheller 2006) and (Torri-Tarelli, Grohovaz et al. 1985, Jahn and Fasshauer 2012).***

The SNARE complex that forms and drives membrane fusion is structurally a coiled-coil of 4 helices named SNARE domains. Syntaxin and Synaptobrevin contribute 1 helix each, SNAP25 contributes 2. The hydrophobic residues of the SNARE motifs are oriented inward to form the hydrophobic layers of the coiled-coil like in classical leucine zippers(Fasshauer, Sutton et al. 1998) (Figure 1.11A). However, the layer in the middle of the complex, called the "0" layer or "ionic" layer, is formed by ionic interactions between an arginine (Synaptobrevin) and three glutamines (Syntaxin and SNAP25) (Figure 1.11B). For this structural feature common to all SNAREs isoforms, often the SNARE domains are classified as Q- or R-SNAREs depending on the residue they contribute to the "0" layer(Bracher, Kadlec et al. 2002). The SNARE complex is so stable that partially resists to the deanturing condition of SDS-PAGE and can be only disassembled in boiling SDS-PAGE loading buffer containing sodium dedocyl sulfonate (SDS)(Fasshauer, Antonin et al. 2002).

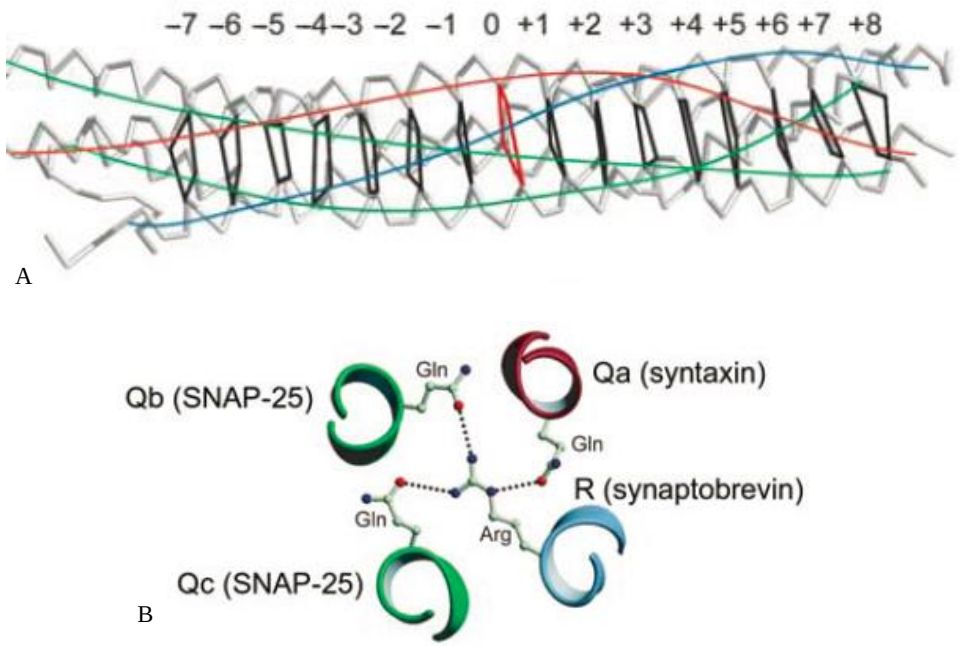

Figure 1.11 ***The backbone of the SNARE complex. (A) The C-termini are at the right, while the N-termini are at the left. The hydrophobic amino acids face to the center of the helix. The backbone of Syntaxin is highlighted in red, Synaptobrevin in blue and the SNAP25 two SNARE domains in green. The zero layer is outlined in red while the hydrophobic layers are black. (B) The zero layer shown as a section. Figures a and b are from(Fasshauer, Sutton et al. 1998, Bracher, Kadlec et al. 2002).***

In *vitro*, syntaxin and SNAP25 can form a stable complex containing two syntaxin molecules, one of which is occupying and possibly obstructing the binding site of synaptobrevin(Fasshauer and Margittai 2004). It has been found that syntaxin and synaptobrevin can also be assembled in vitro without SNAP25(Fix, Melia et al. 2004), however the most stable complex is given by the hetero-trimer.

It is important to mention that the SNARE complex forms in the direction of N- to C- terminal. To show this, mutations were conducted in the N- and C- terminal. Mutations in the N-terminal slowed the fusion, in contrast, C-terminal mutations had no effects on SNARE assembly(Sørensen, Wiederhold et al. 2006). Based on this fact, in this project, the introduction of a cysteine in Syntaxin and Synaptobrevin for conjugation purpose, was deliberately at the C-terminal. We used SNAREs, either cysteine-linked through Sulfo-SMCC to BSA or recombinantly fused to GST, to assess their ability to modularly bind upon adsorption on NPs.

1.2.2 SpyCatcher/SpyTag proteins

In most proteins, including SNARE proteins, the forces that stabilise complexes are non-covalent, such as hydrophobic, ionic interactions and hydrogen bonds(Kang and Baker 2011). Disulphide bonds are the only well-known covalent bonds in protein-protein complexes.

Disulphide bonds form between two cysteine residues and has been proven that these can stabilize proteins against thermal unfolding(Hagihara, Mine et al. 2007), suggesting that they contribute to intramolecular stability. In the major pilin subunit from the Gram-positive human pathogen *Streptococcus pyogenes,* Baker's group found a new intermolecular covalent bond of proteins, between a carboxyl terminal and the amino group of a lysine of the next molecule, which is referred to as isopeptide bonds(Kang, Coulibaly et al. 2007). Isopeptide bonds have the same structure of peptide bonds, however, they have the following features(Kang and Baker 2011):

1. the majority of the reactions occur between a lysine ε-amino group on one protein and a main chain α-carboxyl group on another protein;
2. the formation is enzyme-mediated, and involves a transient thioester intermediate formed by a cysteine on the active site of a participating enzyme; the intermediate is then reacted through nucleophilic attack by the lysine ε-amino group to achieve an isopeptide bond.

Recently, Howarth and his colleagues explored the immunoglobulin-like collagen adhesion domain (CnaB2) which contains a single isopeptide bond (Figure 1.12A)(Zakeri, Fierer et al. 2012). Interestingly, this is an intramolecular isopeptide and its formation is self-catalysed. Due to this unique features, CnaB2 was splitted into two poly-peptides, followed by rational modification, to assess whether it was possible to obtain an intermolecular isopeptide bond formation from the split protein, with potential applications in bio-conjugation. The group produced a peptide tag of 13 amino acids, SpyTag, able to form an isopeptide bond with its protein partner of 138 amino acids, SpyCatcher (Figure 1.12B)(Zakeri, Fierer et al. 2012). The name Spy comes from the fact that the original protein is found in invasive strains of *S.pyogenes*(Oke, Carter et al. 2010). The peptide bond formed by SpyTag and SpyCatcher is so stable that could remain folded in extreme pH (pH2) and high temperature (up to 100 ℃) conditions(Hagan, Björnsson et al. 2010).

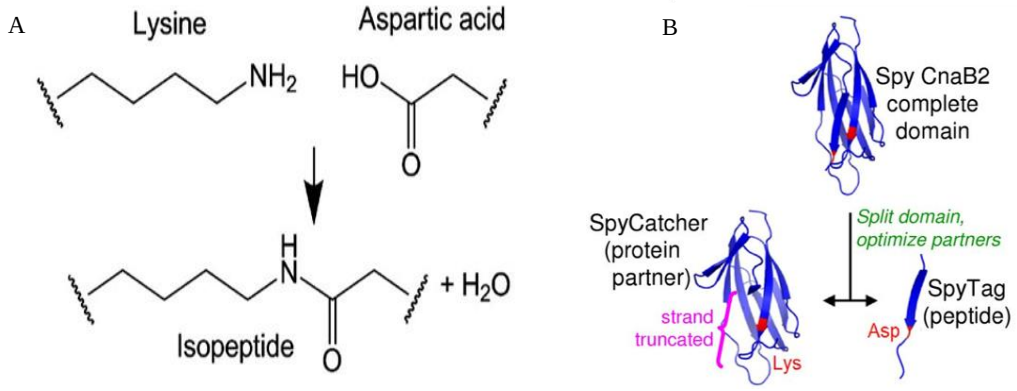

Figure 1.12 ***Isopeptide bond structure*** *(A) the isopeptide bond formation between SpyTag and SpyCatcher. (B) construction of SpyTag and SpyCatcher from* **S.pyogenes** *(Spy): CnaB2 was dissected into a large N-terminal fragment (SpyCatcher, left) and a small C-terminal fragment (SpyTag, right). Reactive residues are highlighted in red(Zakeri, Fierer et al. 2012).*

SpyTag and SpyCatcher can rapidly form covalent bonds without adding enzymes and are powerful bio-conjugation tools. We used this pair of proteins to study interactions of GNPs and protein. GST was fused to SpyCatcher to form a sacrificial layer adsorbed on GNPs and we demonstrated its ability to bind SpyTag directly on the GNP surface.

1.3 Recombinant Synthesis of Protein

Recombinant proteins are identified as proteins encoded by a gene that is cloned in an organism which supports the gene expression and messenger RNA translation. The gene normally does not exist in the genome, but could be synthesized by laboratory methods such as cloning. Following cloning into a host vector, the recombinant DNA could be expressed and the recombinant protein is produced. Finally, the purification process is introduced to harvest the proteins from the host organism. In the context of this work, we made extensive use of designer recombinant proteins for the decoration of GNPs.

1.3.1 Cloning

Cloning is a technique that generates a target DNA sequence containing a gene or a DNA fragment of interest, combines it to an appropriate replicon in *vitro*, then insert it into a host organism such as plasmid, finally express the gene by the host. Here, we summarize the cloning procedure into five steps:

Generation of target DNA insert.

The target DNA sequence can be generated in various ways, including polymerase chain reaction (PCR), chemically synthesizing DNA, cutting the DNA from existing fragments by restriction enzymes, primer extension and annealing. The two main ways to obtain the insert DNA are PCR and the use of restriction enzymes to cut the insert DNA from vectors, which were both used in this work. The PCR process quickly and easily amplifies the target DNA sequence and adds through the primers the restriction sites to the ends of DNA, so it can be inserted into a plasmid. Primers are designed based on the existing DNA sequence or public DNA database. If the target DNA exist in other DNA fragments, it could be separated by restriction enzymes and directly sub-cloned into the destination vector. To ensure that the insert DNA are kept in the frame, the selection of restriction sites and vectors have to be carefully checked. The full sequence including the insert DNA and vector can be mapped by using online resource such as http://web.expasy.org/translate/.

Preparation of the expression vectors by restriction endonucleases.

Before the ligation, the vector is digested by restriction enzymes to obtain the compatible overhangs with the generated target DNA. Expression vectors, and more generally all vectors engineered for the purpose of cloning, have a multiple cloning site specifically design for the convenient insertion of a digested fragment. This includes many standard restriction sites all in close proximity, with good chances that their position matches a desired design. In expression vectors the cloning site is under a promoter that promotes expression of the inserted fragments. Restriction enzymes that generates overhangs upon digestion are generally preferred, unless there are reasons to prefer blunt ligation (for example routine cloning of chemically synthesised inserts by companies that provide custom gene synthesis). Digestion with two restriction enzymes that generates two different overhangs is also favourable, as it guarantee correct orientation and prevents self-ligation of the vector compared to the case of a single restriction enzyme. In the case that the vector is cut by a single restriction enzyme, the insert could anneal in both orientation, in an undefined number of copies and the ends may be able to be religated. To prevent this, the vector should be treated with alkaline phosphatase.

Ligation of the target DNA and digested vector.

Ligation is accomplished by simply mixing the target DNA and vectors which are digested with identical or compatible restriction enzymes. The overhangs are annealed through hydrogen bonds between bases and the phosphodiester linkage is catalysed by ligase, such as T4 DNA ligase, and the ligation is conducted in T4 DNA ligase buffer containing ATP.

Transformation of completed vector and screening.

E.coli is commonly used to take up the completed DNAs and was the host of choice for all the recombinant proteins in this work. The transformants are spread on the plate of selective media (containing antibiotics) on which only the completed vectors which include a gene for antibiotic resistance could grow. Following the transformation into *E.coli*, the colonies carrying recombinant vectors are screened by gel electrophoresis of the vectors digested by restriction enzymes, for selecting those with the correct DNA insert. Alternatively, screening can be further simplified by choosing a vector and *E.coli* strains that are compatible with blue/white screening, which take advantage of intracistronic α-complementation to regenerate β-galactosidase activity.

Verification of the DNA insert by sequencing.

The target DNAs have a risk for mutation during the process, especially if PCR is involved. Because of this, the recombinant vectors that result positive after the screening, are typically Sanger-sequenced to determine the final sequence, generally using standard primers that anneal near the 5' or 3' ends of the multiple cloning site of the vector.

1.3.2 Expression

Expression vectors typically include a promoter that promotes the transcription and subsequent translation of the insert and repressors such as *lac*,that take control of the expression only in presence of an inducer molecule. Often, the protein of interest is fused to an affinity tag encoded directly into the vector, like in the case of the expression plasmid pGEX-KG used in this work, which is meant for the expression of C-terminal fusion to Glutathione-S-Transferase (GST). This facilitates the purification of the protein by using glutathione modified resins for which the fusion protein has high affinity. The affinity tag can be either removed proteolitically or retained. Another common affinity tag in expression vectors, for example the pET family, is represented by His-tag, which has high affinity to nickel bound to resins(Gibert, Bakalara et al. 2000).

In vivo and *vitro* are the two methods that can be used for recombinant protein expression. The *in vivo* expression is the well-established strategy for recombinant protein expression through transfecting cells with the DNA vector which contains the gene of desire protein. During the cell culture, the gene is transcribed and translated to proteins. The subsequent purification is followed to extract proteins from the cell lysate. Some of the bacterial, such as *Escherichia coli*, have the ability to express recombinant protein in a large quantity so that it is used in industrial process and the development of commercial goods(Rosano and Ceccarelli 2014).

However, muli-domain eukaryotic proteins have a high risk of losing the function in bacteria expression because cells are not equipped to reach the requirement of post-translational modifications or molecular folding(Chang, Kaiser et al. 2005). Eukaryotic protein domains, such as the SNARE domains used in this work, are suitable for expression in bacteria when post-translational modifications are not required, they are largely unstructured and therefore do not have critical folding. They have been successfully expressed in *E. coli* for at least two decades and this work makes use of well-established and biochemically well-characterized SNAREs(Chapman, An et al. 1994).

Cell-free protein expression is a new developed in vitro strategy of proteins offering a simply and quickly method in a quasi-cell environment that makes use of purified enzymes and cell-extracts for transcription and translatio. The cell-free system has various advantages than cell based expression (*invivo*): time-saving (24-48 hours for protein expression), the ability to adapt to high-throughput formats, increased tolerance to additives and less sensitivity to toxic or proteolytic proteins(Arduengo, Schenborn et al. 2007). However, it is only suitable and cost-effective for limited amounts of protein, compared to the in vivo alternatives. Therefore cell-free systems were not considered as an option for this work, which required significant yields of expressed proteins for their use in chemical modification steps.

1.4 Protein chemical crosslinking

Protein chemical crosslinking provides a method of combining two or more proteins through covalent bonds by using one or more of the reactivities explained above in the form of crosslinkers (CL). CL typically are directed towards sulfhydryls, primary amines and carboxyls.

CL are either homobifunctional or heterobifunctional molecules depending on whether they offer identical or different reactive groups respectively. Generally, the homobifunctional CL are used to react with primary amine groups (lysine residues) or sulfhydryls (cysteine residues). However, the main issue of homobifunctional CL is their susceptibility to produce undefined or undesirable conjugates. Controlling a reasonable concentration ratio of the two target proteins is difficult. Under the wrong concentration conditions, the active proteins combine with the proteins themselves forming the undesirable intra-protein crosslinking between the same proteins leading to low productivity of expected protein conjugates. If the two target

proteins have similar molecular weights, then it is difficult to separate the intra-protein crosslinking from expected protein conjugates.

The heterobifunctional CL is employed to combine proteins through different functional groups, such as a sulfhydryl and an amine group, or an amine and a carboxyl group. In these crosslinking reactions, the process normally consists of two steps to maximize the amount of protein conjugates. First, the CL reacts with one of the protein to form an activated protein or an intermediate, then the excess CL is removed. Second, the activated protein is incubated with the other protein for making conjugates. For example, SMCC (succinimidyl *trans*-4-(maleimidylmethyl) cyclohexane-1-carboxylate) is a CL for linking sulfhydryl and an amine groups through the maleimide and NHS (N-hydroxysuccininmide) ester respectively. The NHS ester reacts with amine groups of one protein first and after removing the excess SMCC, the other protein containing sulfhydryls are added to the activated protein.

Primary amines ($-NH_2$) exist at the N-terminals of peptides and the side chains of lysine residues. CL reagents providing reactive acylating groups are widely used for crosslinking of primary amines, such as NHS esters and imidoesters. The NHS ester reacts with primary amines in mildly alkaline conditions to form amide bonds and release NHS groups(Lomant and Fairbanks 1976). The high alkaline condition increases the hydrolysis of NHS ester, therefore, pH7.2 to pH8.0 is an important condition (Hermanson 1996). Sulfo-NHS ester is similar to NHS ester except that it has a sulfonate ($-SO_3$) on the NHS ring. The sulfonate group has no effect on the reaction between primary amines and ester, but it increases the solubility of the CL in aqueous buffers. The NHS ester is able to react with sulfhydryls and hydroxyls, however, the products are not stable because they are hydrolysed quickly in aqueous buffers(Hermanson 1996).

The imidoester is the most specific acylating reagent to modify amines. Compared to NHS esters, the imidoester crosslinkers perform better at higher alkaline conditions. At a pH below 8, the half-life of hydrolysis is short, at a pH of 10, the half-life and reactivity with primary amines increases. Moreover, the side reactions are negligible at pH=10(Browne and Kent 1975).

The carbodiimide is a special CL which does not introduce space chains into proteins and, as a consequence, the conjugates combined by carbodiimide groups are spatially close.

The modification and crosslinking of sulfhydryl are achieved by maleimide reactions. The maleimide groups specifically react with sulfhydryls at a pH of 6.5-7.5(Partis, Griffiths et al. 1983). At pH>8, the maleimide reacts with primary amines quicker than sulfhydryl, and the

maleimide are hydrolysed to maleamic acid which is non-reactive with sulfhydryl. Nevertheless, maleimide groups have no activity with carboxyl, hydroxyl or any other functional groups.

1.5 Proteins conjugation to gold nanoparticles

The layer of biomolecules that covers GNPs is called corona and it forms upon the interaction of GNPs with biological sources. In section 1.1, we introduced that GNPs can be decorated by amino acids, peptide, nucleic acids and proteins. Functionalized GNPs are useful tools for biological applications, such as gene and drug delivery and biosensors.

Since the research in my project focuses on the interaction between proteins and GNPs, here we introduce proteins adsorption onto gold nanoparticle surfaces.

1.5.1 GNP-protein binding

The Vroman effect suggests that at the early stage of the interaction of nanoparticles with biological fluids, most abundant proteins are adsorbed onto nanoparticles, however, after hours' incubation, the subsequent protein-protein competition shows they are replaced by higher affinity proteins(Vroman, Adams et al. 1980). The high affinity adsorption is also known as the 'hard corona', while the low affinity proteins form a 'soft corona' surrounding NPs. From the physical-chemical point of view, the hard corona is a long-lived structure that needs several hours to be exchanged (Monopoli, Walczyk et al. 2011). Another hypothesis is that hard corona proteins interact with NPs directly forming tightly bound proteins that do not readily desorb, and the soft corona proteins interact with the hard corona through weak protein-protein interactions(Walkey and Chan 2012).

According to the way proteins interact with NPs, the binding is defined in three ways: physisorption, nonspecific chemisorption and selective orientation-controlled adsorption. Practically the selective orientation-controlled adsorption is the only promising way that preserves the proteins' biological functions, whereas the other two lead to unpredictable results.

In physisorption the protein structures are largely distorted and the protein functions are compromised (Torcello-Gómez, Santander-Ortega et al. 2011). The reason for this effect is that interactions involved in the physisorption are the same factors that affect protein stability and structures, such as hydrophobic, electrostatic and hydrogen bonding(Avvakumova, Colombo et al. 2014). Nonspecific chemisorption is a stronger interaction than physisorption, because

proteins become conjugated to NPs by covalent binding, which is permanent. This approach is often achieved by modifying the NPs with functional groups including amine, thiol and carboxyl. The most commonly used chemistry is Au-S as we described in section **1.1**. However, despite sulfhydryls can be precisely localised on a protein structure, most of the chemisorption poorly control the orientation of interactions.

To control the protein orientation on NP surfaces, there are three important requirements (Avvakumova, Colombo et al. 2014):

(1) A tight irreversible linkage to reduce the system free energy.
(2) Site-specific binding.
(3) Controlled spatial orientation of the biomolecule to make all ligands active.

Based on the above rules, several developed methods exploited specific interactions including the use of biological counterparts(Yang, Mao et al. 2009) and chemical ligands(Hou, Qiao et al. 2012). All these methods improved the control of orientation, however, the modifications required on proteins decreased the biological activity resulting in activity impairment(Mahon, Salvati et al. 2012).

A new approach has been developed here to achieve the selective orientation-controlled adsorption. Bovine Serum Albumin (BSA) and Glutathione-S-Transferase (GST) have been linked to target proteins, either by chemical crosslinking (BSA) or recombinant fusion (GST). BSA and GST have been used as intermediates to bind GNP surfaces by chemisorption. Whilst BSA and GST firmly bind GNPs, the target proteins (SNARE proteins and SpyTag/SpyCatcher) are not directly involved in the chemisorption and still maintain their biological activities and are potentially able to selectively bind other molecules. The details of SNARE proteins and SpyTag/SpyCatcher are introduced in section **1.5**.

1.5.2 Physicochemical study of the GNP-Protein binding

From the physicochemical point of view, the adsorption of proteins to nanoparticles follows an equilibrium where proteins adsorb and desorb to the NPs surfaces. The reaction is in equilibrium when concentrations do not change. In this project, the Hill equation was used to set a simple model for the adsorption of proteins to GNPs(Hill 1910). The adsorption can be described as below:

$$M + S \underset{\text{Koff}}{\overset{\text{Kon}}{\rightleftharpoons}} MS \quad \text{(Equation 1.1)}$$

In the equation 1.1, *M* is the molecule that binds to a free site *S* on the surface of GNPs, *MS* is the site occupied by the protein, and K_{on} is the association constant and has the molar unit (M^{-1} s^{-1}), K_{off} is the dissociation constant and has the molar unit (s^{-1}). According to the law of mass action of Waage and Guldberg(Waage and Guldberg 1964):

$$\frac{d[MS]}{dt} = [M] \cdot [S] \cdot K_{on} - [MS] \cdot K_{off} = 0 \quad \text{(Equation 1.2)}$$

The equilibrium dissociation constant (K_D) is defined as:

$$K_D = \frac{K_{off}}{K_{on}} = \frac{[M] \cdot [S]}{[MS]} \qquad \text{(Equation 1.3)}$$

The maximum surface adsorption [S_{MAX}] is the sum of the free surfaces of GNPs and the adsorbed surfaces:

$$[S_{MAX}] = [S] + [MS] \qquad \text{(Equation 1.4)}$$

The equation 1.3 and 1.4 are rearranged to define [MS]:

$$[MS] = [S_{MAX}] \frac{[M]}{K_D + [M]} \qquad \text{(Equation 1.5)}$$

This model assumes that a molecule M binds to a free site S is not interacting with already occupied sites and that the proteins form a monolayer (single occupancy of the free sites S).

The concentration of the molecule [M] is the independent variable, whereas the concentration of the bound molecules [MS] is not directly measurable, but it is proportional to the measurable increase in diameter d of the nanoparticles (Δd), for example by Dynamic Light Scattering (DLS). Similarly, [S_{MAX}] is proportional to the maximum measurable diameter increase (Δd_{MAX}) in such a way that:

$$[\mathrm{MS}]/[S_{MAX}] = \Delta d / \Delta d_{MAX}$$

This is again only valid under the assumption that a monolayer forms all around the nanoparticle (known as corona). The equation 1.5 then becomes:

$$\Delta d = \Delta d_{MAX} \frac{[M]}{K_D + [M]} \qquad \text{(Equation 1.6)}$$

This is the equation that was used in this project to experimentally determine the binding affinity of a protein to NPs by using DLS data (Δd and Δd_{MAX}) acquired at different concentrations [M].

Based on IUPAC's Gold Book(McNaught and McNaught 1997), the definition of reaction rate is:

$$\frac{d[MS]}{dt} = -K \cdot [MS] \Longrightarrow \ln[MS] = \ln[[MS]_{MAX}] - Kt \quad \text{(Equation 1.7)}$$

K is the rate constant. In my project, $[MS]_{MAX}$ is proportional to the maximum diameter increased (Δd_{MAX}), and [MS] is proportional to the size increase of GNPs (Δd), hence equation 1.7 is rearranged as:

$$\Delta d_{MAX} = \Delta d(1 - e^{-Kt}) \quad \text{(Equation 1.8)}$$

Therefore, from the same experimental data used to calculate K_D it is also possible to determine the rate constant K.

1.5.3 Parameters affecting protein corona

According to the above section, we have tools to understand how proteins are adsorbed onto GNPs surfaces. However, more and more researchers are working on exploring the parameters affecting the protein corona. Lundqvist and colleages studied the hard corona formed from human plasma for NPs with different size and surface properties(Lundqvist, Stigler et al. 2008). This shows that many of highly abundant proteins, regardless of size and surface charge, all form part of the corona. However, there are various parameters that are important, hydrophobicity, surface charge and NPs size are the three most relevant factors that affect the corona formation. In the following description, each parameter will be given a detailed explaination.

Hydrophobicity

NPs with hydrophobic surfaces can adsorb more protein, as evidenced by gel filtration experiments (Cedervall, Lynch et al. 2007, Treuel, Brandholt et al. 2014). Human serum albumin (HSA) was incubated with different hydrophobic NPs and the amount of HSA adsorbed was evaluated by the elution volume and intensity of the peak corresponding toHSA-NPs conjugates. It was shown that the most hydrophobic NPs gave the largest conjugates, which had the highest peak and went out the column first.

The adsorption of protein onto hydrophobic and hydrophilic NPs was also compared. The surfaces with hydrophobic or hydrophilic features were controlled via the ratio between co-monomers N-iso-propylacrylamide/N-tert-butylacrylamide (the ratio of 100:0 giving the most

hydrophobic NPs). After incubation with HSA, the most hydrophobic NPs were fully covered with a single layer of proteins, while, the hydrophilic NPs were barely adsorbed with HSA(Lindman, Lynch et al. 2007).

Surface Charge

The surface charge of NPs plays an important role in protein adsorption. It is a general preference that proteins with isoelectric points (pI) >5.5 adsorb onto negative NPs surfaces bearing acidic functional groups (Gessner, Lieske et al. 2003), whereas proteins with pI less than 5.5 are preferentially adsorbed to positive charged NPs, such as the strong basic (NH_2) functionalized NPs. Opsonization is the process by which a foreign organism or particle becomes covered with opsonin proteins, thereby making it more visible to phagocytic cells. A correlation between surface charge and opsonization was demonstrated in vitro, showing neutral NPs have a much slower opsonization rate than charged NPs(Owens and Peppas 2006).

The surface charge also affects protein functions. Native protein conformations are controlled by the shape complementarity of the hydrophobic residues that allow close packing of the cores. When proteins interact with NPs, the native structure is distorted, as repulsive electrostatic forces are counterbalanced by a large entropy loss. Hence, proteins function are disrupted because of the interaction(Lynch and Dawson 2008).

Nanoparticles Size

Generally, the highly curved NPs surface discourage the adsorption. Lundqvist used polystyrene NPs with different sizes (50nm and 100nm) and the lower curved NPs were able to adsorb more proteins than higher curved NPs(Lundqvist, Stigler et al. 2008). Lynch used isothermal titration calorimetry (ITC) to determine the thermodynamics of the binding of HSA to NPs of 50:50 N-iso-propylacrylamide/N-tert-butylacrylamide (NIPAM/BAM) with a size range of 70nm-700nm,(Lindman, Lynch et al. 2007). They found that the smaller the NPs are, (larger surface areas at the same weight-per-volume concentration), the more protein they adsorb(Cedervall, Lynch et al. 2007). Conclusively, the NPs size has an important role on the amount of proteins adsorbed on NPs.

1.6 Aims of the project

As introduced above, protein-gold nanoparticles conjugates are widely employed in various applications, such as biosensors, drug delivery and gene delivery. Although conjugates are

fundamental elements for biosensors and delivery systems, the adsorption mechanism of proteins onto gold nanoparticles (GNPs) has been investigated only to limited extent. The main aims of this project are: 1. to understand the interactions between proteins and gold nanoparticles and 2. to engineer proteins that efficiently bind to gold surfaces in an expected orientation.

The primary aim was to investigate the role that electrostatic forces and thiol groups play in the adsorption mechanism of proteins to gold nanoparticles. To do this, Glutathione-S-Transferase (GST) was used as a model protein. For the study of electrostatic forces, GST was adsorbed onto GNPs under different pH values, and hence different surface charges. For understanding the role of thiol groups, cysteines of GST were chemically blocked by N-ethylmaleimide (NEM). The affinity and kinetics of GST and NEM-GST adsorption to gold nanoparticles were compared.

The second aim was to investigate whether GST and Bovine Serum Albumin (BSA), which are both able to stably bind gold, could be used as an interface for further proteins conjugation to GNPs. This was done by verifying whether the functions of self-assembling proteins was preserved upon modification with either interface (GST or BSA). The work focused on two convenient protein-protein conjugation systems: SpyCatcher and SNAREs. These were recombinantely fused to GST or chemically cross-linked to BSA and adsorbed to gold nanoparticles. The aim was to verify whether the self-assembling proteins were able to pair with their partner proteins in solution. Also, SNARE-BSA conjugates were used to attempt self-assembly of GNPs dimers. The project overall found that both GST and BSA are suitable interfaces for conjugation to gold, especially due to the availability of thiol groups. SpyCatcher and SNAREs conjugation systems are both able to work in combination to GNPs when either GST or BSA are used as an interface.

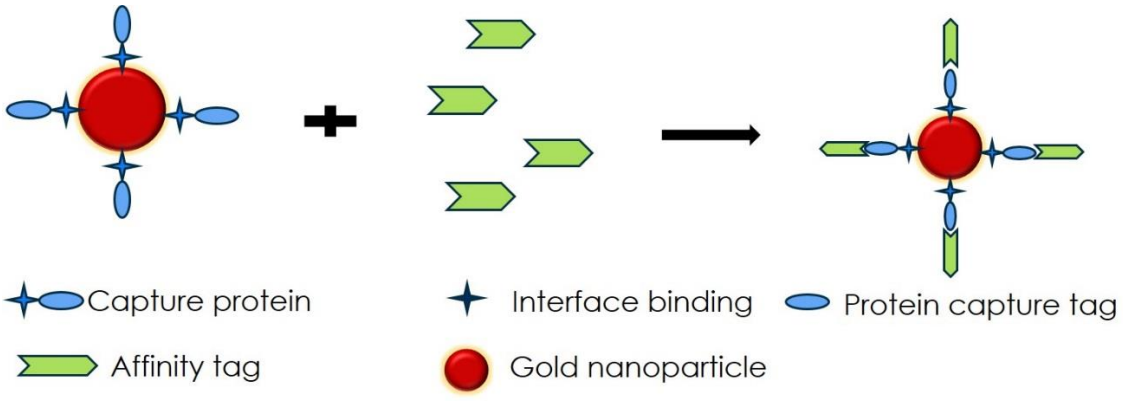

*Figure 1. 13: **Schematic of the modular assembly of proteins onto gold nanoparticles.***

This project provides a promising tool for modular assembly of proteins to nanomaterials. Figure 1.13 shows how self-assembling proteins could be used for conjugation to GNPs. The interface binding tested were GST and BSA. The capture protein was either a recombinant fusion of SNAREs or SpyCatcher to GST or a SNARE chemically crosslinked to BSA. The affinity tag was either a SNARE or SpyTag. Interestingly, this modular approach is not limited to GNPs, but to adapt to different nanomaterials, the interface binding could be possibly changed and investigated separately. For further applications, the affinity tag could be synthesized or bound with target molecules, such as antibodies, DNA and enzymes, which would capture the analytes in testing samples. The establishment of this modular platform for protein-nanoparticle conjugation was the main achievement of this project and the work will be discussed in detail in the next sections.

Chapter 2. Methods

The following flow chart lists the connections between proteins and GNPs, and purposes of methods.

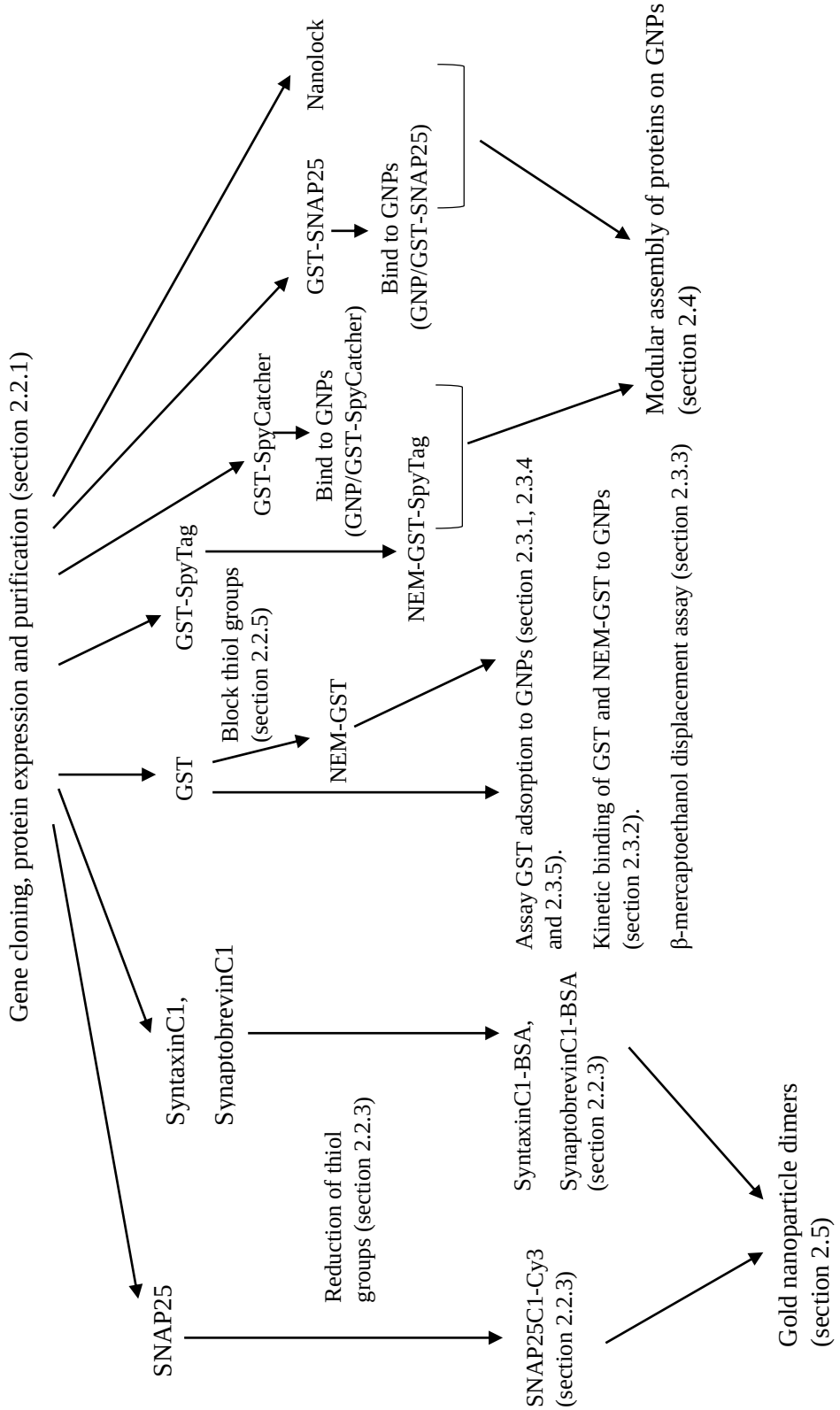

2.1 Synthesis and Characterization of Gold Nanoparticles

2.1.1 Synthesis of GNPs by sodium citrate method

Gold nanoparticles were synthesized using the well-known sodium citrate method(Turkevich, Stevenson et al. 1951). Briefly, all glassware which was used for the synthesis was immersed overnight in aqua regia (nitric acid and hydrochloric acid in a ratio 1:3), washed thoroughly with Milli-Q water and dried in oven. 0.125mL 2% $HAuCl_4$ in 24.375mLMilli-Q water were heated on a hot plate set at 300 ℃ while stirring at 150rpm using a magnet. When the mixture was boiling thoroughly, 1% sodium citrate was added rapidly, under constant stirring. The expected size of gold nanoparticles is determined by the volume of sodium citrate used. We synthesized two sets of GNPs, 15nm and 30nm, by adding 1% sodium citrate volumes of 0.58mL and 0.4mL respectively. The colour of solution changed from transparent to dark blue. The solution was left boiling for about 10 extra minutes until the colour suddenly changed from dark blue to wine-red. Heating and stirring was kept constant for 5 extra minutes, then the heating was turned off, while keeping the stirring on until the solution reached room temperature. The gold nanoparticle suspension was stored in a very clean plastic tube at room temperature in dark.

In order to compare the quality of GNPs synthesized by sodium citrate in the lab with commercial GNPs products, a batch of 40nm GNPs at a concentration of 5OD was bought from BBI Solutions.

2.1.2 Characterization of GNPs by atomic force microscopy

GNPs sample preparation for Atomic Force Microscopy (AFM) was based on a US National Institute of Standards and Technology (NIST) protocol(Grobelny, DelRio et al. 2011). A layer of mica, supported on a regular microscope glass slide, was removed by a sticky tape. This step was repeated many times until the exposed surface was smooth. 30µL of 0.01% poly-L-Lysine (PLL), providing a positively charged surface, was dropped on the flat mica substrate and incubated for 30min at room temperature. The PLL solution on mica was blown away using compressed air. 30µL of GNPs solution was applied onto the positively charged mica surface for 5 min at room temperature and finally dried with compress air.

The three sets of GNPs (15nm and 30nm GNPs from lab synthesis and 40nm GNPs from BBI Solutions) were prepared in the above way for AFM observation with a Bruker, Catalyst Bioscope.

The images were taken using Peak Force tapping mode and ScanAsyst Air probes (Bruker) at room temperature. The images were recorded at the scan rate of 1 Hz, 256 lines and scan size of 1 μm.

2.1.3 Characterization of GNPs by nanoparticle tracking analysis

Nanoparticle Tracking Analysis (NTA) was performed using Malvern Nanosight LM14. The three samples of GNPs described above were diluted 1:500 with Milli-Q in a volume of approximately 400μL to match the ideal number of particles/frame in the camera. This concentration corresponds to a number between 10^5 and 10^{10} particles/mL(Filipe, Hawe et al. 2010). Data were acquired using a 1 minute video recording at room temperature.

2.1.4 Characterization of GNPs by dynamic light scattering

The hydrodynamic diameter of GNPs was determined by Dynamic Light Scattering (DLS, Malvern Zetasizer Nanoseries). The three sets of GNPs (15nm, 30nm and 40nm) were diluted 5 times with filtered Milli-Q water. 1mL GNPs samples were added to disposable cuvettes (Polystyrol cuvette, Sarstedt). Then the cuvettes were covered with lids which were used to keep the samples at the set temperature of 20 ℃.

The instrument was set at 173 ° scattering angle. First, the instrument was equilibrated for 2 minutes. Then 3 readings of hydrodynamic diameter (z-average) were acquired with 16 sub runs each.

2.1.5 Characterization of GNPs by ultraviolet-visible spectroscopy

The GNPs samples were analysed by Ultra-Violet-visible spectroscopy (UV-vis) using a Shimadzu UV spectrophotometer, UV-1800. Samples were prepared in semi-micro disposable cuvettes (Sigma) with 1mL GNPs solution. All the UV-vis spectra were scanned from 400nm to 700nm. A graph of optical density (OD) versus wavelength was plotted and the wavelength (λ) and absorbance (A) of the Surface Plasmon Resonance (SPR) peak were determined.

Based on published work (Haiss, Thanh et al. 2007), equation 2.1 gives a precise determination of diameters of GNPs ranging from 25nm to 120nm, while equation 2.2 provides a good way to calculate the size of GNPs between 5nm and 50nm.

$$d = \frac{\mathrm{In}(\lambda - \lambda 0/L1)}{L2} \qquad \text{(Equation 2.1)}$$

The calculation of Equation 2.1 is based on the wavelength (λ) of the peak absorbance and λ_0, L_1 and L_2 are empirical parameters with values of 512nm, 6.53 and 0.0216 respectively, which have been given previously (Haiss, Thanh et al. 2007).

$$d = \left(\frac{A(5.89\times10^{-6})}{C_{Au}\exp(C1)}\right)^{1/C2} \qquad \text{(Equation 2.2)}$$

Equation 2.2 is calculated from the absorbance (A) at the SPR peak, C_{Au} (in moles per litre), which is the initial concentration of $HAuCl_4\ 3H_2O$ used to synthesize the GNPs (in this experiment was 2.42×10^{-4} M), C_1= - 4.7 and C_2=0.30 are empirical parameters that have been given previously (Haiss, Thanh et al. 2007).

2.2 Protein Biochemistry

2.2.1 Recombinant protein synthesis and purification

All recombinant proteins were encoded in pGEX-KG vectors as Glutathione-S-Transferase (GST) C-terminal fusions, with a thrombin-cleavable site at the N-terminal.

Mouse SNAP25 (synaptosomal-associated protein of 25 kDa, from NCBI Reference Sequence: NP_035558.1) has 4 cysteines residues in the loop that links the two SNARE domains. In this project three cysteines were mutated into alanine leaving the only one cysteine for the conjugation of a single fluorophore. The plasmid for the newly designed SNAP25, named SNAP25C1 was made by introducing a codon optimized (EMBOSS Backtranseq, available at www.ebi.ac.uk), chemically synthesized (Dundee Cell Products Ltd, UK) DNA insert into the *Eco*RI restriction site of the vector. The resulting amino acid sequence after GST tag removal by thrombin-cleavage was designed and shown in Table 2.1.

	Sequence
SNAP25C1	gspgisgggggilMAEDADMRNELEEMQRRADQLADESL ESTRRMLQLVEESKDAGIRTLVMLDEQGEQLERIEEGMDQINKDMKEAEKNLTDLGKFCGL AVAPANKLKSSDAYKKAWGNNQDGVVASQPARVVDEREQMAISGGFIRRVTNDARENEMDE NLEQVSGIIGNLRHMALDMGNEIDTQNRQIDRIMEKADSNKTRIDEANQRATKMLGSGef
SynaptobrevinC1	gspgNLTSNRRLQQTQAQVDEVVDIMRVNVDKVLERDQKLSELDDRA DALQAGASQFETSAAKLGSC
SyntaxinC1	gspgisgggggildsmgrpIETRHSEIIKLENSIRELHDMFMDMAMLVES QGEMIDRIEYNVEHAVDYVERAVSDTKKAGSC
Nanolock	gsEGRHKDIVRLESSIKELHDMFMDIAMLVENQGEMLDNIELNVMHTVDHVEKARDEAKRA GILDSMGRLELKLMSATAATVPPAAPAGEGGPPAPPPNLTSNRRLQQTQAQVDEVVDIMRV NVDKVLERDQKLSELDDRADALQAGASQFETSAAKL

Table 2. 1 ***SNARE proteins sequences. Amino acids in small are from the vector, and the upper case amino acids are from proteins sequences. In the SNAP25C1 sequence, alanines in red are mutated from cysteines in the original mouse sequence. The GSC added to the C-terminal of SynaptobrevinC1 and SyntaxinC1 are highlighted in yellow.***

A second version of the protein with all cysteines mutated into alanines, named SNAP25, was encoded in an already available pGEX-KG derivative which has been already extensively described(Poirier, Hao et al. 1998) and was used as a control throughout the project.

For conjugation to BSA and successive absorption on GNPs, the C-terminal of both Synaptobrevin and Syntaxin was modified with one extra cysteine and the resulting proteins named SynaptobrevinC1 and SyntaxinC1 respectively. The cysteine was designed to be separated from the SNARE domain by a glycine and serine, forming a 3 amino acids GSC short sequence. SynaptobrevinC1 was derived from rat Synaptobrevin2 sequence (aminoacids 25-84) and SyntaxinC1 from rat Syntaxin 1A (aminoacids 195-254). Both DNA inserts were amplified from existing plasmids using the primers in Table 2.2. The amplified products were double digested with the restriction enzymes also shown on Table 2.2 and ligated into pGEX-KG cut with the same enzymes. Two plasmids encoding the same proteins, but without the nucleotides for the GSC end, were cloned the same way for control purpose and named Syntaxin and Synaptobrevin.

	Primers	Restriction Enzyme
SynaptobrevinC1	Synaptobrevin_Forward:GGATCCCCGGGCAATCTTACCAGTAACAGG	*SmaI*
	Synaptobrevin_Reverse:GAGTCTAGATTAGCAGCTGCCGAGCTTGGCTGCAC	*XbaI*
SyntaxinC1	SYX_Forward:CATGGGTCGACCGATCGAGACCAGGCACAG	*SalI*
	SYX_Reverse:CTTGAGCTCTAGCAGCTGCCGGCCTTCTTGGTGTC	*SacI*

Table 2. 2 ***Primers and restriction enzymes for SNARE proteins. The restriction sites are underlined. The sequence encoding the GSC is highlighted in yellow.***

The resulting sequence of thrombin-cleaved SynaptobrevinC1 and SyntaxinC1 are shown in Table 2.1.

In order to make the naturally ternary SNARE complex into a binary group, Synaptobrevin and Syntaxin were fused into one protein and named Nanolock. This plasmid was kindly donated by the Medical Research Council and it has been previously reported(Ferrari, Darios et al. 2010). Briefly, Nanolock protein was made by combining rat syntaxin3 (amino acids 195-253) to rat synaptobrevin2 (amino acids 1-84), encoded in pGEX-KG vector. The thrombin-cleaved amino acid sequences of Nanolock is shown in Table 2.1.

The SpyCatcher protein sequence used in (Zakeri, Fierer et al. 2012) was reverse translated by 'Sequence Manipulation Suite' (http://www.bioinformatics.org/sms2/rev_trans.html) for chemical synthesis, outsourced and provided cloned in pBluescript. The software also optimised the codon usage for expression in *E.coli*. The 5' end of the resulting DNA sequence was modified with `TGATCA` which is the *BclI* restriction sites. The sequence `GGATCCTAGGAGCTC`, containing the stop codon `TAG` and restriction sites for *BamHI* (`GGATCC`) and *SacI* (`GAGCTC`) was added to the 3' end of the DNA sequence to make a synthetic DNA insert for subcloning from pBluescript into pGEX-KG (Table 2.3). *BamHI* and *SacI* near the 3' end of the insert were included to facilitate the subsequent insertion of a second

fragment designed the same way. This strategy was designed for future need of fusing several building blocks placed in tandem, as it would be suitable to originate a protein the type gsPROTEIN1gsPROTEIN2gsPROTEIN3gs (where gs is from the pGEX-KG vector). The DNA insert encoding SpyCatcher was synthesized (Dundee Cell Products Ltd, UK) and cloned in the form of un-methylated pBluescript vector. The pGEX-KG plasmid (expression vector) was cut by *BamHI* and *SacI*. The pBluescript plasmid (origin vector) was cut by *BclI* and *SacI* to obtain the insert DNA with sticky end which was ligated with the opened pGEX-KG (Table 2.3) using T4 ligase.

Expression pGEX-KG vector: *BamHI*/*SacI* cut

GGATCC……GAGCTC

CCTAGG……CTCGAG

Origin pBluescript vector: *BclI*/*SacI* cut

TGATCA……GGATCCTAGGAGCTC

ACTAGT……CCTAGGATCCTCGAG

Table 2.3 ***Cloning strategy for SpyCatcher. The overhangs from vectors and insert cuts are highlighted in yellow. The extra BamHI (red) site just before stop codon TAG converts the vector in a new potential acceptor of an insert with same design. The dots represent the actual insert.***

The theoretical thrombin-cleaved amino acidic sequence of SpyCatcher resulting from this cloning strategy is shown in Table 2.4.is the following:

	Sequence
SpyCatcher	gsGAMVDTLSGLSSEQGQSGDMTIEEDSATHIKFSKRDEDG KELAGATMELRDSSGKTISTWISDGQVKDFYLYPGKYTF VETAAPDGYEVATAITFTVNEQGQVTVNGKATKGDgs
GST-SpyTag	mspilgywkikglvqptrllleyleekyeehlyerdegdkwrnkkfe lglefpnlpyyidgdvkltqsmaiiryiadkhnmlggcpkeraeismlegavldirygvsriayskdf etlkvdflsklpemlkmfedrlchktylngdhvthpdfmlydaldvvlymdpmcldafpklvcfkkri eaipqidkylksskyiawplqgwqatfgggdhppksdlvprgsAHIVMVDAYKPTKgs

Table 2. 4 ***Protein sequences of SpyCatcher and GST-SpyTag. The Amino acids in small are from the vector whereas the upper case amino acids are from proteins sequences***

The DNA insert of SpyTag was designed for the same cloning strategy, but given the short length, it was simply obtained by two annealed complementary oligos which contain sticky ends for the subsequent subcloning into pGEX-KG. The target amino acid sequence of SpyTag

(AHIVMVDAYKPTK)(Zakeri, Fierer et al. 2012) was reversed translated by 'Sequence Manipulation Suite' (http://www.bioinformatics.org/sms2/rev_trans.html). The software also optimised the codon usage for expression in *E.coli*. The reverse translated sequence of SpyTag amino acid was named oligo1. Oligo2 was designed as the reverse-complementary sequence of oligo1, obtained using Bio-Web resources (http://www.cellbiol.com/scripts/complement/dna_sequence_reverse_complement.php). The leading sequence GATCA and the end sequence GGATCCTAGGAGCT were added to oligo1. A stop codon TAG was added just after the introduced *BamHI* (GGATCC) of oligo1. For oligo2, the leading sequence CCTAGGATCC and an end nucleotide T were added to match the sticky ends of the destination vector. The end codons of oligo1 and oligo2 were designed for the ligation into the pGEX-KG vector (Table 2.5).

Expression pGEX-KG vector: *BamH1*/*Sac*1 cut
GGATCC……GAGCTC
CCTAGG……CTCGAG
Annealed complementary oligos
5' GATCA……GGATCCTAGGAGCT 3'
3' T……CCTAGGATCC 5'

Table 2.5 ***Schematic of the cloning strategy of SpyTag. The pGEX-KG vector was cut by BamHI and SacI, where the sticky end of oligos were located (highlighted in yellow). The dots represent the DNA insert of SpyTag. The annealed oilgos was introduced with a BamHI site (red) before the stop codon TAG.***

The pGEX-KG vector was cut by *BamHI* (GGATCC) and *SacI* (GAGCTC), and then the removed sequence of vector was ligated with the annealed complementary oligos (Sigma).

SpyTag was kept as a fusion to the GST affinity tag after affinity purification. The theoretical protein sequence of GST-SpyTag is shown in Table 2.4.

Cloning of all the plasmids was made using XL1 Blue *E. coli* rubidium chloride competent cells (Agilent). Clones presenting the expected inserts and orientation were Sanger sequenced in two directions using pGEX5 and pGEX3 primers to confirm the sequences before proceeding to expression and purification.

All the proteins were expressed in *E.coli*, bacterial strain BL21-gold (DE3) pLysS competent cell (Agilent). 30µL of competent cells were transformed with 1µL of vector. 300µL of Super Optimal Broth (SOB) medium (pre-warmed at 37℃) was added to the transformed cells and

incubated in a shaker for 1 hour at 37℃. The transformants were spread on Luria-Bertani (LB) plates containing ampicillin (100µg/mL) and chloramphenicol (30µg/mL) and incubated at 37℃ overnight. 5mL of 2xTY (Tryptone, Yeast extract) medium containing ampicillin (50µg/mL) and chloramphenicol (50µg/mL) were inoculated with a colony picked from the plates. The culture was incubated at 37℃ overnight in a shaker. The overnight culture was diluted into 0.5L of 2xTY medium containing ampicillin (50µg/mL) and chloramphenicol (50µg/mL) in a 2L conical flask and grown at 37℃ in a shaker until the OD (optical density) value at 600nm culture reached 0.5-0.7. 100µM IPTG (Isopropyl β-D-1-thiogalactopyranoside, Melford) was added to induce protein expression and the culture was incubated at 18℃ in a shaker overnight.

Bacteria were harvested by transferring the culture into 0.5L polycarbonate bottles. The cultures were centrifuged at 3000g for 20min using a JLA 10.500 rotor in a J25 centrifuge (Beckman, Avanti J-26s XP). The pellet was suspended using 10mL Lysis Buffer (20mM HEPES pH 7.4, 500mM NaCl and 1mM EDTA). All the lysates were collected and transferred into a 50mL Falcon tube. 300µL of a 1ml solution containing a dissolved tablet of Complete Protease Inhibitor Cocktail (Roche) was added to the lysate to prevent protease degradation. In order to break the cell walls, the lysate was instant-frozen in liquid nitrogen for 10min, and thawed at 42℃ for 30min. 1mM of $MgCl_2$ and 400µL of 1mg/mL deoxyribonuclease I (from bovine pancreas, ≥400 Kunitz unit/mg Sigma) was added to Falcon tube and rotated at room temperature for 10min to digest DNA and reduce the viscosity of the lysate. 2% TritonX-100 detergent was added to the lysate and incubated for 20min at 4℃. The lysate was transferred into a centrifuge tube and spun down at 10000g for 20min at 4℃ using a JA-25.50 rotor in a J25 centrifuge (Beckman, Avanti J-26s XP).

The GST-fusion proteins were affinity-purified using glutathione resin. The supernatant was mixed with glutathione-sepharose beads under gentle rotation at 4℃ for 1.5 hours. The beads were washed twice using High Salt Buffer (20mM HEPES, 1M NaCl, 1mM EDTA, 0.1% TritonX-100), followed by two washes using Low Salt Buffer (20mM HEPES, 100mM NaCl, 1mM EDTA, 0.1% TritonX-100). In order to elute the affinity purified proteins from the glutathione resin, the beads were transferred into a 2mL eppendorf tube, washed with Buffer A (containing 20mM HEPES and 100mM NaCl, pH7.4), the volume adjusted to 1.5mL. The GST affinity tag was cleaved by incubating with 16.7U of thrombin (from bovine plasma, Sigma) for 1 hour at room temperature, shaking at 1000rpm. The eluate was separated from the beads using spin columns (Generon) and 30µL of Complete Protease Inhibitor Cocktail (from the

same stock used during bacterial lysis) was added to stop thrombin activity.

For some of the proteins (GST, GST-SNAP25, GST-SpyCatcher and GST-SpyTag) which were kept as GST C-terminal fusions, the beads were eluted with 5ml gluthathione (GSH) buffer (15mM Glutathione H, 250mM NaCl, 20mM HEPES, pH8.5) at 4°C for 30 minutes with 3000rpm shaking. The beads were spin down at 3000g for 1 minute. The first eluate was saved in a Falcon tube. 1ml GSH elution buffer was added to beads for another 15 minutes incubation at 4°C for with 3000rpm shaking. Then the beads were separated by centrifugation at 3000g for 1 minute. The second eluate was saved in an Eppendorf tube. The first and second elute were mixed before concentrating.

The combined eluates were concentrated to about 0.55ml using a Vivaspin 2 concentration column (Satorius), MWCO (Molecular Weight Cut-Off) of 10kDa for further purification by size exclusion chromatography.

The concentrated eluate was injected into an Akta FPLC (Fast Protein Liquid Chromatography) device (GE Healthcare) equipped with a Superdex 200 10/200 GL column (GE Healthcare). The collected fractions presenting high absorbance at 280nm were examined by Instantblue (Expedeon Company) stained SDS-polyacrylamide gel electrophoresis (SDS-PAGE) and pulled-together for conservation at -80ºC. The concentration of the resulting purified proteins was measured using BCA (bicinchoninic acid, protein assay, Thermo Scientific Pierce) kit.

2.2.2 Protein functional assays

SNAREs functionality was assessed by formation of a SNARE complex by simple mixing of 5µM of SNAP25C1, SynaptobrevinC1 and SyntaxinC1 or 5µM of SNAP25 and Nanolock in Buffer A with 0.8% OG (n-Octyl-β-D-glucoside, Sigma). The assembly was performed at room temperature for 1 hour and in a volume of 10µL. SNARE complex is unusually strong and cannot be denatured in SDS, therefore its assembly was assessed simply by using SDS-PAGE. However, heating a mixture containing SNARE complex in presence of SDS does break the quaternary structure. Therefore, 10 µL complex solution was equally aliquoted into two tubes, 5 µL of 2X SDS gel loading buffer was added to each tube and only one of the tubes was heated at 100 ℃ for 2 minutes. The heated and non-heated complex samples were run in 12% acrylamide SDS-PAGE in cold buffer, representative of the individual components and complex respectively. The cold buffer was necessary to prevent partial disassembly of the SNARE complex due to the heating from the electrophoresis apparatus. The complex formation

was assessed from the appearance of high molecular weight compounds that were absent in the heated samples.

The formation of a SpyCatcher/GST-SpyTag complex formed thorough isopeptide bond was assessed by mixing 5μM of SpyCatcher and GST-SpyTag. The isopeptide bonds are covalent bonds that cannot be dissociated in SDS-PAGE. Hence, 5 μL of 2X SDS gel loading buffer was added to 5 μL SpyCatcher/GST-SpyTag and the mixture was heated at 100 ℃ for 5 minutes. The heated sample was run in 12 % precast SDS-PAGE (RunBlue SDS Protein Gels, expedeon) to verify conjugation by change of the molecular weight.

2.2.3 Chemical modification of proteins

Thiol reduction of single-cysteine SNARE proteins

The single-cysteine SNARE proteins, SNAP25C1, SynaptobrevinC1 and SyntaxinC1, were reduced by Tris-(2-crboxethyl) Phosphine (TCEP) to break disulphide bonds. For the purpose of finding the best conditions for the reduction, the concentration of TCEP and incubation time were optimized. SNAP25C1 was used for optimization. Different concentrations of TCEP (0mM, 0.1mM, 0.5mM and 1mM) were added to 50 μM SNAP25C1and incubated at 4 ℃ overnight. Then the solution was spun in a Zeba Spin Desalting Columns, 7K MWCO (Thermo Scientific) to remove TCEP. 5μL of 2X SDS gel loading buffer (without β-mercaptoethanol) was mixed with 5μL reduced SNAP25C1. β-mercaptoethanol is a weaker reductant of disulphide bonds than TCEP, however it is still able to reduce SNAP25C1, therefore, in order to check the reduction efficiency of TCEP, SDS gel loading buffer without β-mercaptoethanol was employed. The reduced SNAP25C1 was run on 12% SDS-PAGE. 50 μM SNAP25C1 was reduced by 1mM TCEP for overnight, 8 hours, 5 hours, 3 hours, 1 hours and 0 hour separately. TCEP was removed by Zeba Spin Desalting Columns, 7K MWCO (Thermo Scientific). Reduced SNAP25C1 was mixed with 2X SDS gel loading buffer (without β-mercaptoethanol) for the SDS-PAGE analysis. In all the following experiments, the single-cysteine SNARE proteins were reduced by 1mM TCEP overnight before use, as this were the conditions that gave the best reduction in the optimization.

Cy3-maleimide conjugation to SNAP25C1

The cysteine of SNAP25C1 was labeled with Cy3-maleimide. 0.5g Cy3-maleimide (GE Healthcare) was dissolved in 50μL dimethylformamide (DMF) anhydrous for storage. 5μL Cy3-maleimide solution and 0.1mg reduced SNAP25C1 were gently mixed and incubated at room temperature for two hours with additional mixing every 20 minutes. Further incubation was performed at 4℃ overnight. Finally, the labeled SNAP25C1 was separated from the excess of Cy3-maleimide using Zeba Spin Desalting Columns, 7K MWCO. The SNAP25C1-Cy3 conjugate was run in the SDS-PAGE gel to verify molecular weight and fluorescence. SNAP25C1-Cy3, SynaptobrevinC1 and SyntaxinC1 were mixed and incubated at room temperature for 1 hour in the presence of 0.8% OG to verify the functionality of the modified SNAP25. 10μL of 2X SDS gel buffer were added to 10μL single-cysteine SNARE proteins complex. Half amount of this mixture was boiled at 100℃ for 2 minutes. The boiled and non-boiled complex samples were run in 12% SDS-PAGE in cold buffer.

Optimization of SNARE-BSA conjugation

SynaptobrevinC1 and SyntaxinC1 were designed to combine with BSA through Sulfosuccininidyl 4-[*N*-maleimidomethyl] cyclohexane-1-carboxylate (Sulfo-SMCC, Figure 2.1). Sulfo-SMCC is a water soluble heterobifunctional crosslinker which could combine amine- and sulfhydryl- through N-hydroxysuccinimide (NHS) ester and maleimide. For a long time storage, 20mM Sulfo-SMCC was dissolved in dimethyl sulfoxide (DMSO) and kept at -20℃.

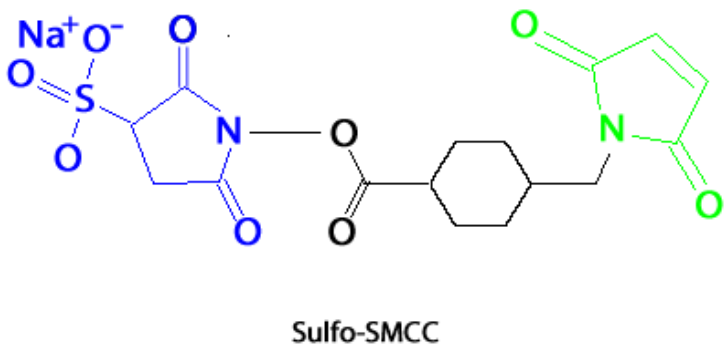

Figure 2.1 ***The chemical structure of Sulfo-SMCC, the NHS ester group (blue) links to amino groups, while the maleimide group (green) links to sulfhydryl groups.***

The cysteine of SynaptobrevinC1 or SyntaxinC1 were expected to combine with maleimide, and then BSA was expected to combine with activated SynaptobrevinC1 or SyntaxinC1 by the action between amines and NHS ester. In order to combine SNARE protein and BSA in the expected orientation, SynaptobrevinC1 or SyntaxinC1 were incubated with Sulfo-SMCC first,

then BSA was added to the activated SNARE. The scheme of the combination is shown in Figure 2.2. Both SynaptobrevinC1 and SyntaxinC1 were linked to BSA in the same way, therefore, SyntaxinC1 was used as an example for optimization.

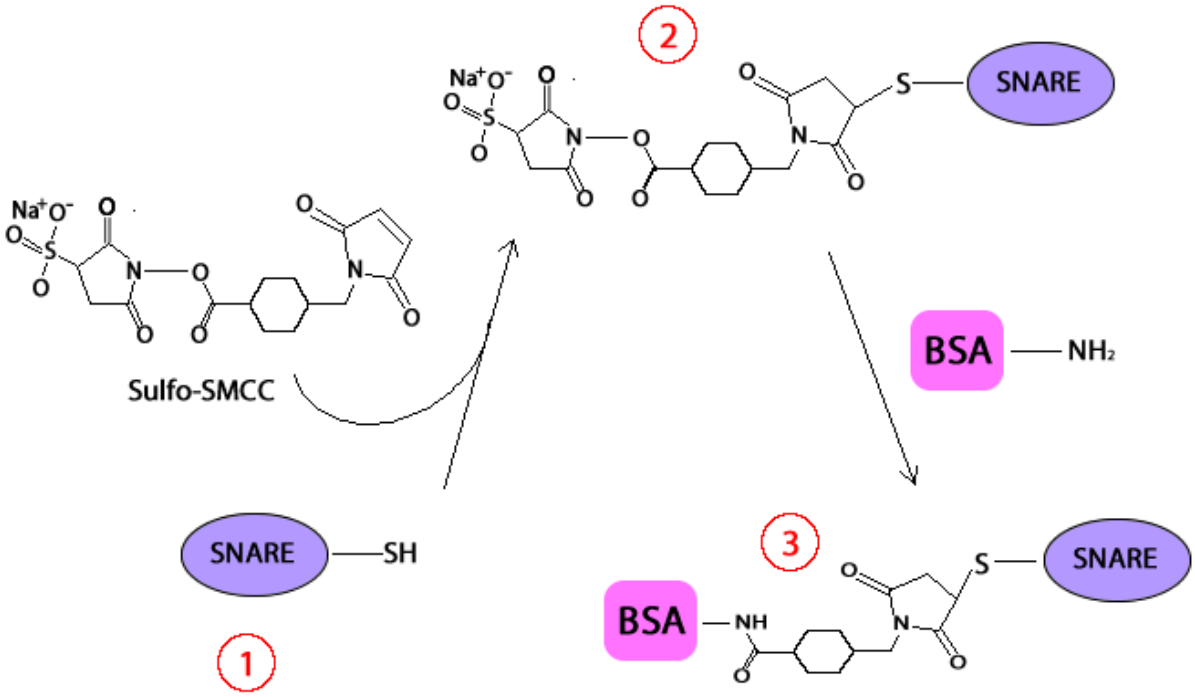

Figure 2.2 ***Schematics of crosslinking reaction. SNARE proteins were linked to maleimide firstly and then BSA was combined with NHS-ester.***

To ensure the free cysteine of SyntaxinC1 would not be oxidized during maleimide reaction, TCEP was kept in the maleimide step of the conjugation reaction. This was also because Zeba Spin Desalting Columns (Thermo Scientific) do not have 100% recovery, therefore removal of TCEP at this stage was avoided to minimise protein loss. To verify TCEP does not compromise the conjugation, the maleimide reaction with or without TCEP were compared. 50 µM SyntaxinC1 were reduced by 1mM TCEP overnight, then TCEP was removed by desalting columns. In another reaction, TCEP was kept after reduction. The two different treatments of SyntaxinC1 were incubated with 1mM Sulfo-SMCC for 1 hour at room temperature separately. 30 µM BSA were reacted with 30 µM SyntaxinC1-NHS for 1 hour at room temperature. The conjugate was checked by 12% SDS-PAGE.

The relative concentration of Sulfo-SMCC and BSA was then optimized. Different concentrations of Sulfo-SMCC (1mM, 5mM, and 10mM) were incubated with reduced 50 µM SyntaxinC1 at room temperature for 1 hour. The excess of Sulfo-SMCC was removed by Zeba Spin Desalt Columns, 7K MWCO (Thermo Scientific). 30 µM BSA were added to 30 µM

SyntaxinC1-NHS and incubated 1 hour at room temperature. The Syntaxin-BSA conjugate was analysed by 12% SDS-PAGE to verify the crosslinking reaction.

50 µM of reduced SyntaxinC1 and 1mM Sulfo-SMCC were mixed for 1 hour incubation at room temperature. Excess Sulfo-SMCC was removed by Zeba Spin Desalting Columns, 7K MWCO (Thermo Scientific). 10 µM, 30 µM and 40 µM BSA were added to 30 µM SyntaxinC1-SMCC separately for 1 hour incubation. 12% SDS-PAGE gel was employed to verify the conjugate.

The crosslinking reaction has two steps. First, Sulfo-SMCC was reacted with SyntaxinC1, then BSA was linked to the activated SyntaxinC1. The incubation time of the two reactions was optimized to achieve highest efficiency and prevent over-crosslinking.

50 µM of reduced SyntaxinC1 was reacted with 1mM Sulfo-SMCC at room temperature for overnight, 5 hours, 1 hour and 0.5 hour separately. Zeba Spin Desalt Columns (7K MWCO, Thermo Scientific) was used to remove excess Sulfo-SMCC. 30 µM BSA was added to 30 µM activated SyntaxinC1 for 1 hour incubation at room temperature. 10µL 1X SDS gel loading buffer was mixed with 2µL conjugate. This conjugate was checked in 12% SDS-PAGE gel to find the best incubation time.

For the BSA reaction, 50 µM of reduced SyntaxinC1 was mixed with 1mM Sulfo-SMCC for 1 hour incubation at room temperature. Excess Sulfo-SMCC was removed by Zeba Spin Desalt Columns (7K MWCO, Thermo Scientific). 30 µM BSA were added to 30 µM SyntaxinC1-NHS for overnight, 5 hours, 1 hour and 0.5 hour incubation at room temperature and analysed by SDS-PAGE.

Orientation of SNARE-BSA conjugates

In order to check whether conjugates of SyntaxinC1-BSA and SynaptobrevinC1-BSA were linked in the expected orientation, 50 µM of Synaptobrevin, SynaptobrevinC1, Syntaxin and SyntaxinC1 were mixed with 1mM Sulfo-SMCC separately for 1 hour incubation at room temperature. The excess Sulfo-SMCC was removed by Zeba desalting columns. 30 µM of Synaptobrevin-SMCC, SynaptobrevinC1-SMCC, Syntaxin-SMCC and SyntaxinC1-SMCC were added to 30 µM BSA separately. The incubation lasted for 0.5 hour at room temperature. The results were verified by 12% SDS-PAGE.

SNARE complex formation by SNARE-BSA conjugates

SNARE-BSA conjugates and SNAP25C1-Cy3 were mixed to form SNARE complex. 5μM conjugated SyntaxinC1-BSA and SynaptobrevinC1-BSA were mixed with 5μM SNAP25C1-Cy3 and incubated at room temperature for 1 hour. 10μL complex solution was equally aliquoted into two tubes, 5μL of 2X SDS gel loading buffer was added to each tube and only one of the tubes was heated at 100℃ for 2 minutes. The samples were run in 12% SDS-PAGE in cold running buffer.

All the SDS-PAGE gels were stained by Instant Blue (Expedeon) for 30 minutes, then distained by water for 10 minutes. The gels were analysed by ChemiDoc MP (BioRad).

2.2.4 Estimation of protein concentration

Apart from the fluorescent SNAP25C1-Cy3, the concentration of the other proteins was measured by BCA (Bicinchoninic acid) kit (Thermo Scientific) according to the manufacturer protocol.

Briefly, BSA standards were prepared by diluting 2mg/ml BSA stock (provided in the BCA kit) with filtered Milli-Q water (Table 2.6). Working reagent was prepared by mixing 50 parts of BCA Reagent A with 1 part of BCA Reagent B.

Vial	Filtered Milli-Q water (μL)	Volume and Source of BSA (μL)	Final BSA Concentration (μg/mL)
A	0	300 of stock	2000
B	125	375 of stock	1500
C	325	325 of stock	1000
D	175	175 of vial B dilution	750
E	325	325 of vial C dilution	500
F	325	325 of vial E dilution	250
G	325	325 of vial F dilution	125
H	400	100 of vial G dilution	25
I	400	0	0=Blank

Table 2. 6 ***Preparation of BSA standards***

25μL of each BSA standard or protein samples were pipetted into a 96 well microplate. 200μL working regent were added to each well and mixed with proteins thoroughly by pipetting.

Under this conditions, the working measurement range is 20-2000 µg/mL according to the manufacturer of the BCA kit. The plate was covered with a lid, and then incubated at 37 ℃ for 30 minutes. The plate was allowed to cool down to room temperature. The absorbance of proteins was measured at 562nm on a plate reader (TECAN infinite M200 Pro).

The concentration measurement of SNAP25C1-Cy3 was not carried out by BCA assay, as Cy3 has the maximum absorbance at 552nm which could affect the absorbance of BCA measurement at 562nm. SNAP25C1 has a very little difference of molecular weight compared to SNAP25C1-Cy3, therefore the gel filtration could not separate those two molecules, the concentration of true SNAP25C1-Cy3 was estimated by measuring the concentration of Cy3, based on its absorbance and extinction coefficient. Molar concentration of Cy3 and SNAP25C1 were calculated by Equation2.3 and Equation2.4 respectively (based on the maleimide-Cy3 protocol from GE Healthcare). The Equation2.5 is the molar concentration ratio which indicates the number of Cy3 combined to SNAP25C1 and the efficiency of the maleimide-thiol reaction.

$$[Cy3] = (A552)/150\,000 \quad \text{(Equation 2.3)}$$

$$[SNAP25C1] = [A280-(0.08 \bullet A552)]/28990 \quad \text{(Equation 2.4)}$$

$$C/S = [Cy3]/[SNAP25C1] \quad \text{(Equation 2.5)}$$

A552 and A280 were the absorbance at 552nm and 280nm respectively. The absorbance was measured by Nanodrop (Thermo Scientific). Molar extinction coefficients of $28990 M^{-1}cm^{-1}$ at 280nm for SNAP25C1 and $150000 M^{-1}cm^{-1}$ at 552nm for Cy3 were used in the equations. For the concentration of SNAP25C1, the calculation was corrected at 280 nm (approximately 0.08 of the absorbance at 552 nm). Equation 2.3 was used to calculate the Cy3 concentration which equals the concentration of SNAP25C1-Cy3, as the excess Cy3 was removed during gel filtration and does not contribute to the overall fluorescence of the preparation. The C/S value estimated the reaction efficiency between maleimide and cysteine.

2.2.5 Blocking of thiol groups by N-ethylmaleimide

The thiol groups of GST and GST-SpyTag were blocked by *N*-Nethylmaleimide (NEM, Sigma) to obtain NEM-GST and NEM-GST-SpyTag respectively. NEM was equilibrated at room temperature before opening to prevent condensation in the bottle and subsequent hydrolysis and loss of function.

For long time storage, 100mM NEM was dissolved in DMSO. A minimum of a 10-fold molar excess of NEM was added to sulfhydryl groups, since each GST molecule has 4 cysteines, 1.2mM NEM was added to 30 μM GST or GST-SpyTag. The reaction was performed at room temperature for 2 hours. The excess NEM was removed by Zeba Spin Desalting Columns, 7K MWCO. The remaining thiol groups of NEM-GST and NEM-GST-SpyTag were determined by Ellman's Reagent (5, 5'-Dithio-bis-(2-nitrobenzoic acid)).

4mg Ellman's reagent was dissolved in 1mL reaction buffer (0.1M sodium phosphate buffer: 0.1M KH_2PO_4, 0.1M Na_2HPO_4, 1mM EDTA, pH8.0). L-Cysteine was used as standard solution (Table 2.7). L-Cysteine (Sigma) was dissolved in reaction buffer to make a 400 μM stock, then diluted to 10 μM, 50 μM, 100 μM, 150 μM, 200 μM, 250 μM, 300 μM by reaction buffer. The working buffer was made by mixing Ellman's reagent and reaction buffer with the ratio of 1:2. 50 μL L-Cysteine standards or protein samples were mixed with 150 μL working buffer for a 10 minutes incubation at room temperature in 96 well micro plate. The absorbance was measured at 412 nm (TECAN infinite M200 Pro). The standard curve was based on the absorption of different concentration of L-Cysteine solution and the thiol concentration of NEM-GST and NEM-GST-SpyTag was calculated based on the equation of the standard curve.

	400uM L-Cysteine	Reaction Buffer
400uM	500uL	0uL
300uM	56.25uL	43.75uL
250uM	62.5uL	37.5uL
200uM	75uL	75uL
150uM	30uL	30uL
100uM	70uL	70uL
50uM	30uL	30uL
10uM	10uL	90uL
0uM	0uL	100uL

Table 2. 7 ***Preparation of L-Cysteine standard solution.***

2.3 Adsorption of proteins on GNPs

2.3.1 Equilibrium binding of proteins to GNPs

40nm BBI GNPs were used for the equilibrium binding study. 100 µL 1OD GNPs were mixed with 900 µL buffer phosphate buffer of four different pH, prepared by mixing fixed volumes of 0.1M KH_2PO_4 and 0.1M Na_2HPO_4 (Table 2.8) to a final concentration of 0.01M phosphate. The final pH of each phosphate buffer was measured by the calibrated pH meter (H12210 Henna Instruments), the pH values were confirmed as 6.0, 6.5, 7.3 and 8.0.

0.1M KH_2PO_4 (mL)	0.1M Na_2HPO_4 (mL)	pH value
90	10	6.0
70	30	6.5
20	80	7.3
5	95	8.0

Table 2. 8 ***Preparation of phosphate buffer at different pH value***

For the adsorption analysis of GST-SNAP25/SNAP25 and GST-SpyCatcher/SpyCatcher, 100 µL 1OD GNPs was added to 900 µL Buffer B (10mM HEPES, 10mM NaCl, pH7.3).

The adsorption of proteins to GNPs results in size increasing which was measured by Dynamic Light Scattering (DLS, Malvern Zetasizer Nanoseries). There was a 2 minutes equilibration time to prepare the instrument temperature reaching up to 20 ℃. The scattering angle was fixed at 173 °. 3 readings of hydrodynamic diameter (z-average) were taken for each sample. The hydrodynamic diameter of GNPs only was measured first without addition of protein, then increasing volumes of 30 µM proteins were added to GNPs as follows in Table 2.9.

	GNPs (1OD)	Buffer (µl)	Protein volume to add (µl)	Protein total volume (µl)	Total volume (µl)	Protein concentration (µM)
A	100	900	0	0	1000	0
B	100	900	5	5	1005	0.15
C	100	900	5	10	1010	0.3
D	100	900	10	20	1020	0.59
E	100	900	10	30	1030	0.87
F	100	900	10	40	1040	1.15
G	100	900	15	55	1055	1.56
H	100	900	15	70	1070	1.96

Table 2. 9 ***Preparation of DLS measurement***

The increase in diameter (Δd) was calculated by subtracting GNPs diameter at zero concentration. A graph of Δd versus the protein concentration was plotted to determine the affinity curve. The data points were fitted by nonlinear least-squares method (Kemmer and Keller 2010)to an equilibrium binding curve. Finally, the equilibrium dissociation constant (K_D) and maximum increasing diameter (Δd_{MAX}) were calculated from Equation 1.6. The sum of the weighted square roots (SWSR) for these parameters were calculated and minimised by the solver tool of excel, and the confidence interval was assessed using the Fishers' F-distribution with a confidence interval of 95%.

2.3.2 Kinetic binding of GST and NEM-GST to GNPs

For the kinetic binding study, the procedure of DLS was set up as follows: 90 µL 1OD 40nm BBI GNPs were added into a micro disposable cuvette and 15 single size measurements were taken with 30 seconds interval between each reading. The GNPs diameter was measured without any protein in the first reading, then 10 µL GST or NEM-GST with different final concentration (0.02 µM, 0.05 µM, 0.1 µM, 0.2 µM and 0.5 µM) was added to the cuvette during the 30 seconds between first and second reading. The increasing diameter (Δd) of 15 readings was recorded. For different proteins concentration, the graph of Δd (nm) versus time (s) was plotted. The maximum increasing diameter (Δd_{MAX}, nm) of each concentration versus the relevant concentration was plotted and fitted by nonlinear least-squares data fitting procedure.

$K = K_{on}[M] + K_{off}$ (Equation 2.6, [M] is the protein concentration.)

The Δd_{MAX} and rate constant (K) of relevant concentrations were calculated based on Equation 1.8, K versus concentration was plotted and the data points were fitted by linear curve. The association constant (K_{on}) and dissociation constant (K_{off}) were estimated by the Equation 2.6.

2.3.3 Au-S formation determination by β-Mercaptoethanol stability assay

0.4 OD 40nm GNPs (BBI Solutions) were incubated with 1.5 µM GST or NEM-GST at room temperature for 1 hour, 30 minutes, 20 minutes, 10 minutes, 5 minutes, 2 minutes and 0 minute in a total volume of 200 µL. Then 0.2mM β-Mercaptoethanol was incubated with the GNPs proteins conjugates for 20 minutes at room temperature.

With regards to GNPs conjugates with GST-SNAP25, SNAP25, GST-SpyCatcher and SpyCatcher, 0.2OD 40nm GNPs (BBI Solutions) were incubated with 1.5 μM of each protein at room temperature for 20 minutes. 0.2mM β-Mercaptoethanol was mixed with the GNPs conjugates, and the incubation was last for 20 minutes at room temperature.

The absorbance between 400nm and 700nm was measured by Surface Plasmon Resonance (TECAN infinite M200 Pro) with 5nm steps and the absorbance ratio between 530nm (nearest to the expected Surface Plasmon Resonance peak) and 600nm readings ($Ab_{530nm/600nm}$) was used to describe the GNPs aggregation. The $Ab_{530nm/600nm}$ value versus incubation time was plotted for analysing the chemi-sorption of GST and NEM-GST to GNPs.

2.3.4 Zeta-Potential determination of GNPs/GST at different pH values

The zeta-potential of GNPs and GNPs/GST conjugates at different pH (pH6.0, 6.5, 7.3 and 8.0) was measured by Malvern Zetasizer. 1mL of 0.1OD 40nm GNPs (BBI Solutions) was carefully injected into a zeta-potential cuvette (Malvern) by a 1mL syringe paying attention not to introduce air bubbles. The z-potential was determined at each pH for both naked particles and after incubation for 20 minutes with 0.5 μM GST (final concentration).

The Zeta-Potential measurement parameters were set as follows: there was a 2 minutes equilibration time before the measurement, each measurement had 4 readings, each reading had 25 runs, 60 seconds interval was set between each reading. The average value of the zeta-potential was calculated from 4 readings. The graphs of zeta-potential versus pH was plotted for both naked GNPs and GNPs/GST.

2.3.5 Mapping of GST surface charge at different pH

The calculation of surface charge of GST at different pH (6.0, 6.5, 7.3, and 8.0) was based on the Adaptive Poisson-Boltzmann Solver (APBS) solvation model which is an algorithm to solve the Poisson-Boltzmann equation and calculate the electrostatic potential of a surface. GST PDB (protein data bank) structure file (ID 1UA5) was used as the input and the distribution of potential calculated at different pH from the APBS server (University of California San Diego, http://nbcr-222.ucsd.edu/pdb2pqr/) was converted into a 3D plot by Chimera software (University of California San Francisco, https://www.cgl.ucsf.edu/chimera/).

2.4 Modular assembly of proteins on GNPs

2.4.1 Agarose gel electrophoresis of GNPs-protein conjugates

10 µL 1OD 40nm BBI GNPs were mixed with increasing concentrations (0.15, 0.30, 0.59, 0.87, 1.15, 1.56, 1.96 µM) of GST-SNAP25 in a final volume of 20 µL in Buffer B and incubated for 1 hour at room temperature. After incubation, they were mixed with 5% glycerol, loaded in a 0.8% agarose gel and run in 0.25xTBE (22.5mM Tris-borate, 1mM EDTA, pH8.3) for 50 minutes at 75V. A sample of GNPs with no protein was also loaded as the negative control. The agarose gel was imaged by ChemiDoc MP (BioRad) to estimate the migration of the intensely red bands corresponding to GST-SNAP25-coated GNPs.

In order to study the SNARE proteins assemble on GNPs, 1.5 µM GST-SNAP25 were mixed with 1OD 40nm BBI GNPs, incubated for1 hour at room temperature, then mixed with 3 µM Nanolock and incubated for 2 hours at room temperature. A mixture made of GNPs/GST and Nanolock was prepared in parallel and used as the negative control. The two groups of mixture with Nanolock were run in the 0.8% agarose gel (0.25 ×TBE buffer, 50 minutes, 75V).

2.4.2 SDS-PAGE of GNPs-protein conjugates

1OD 40nm GNPs (BBI Solutions) were incubated with 250nM GST-SNAP25 or GST (control) for 1 hour at room temperature. The final volume of this mixture was made up to 50 µL by adding Buffer B (10mM HEPES and 10mM NaCl, pH7.3). 500nM Nanolock was added to GNPs/GST-SNAP25 or GNPs/GST (control) and incubated for 3 hours at room temperature to allow SNARE complex formation.

Similarly, 500nM GST-SpyCatcher were added to 1OD 40nm GNPs (BBI Solutions), and the final volume was made up to 50uL by adding Buffer B, incubated at room temperature for 1 hour. 500nM NEM-GST-SpyTag or NEM-GST (control) were added to GNPs-GST-SpyCatcher respectively, and incubated at room temperature for 3 hours.

All the above GNPs-protein conjugates were centrifuged at 5000g for 5 minutes after incubation. The GNPs pellets were resuspended in 50 µL Buffer B. The centrifugation and suspension were repeated for three times to remove the uncomplexed proteins.

In order to release the proteins from the particles and allow them to migrate into the SDS-PAGE gel, we used harsh conditions to break the Au-S covalent bond between GNPs and adsorbed proteins (GST). 15uL GNPs-protein conjugates were added to 5uL 4X SDS-PAGE loading buffer (0.06M Tris pH6.8, 10% glycerol, 2% SDS, 0.005% bromophenol blue, 5% β-mercaptoethanol), heated at 100 ℃ for 5 minutes, then left in 42 ℃ water bath for 10hours. The proteins were fully recovered after removal of GNPs by centrifugation at 5000g for 5 minutes and loaded in 12% precast SDS-PAGE gel, run at 170V for 55 minutes with fresh running buffer. The gel was stained by InstantBlue for 6 hours, then distained by water for 10 hours on a shaker to display the total protein bound to GNPs samples.

2.4.3 DLS measurement of protein complexes assembled on GNPs

100 µL 1OD 40nm GNPs (BBI Solutions) were diluted to 1mL by filtered Buffer B. The naked GNPs size was determined by DLS as described in **2.3.1.** Then excess GST-SNAP25 at a concentration of 1.5 µM was added and the size of GNPs/GST-SNAP25 measured by DLS. 3 µM Nanolock was added to GNPs/GST-SNAP25 mixture and the size was measured by DLS after 3 hours incubation at room temperature to assess the binding of Nanolock to GNPs/GST-SNAP25. As the negative controls, GST was incubated with GNPs in the same condition as GST-SNAP25 and measured in parallel without and with the same amount of Nanolock.

Similarly, GNPs were saturated by 1.5 µM GST-SpyCatcher and the GNPs conjugate size was measured by DLS, then 3 µM NEM-GST-SpyTag was added and the size was measured again after the incubation of 3 hours. NEM-GST, lacking the SpyTag, was incubated with GNPs/GST-SpyCatcher as negative control.

The experiments were repeated in triplicate on independently prepared samples. All measured sizes were expressed as the average value of the three replicates with standard deviation.

2.5 Assembly of gold nanoparticles dimers using SNARE-BSA conjugates

6.5 µM SyntaxinC1-BSA and SynaptobrevinC1-BSA were incubated with 100 µL of 1OD 40nm GNPs and 1OD 20nm GNPs respectively for 1 hour at room temperature. GNPs/SNARE-BSA conjugates were spun down at 5000g for 5 minutes. Then the GNPs conjugates were suspended in 100 µL Buffer B. GNPs/SyntaxinC1-BSA and GNPs/SynaptobrevinC1-BSA were mixed in a 0.5mL Eppendorf tube. 6.5 µM SNAP25C1-Cy3

was added to the mixture for a 1 hour incubation at room temperature to make GNP dimers. Finally, the dimers were observed by AFM as described in section **2.1.2**.

Chapter3. Results and discussion

3.1 Synthesis and characterization of gold nanoparticles

This section reports the synthesis and characterization of the GNPs that were used for all the subsequent experiments. Two sets of GNPs were synthesized with an expected size of 15nm and 30nm respectively. The different size can be useful in nanoparticle assembly, for example, to assess specific, protein-driven dimerization of GNPs. Commercial GNPs were also bought and their quality compared with lab synthesized GNPs. The sizes of all GNPs were characterized by AFM, NTA, UV-vis and DLS.

3.1.1 Characterization of gold nanoparticles by AFM

AFM allowed direct visualisation and high-resolution imaging of nanoparticles. AFM images were used to observe the shape and size of GNPs and were used to generate a distribution based on the height measurement of hundreds of particles from several images. The height of a particle on a very flat surface such as mica can be determined very accurately by AFM, while the diameter of the same can be affected by the limited lateral resolution of this technique. For this reason the diameter was expressed as height of a spherical particle rather than its lateral dimension.

The AFM study (Figure 3.1A and 3.1B) shows the size of lab synthesized GNPs was homogeneous, and morphology was as spherical as commercial 40nm BBI Solutions GNPs (Figure 3.1C). According to the distribution in Figure 3.1D, 3.1E and 3.1F, most of GNPs had a diameter of 26.2nm, 18.8nm and 37.8nm respectively, which is close to the expected size.

3.1.2 Characterization of Gold Nanoparticles by NTA

Although AFM is a suitable technique for the visualization of GNPs, it is poor from a statistical point of view as only tens or hundreds of particles can be realistically counted. Nanoparticle Tracking Analysis (NTA) instead verifies the size distribution of the GNPs based on measurement of the diffusion coefficient of many GNPs in a dispersion and also estimate the concentration of GNPs.

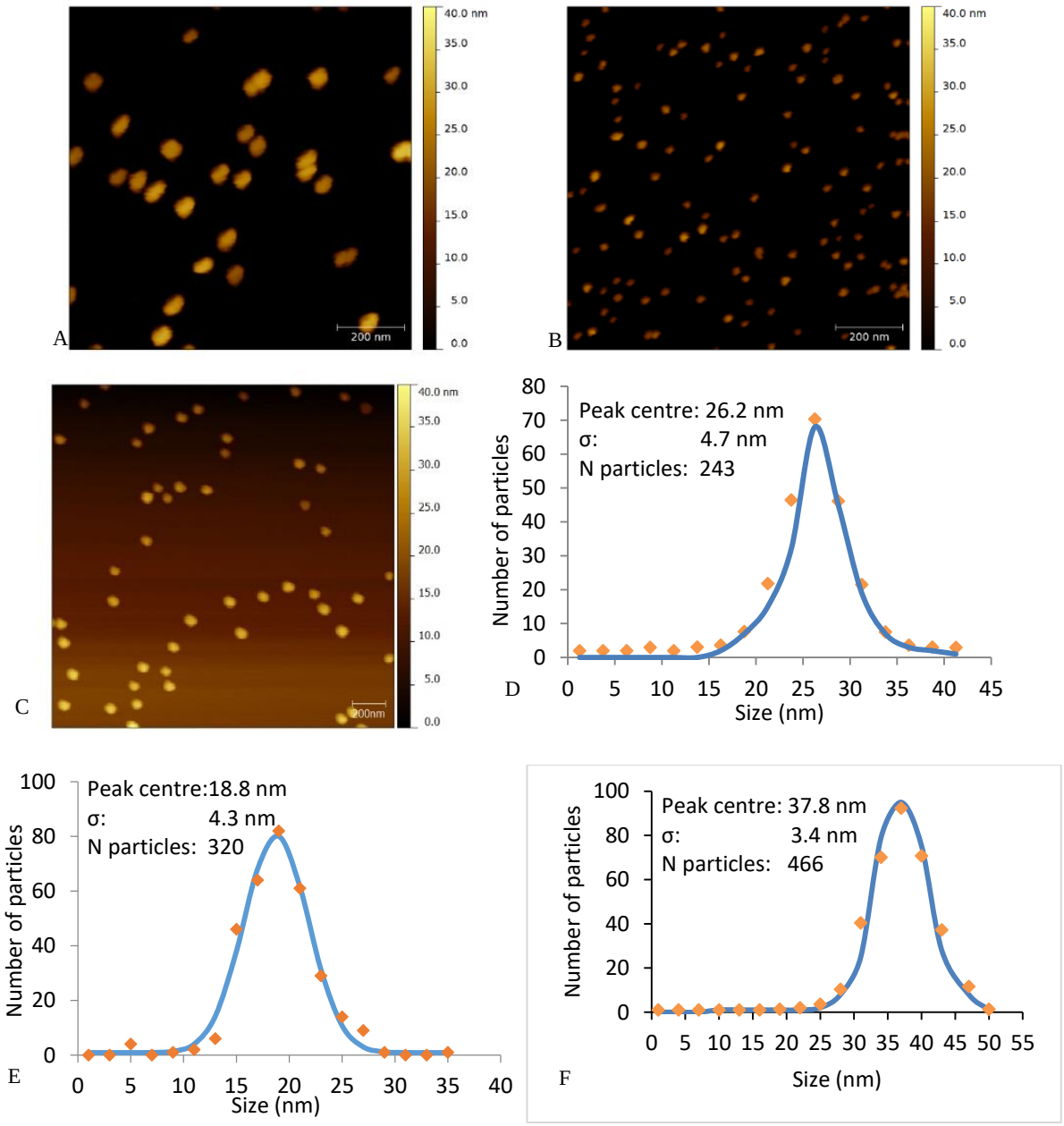

Figure 3. 1 ***AFM images of 30nm (A), 15nm (B) and 40nm (C) GNPs on mica. Distributions of gold particles shown in panels D (30nm), E (15nm) and F (40nm) respectively were obtained combining the particle maximum height from several AFM images (blue lines). The data from N nanoparticles were fitted to a Gaussian distribution (orange dots) to determine the most likely size of particles (Peak centre) and the standard deviation of the distribution (σ).***

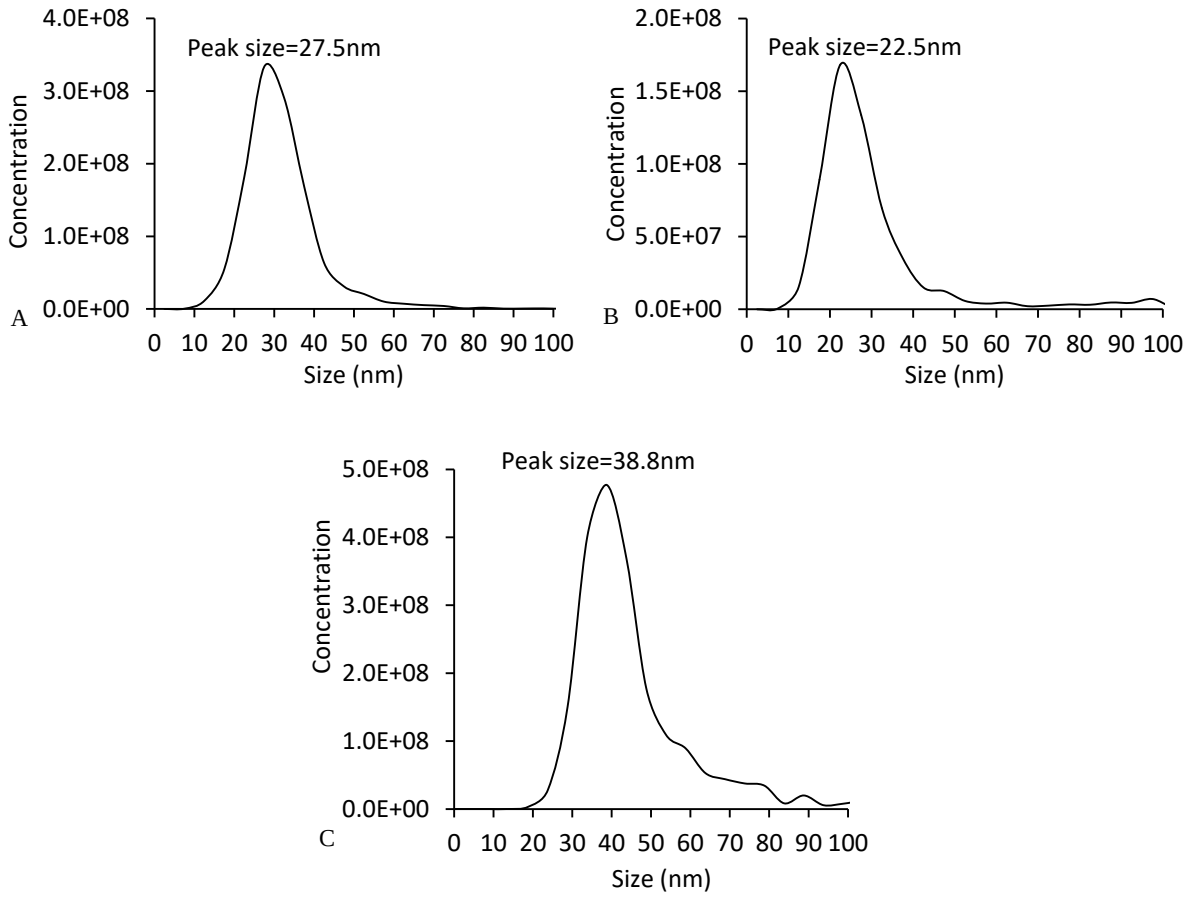

***Figure 3. 2** Size distribution of GNPs by NTA.30nm (A), 15nm (B) and 40nm (C). The 500X diluted concentration of (A), (B) and (C) was 2.38×10^{8}particles/ml, 2.94×10^{8}particles/ml and 3.77×10^{8}particles/ml respectively.*

The peak of the distributions obtained by NTA from the same samples discussed above was 27.5nm, 22.5 nm and 38.8nm for the 30 nm, 15 nm and 40nm dataset respectively (Figure 3.2). Compared with the data obtained by AFM, the results for the 30nm GNPs and 40nm BBI GNPs were closer to the expected values. However, the estimation of the size for the 15nm batch by NTA was 22.5nm, which is 7.5nm bigger than the expected size. This discrepancy may be due to aggregates of GNPs in solution or due to the limited accuracy of NTA measurements, especially for very small particles.

The concentration of the three sets of GNPs was measured by NTA as 2.94×10^{8}particles/ml (15nm), 2.38×10^{8}particles/ml (30nm), and 3.77×10^{8}particles/ml (40nm) respectively. 15nm, 30nm and 40nm GNPs were diluted with Milli-Q water in the proportion of 1:500, therefore, the actual concentration of 15nm, 30nm and 40nm is 1.47×10^{11}particles/ml, 1.19×10^{11}particles/ml and 1.89×10^{11}particles/ml respectively.

3.1.3 Characterization of gold nanoparticles by DLS

The average size of each set was calculated according to scattering intensity distributions. The measured mean GNPs sizes (Z-average) of 15nm, 30nm and 40nm were 13.97nm, 27.88nm and 39.16nm respectively (Figure 3.3). All the measurements showed that the three sets of GNPs were monomodal (only one peak) and monodisperse (narrow width of distribution). These results confirmed the measurements obtained with AFM and, in part, with NTA.

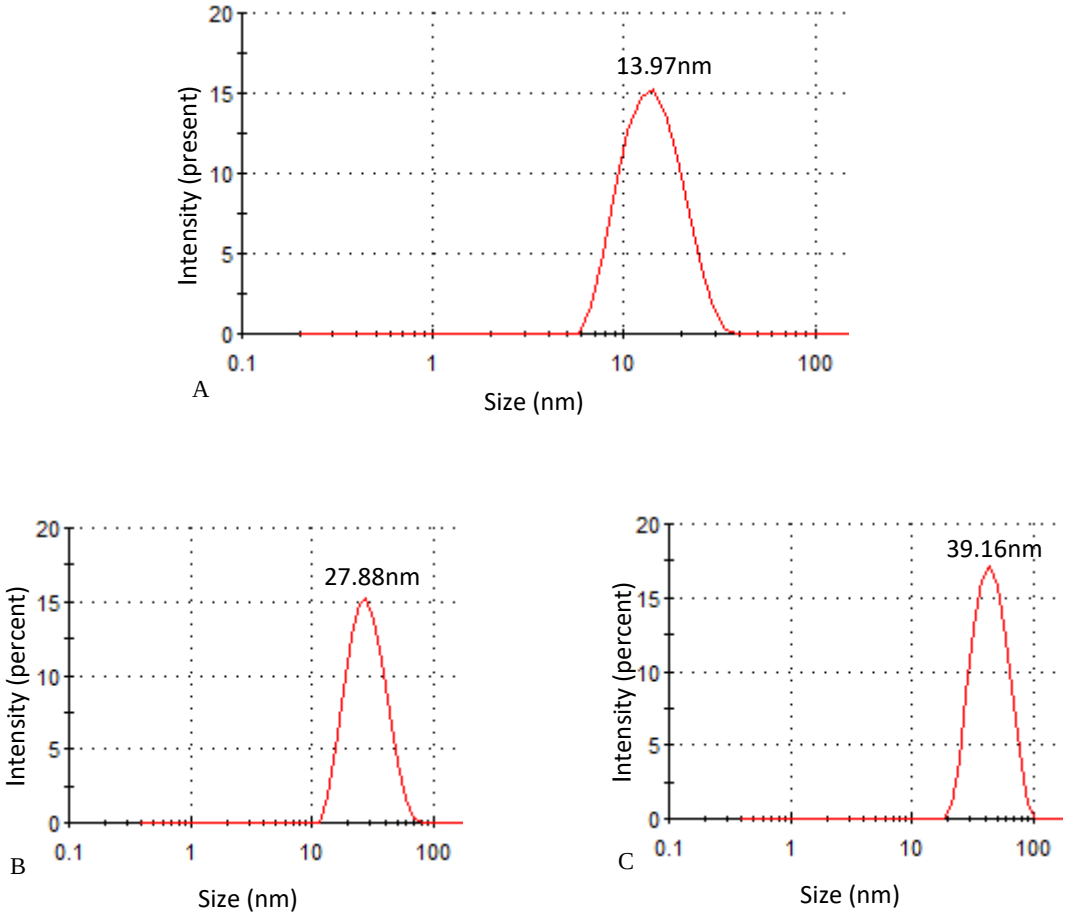

Figure 3. 3 ***GNPs size distribution by DLS. (A) 15nm, (B) 30nm and (C) 40nm.***

Considering that the concentration at which particles are measured is less critical in DLS than NTA, that DLS takes into account the hydrodynamic behaviour of a very large number of particles compared to AFM and NTA, and that in case of monodispersed samples DLS is considered the most accurate way to assess particle size, we concluded that this was the best estimate of particles size. The size measurement was therefore very close to the expected size for all three samples.

3.1.4 Characterization of gold nanoparticles by UV-vis

Based on multipole scattering theory, the size of GNPs can be estimated by absorbance spectra in the visible range. The GNPs solution were measured by UV-vis spectrophotometry to obtain the absorption spectra shown in Figure 3.4.

The wavelength peak of absorbance of GNPs is size-dependent. The absorbance values for 15nm GNPs, 30nm GNPs and 40nm BBI GNPs were 0.932, 0.8874 and 0.907 with peaks at 521.9nm, 525.2nm and 527.3nm respectively.

The peak absorbance for 30nm GNPs and 40nm BBI GNPs were at 525.2nm and 527.3nm respectively, therefore, the GNPs diameter based on Equation 2.1 was 32.6nm and 39.4nm, which is close to the expected size of 30nm and 40nm.

Since Equation 2.1 is optimal for particles larger than 25nm, Equation 2.2 was used instead to estimate the size of the GNPs batch with expected size of 15nm. The measured peak absorbance was 0.866, resulting in GNPs diameter calculated from Equation 2.2 of 17.7nm, close to the expected size of 15nm.

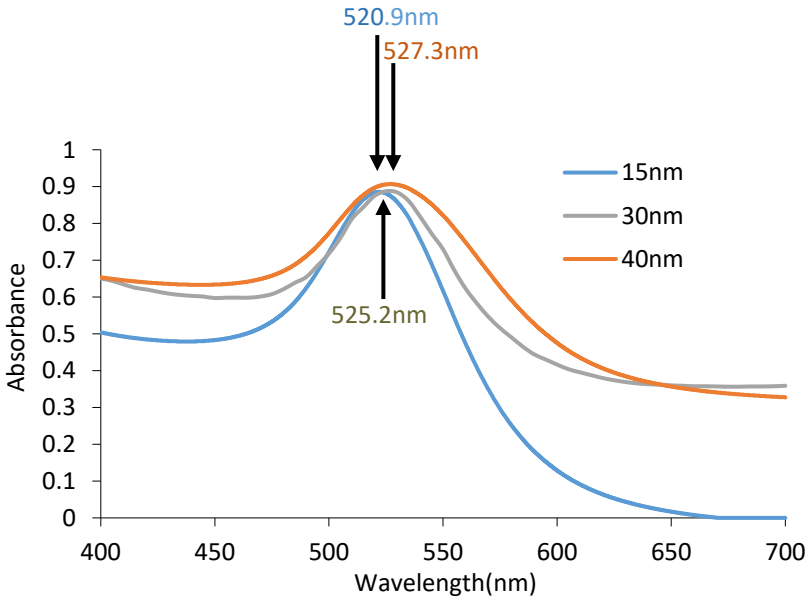

Figure 3. 4 ***UV-vis spectra of GNPs of 15nm, 30nm and 40nm.***

Generally, the calculated diameters of the three sets of GNPs were 17.7nm, 32.6nm and 39.4nm according to Equations 2.1 and 2.2. It is known that the model is prone to an error of about 6%, hence, the calculated values fall within the range of the expected sizes.

Expect size (nm)	AFM(nm)	NTA(nm)	DLS(nm)	UV-vis(nm)
40	37.8	38.8	39.16	39.4
30	26.2	27.5	27.88	32.6
15	18.8	22.5	13.97	17.7

Table 3. 1 ***Summary of GNPs characterization.***

In conclusion, the three sets of gold nanoparticles (15nm and 30nm GNPs were synthesized in the lab, 40nm GNPs was bought from BBI solution) were characterized by AFM, NTA, DLS and UV-vis (Table 3.1). Those techniques provide the size, the morphology and the concentration of GNPs in terms of visual observation, diffusion coefficient and multipole scattering theory. All the results show that all the batches of GNPs have expected sizes, and the lab-made GNPs (15nm and 30nm) have good distribution and morphology as BBI solution GNPs (40nm). Nevertheless, the excess gold chloride of lab synthesised GNPs has to be removed, and the buffer was exchanged in this case with water. The commercial GNPs, 40nm BBI GNPs, are more suitable for subsequent experiments that make use of proteins which are dissolved in salt buffers. Considering the salt stability, the BBI GNPs were used in the subsequent study of proteins adsorption to GNPs and proteins assembly on GNPs.

3.2 Protein recombinant synthesis, chemical modification and assembly

This section includes all the results on the protein biochemistry done in preparation of the experiments reported in the next sections. This included recombinant synthesis, bio-conjugation and assessment of the assembly properties of SNARE proteins and SpyTag/SpyCatcher. The single-cysteine recombinant SNARE proteins (including SNAP25C1, SyntaxinC1 and SynaptobrevinC1) were used for conjugation purpose. SNAP25C1 was linked to maleimide-Cy3, and the assembled complexes containing SNAP25C1-Cy3 were visible under UV light. The cysteine of SyntaxinC1 and SynaptobrevinC1 was conjugated with BSA through Sulfo-SMCC. The BSA-SNARE proteins were used to assemble GNPs as dimers. GST, SNARE fusion proteins (GST-SNAP25 and Nanolock) and SpyTag/SpyCatcher proteins were synthesized as a proof-of-concept for modular assembly of proteins on gold nanoparticles.

3.2.1 Purification of GST

The GST is a popular and easy-obtained affinity tag for recombinant proteins. It was expressed as native element of pGEX-KG vector and eluted by excess of glutathione from glutathione affinity resins. GST has four cysteine that are thought to be involved in forming Au-S covalent bonds between thiol groups and GNPs which are investigate in section **3.3.1.** The investigation of GST was done to study the effect of electrostatic force and covalent bond on GNPs conjugation, and to evaluate whether GST can be used as an interface protein in GST-SNAP25 and GST-SpyCatcher to bind GNPs efficiently, which is one of the primary objectives of this work.

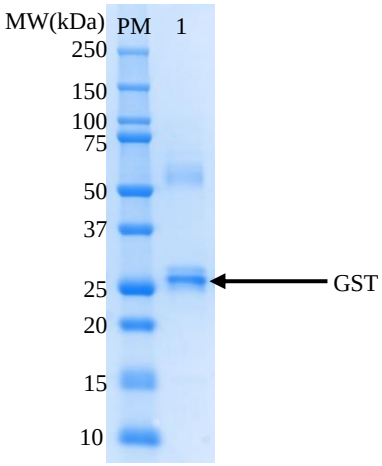

Figure 3. 5 ***The GST protein. Lane 1. PM is the protein marker (BioRad, Precision Plus Protein™ Dual Color). MW is molecular weight.***

The calculated molecular weight of GST is 28.6kDa. The lane 1 of Figure 3.5 showed that the recombinant protein expressed and purified as described in methods has a molecular weight which is slightly bigger than 25kDa, from which we concluded that the intense protein band of lane 1 is compatible with GST, whereas the higher molecular weight bands can be impurities or aggregates.

3.2.2 Synthesis and characterization of single-cysteine recombinant SNARE proteins for chemical conjugation

For the purpose of chemical cross-linking with thiol reactive reagents, the three elements of the neuronal SNARE complex, SNAP25, Synaptobrevin and Syntaxin, were mutated by introducing a single-cysteine residue and named SNAP25C1, SynaptobrevinC1 and

SyntaxinC1. All of these proteins were cloned in pGEX-KG vector and expressed in E.coli. A total of 1.5 ml with an estimated concentration (BCA colorimetric method) of 39 µM, 49 µM and 115 µM respectively was obtained for each protein. In order to verify whether the purified proteins correspond to the expected molecular weight, 6 µg of each of the purified protein were loaded on a SDS-PAGE gel. The calculated molecular weights of SNAP25C1, SynaptobrevinC1 and SyntaxinC1 are 24.5kDa, 7.28kDa and 8.97kDa respectively. The three proteins are shown in the SDS-PAGE gel (Figure 3.6) and they appear to be of the expected molecular weights. An extra band remained after the gel filtration in purified SyntaxinC1 and SynaptobrevinC1. The gel shows that the target bands and extra bands have very closed molecular weight, so that they might not viable for gel filtration separation. Later it was found that these do not interfere with the assembly properties of SNAREs and are likely to be impurities from the original bacterial lysate.

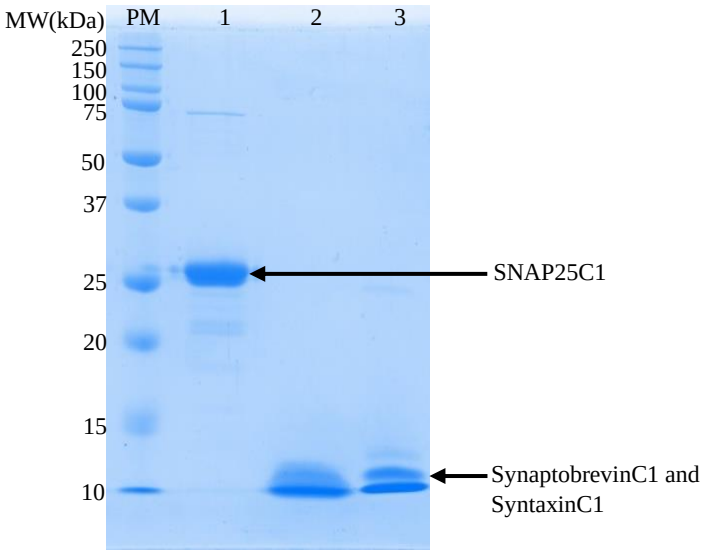

Figure 3. 6 ***SDS-PAGE gel of purified SNARE proteins, PM: protein marker (BioRad, Precision Plus Protein™ Dual Color), 1: SNAP25C1, 2: SynaptobrevinC1, 3: SyntaxinC1. The arrows indicate the bands of the protein marker corresponding to 25 and 10kDa. MW is molecular weight.***

The newly designed SNARE proteins were mixed to verify their ability to assembly and in order to proof this, a heated and a non-heated samples were assessed by SDS-PAGE. In fact, SNARE complex is known to be resistant to SDS denaturation, however, when exposed to very high temperatures in presence of a loading buffer containing SDS, the complex is irreversibly disassembled into the three components. The successful assembly of SNAREs can be assessed by simply comparing the heated (complex completely disrupted) and non-heated sample (complex partly intact).

The expected molecular weight of the SNARE complex is 40.75kDa, however, there is a sharp band around 37kDa in lane 2 of Figure 3.7, non-heated sample. This slightly odd migration is likely due to the tight coiled-coil structure of SNARE complex which runs at different speed compared to the sum of the three linear proteins components. The non-heated sample also shows bands corresponding to Synaptobrevin and Syntaxin as they were used in excess. In the heated sample, lane 1 of Figure 3.7, the quaternary structure of assembled SNARE proteins was broken, and as a result the individual bands of SNAP25C1, SynaptobrevinC1 and SyntaxinC1 are clearly visible in line 1 (Figure 3.7).

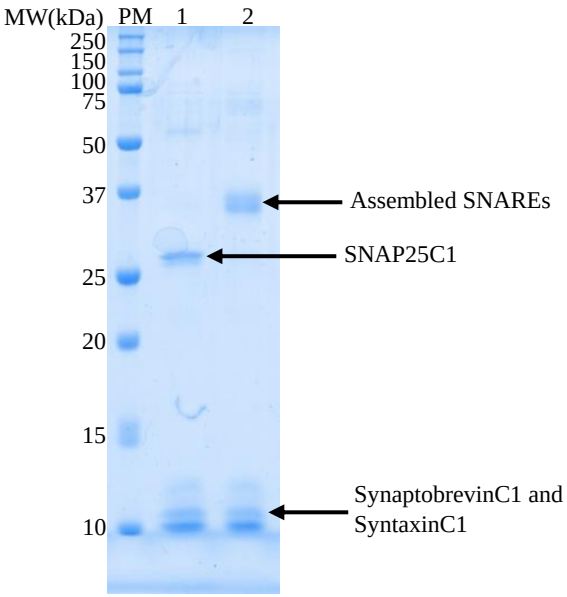

Figure 3. 7 ***SNARE complex assembled by newly synthesized proteins. PM is protein marker (BioRad, Precision Plus Protein™ Dual Color). (1) heated SNARE complex, (2) non-heated SNARE complex. MW is molecular weight.***

The results in Figure 3.7 suggests that the newly synthesized SNAREs are capable of assembly and therefore can be potentially used for bio-conjugation, such as of GNPs, fluorophores or protein domains, by simple mixing. Thanks to SNARE complex unusual stability, it is worth noting that assembly can be assessed simply by SDS-PAGE.

3.2.3 Synthesis and characterization of SNARE proteins fusions

Neuronal SNARE proteins form a ternary complex made of SNAP25, Syntaxin and Synaptobrevin. In order to assemble two elements, for example GNPs, in a binary way, we expressed a Syntaxin and Synaptobrevin fusion into a single polypeptide, named Nanolock. Syntaxin is at the N terminal of Nanolock whereas Synaptobrevin is at the C terminal.

A GST-SNAP25 fusion was also made to adsorb SNAP25 onto GNPs, following the observation that GST binds to gold with high affinity (see section **3.3.4** and **3.3.5**). A GST-SNAP25 fusion was purified by elution with glutathione excess from glutathione affinity resin. GST-SNAP25 and Nanolock were mixed to verify whether they were able to form a SNARE complex.

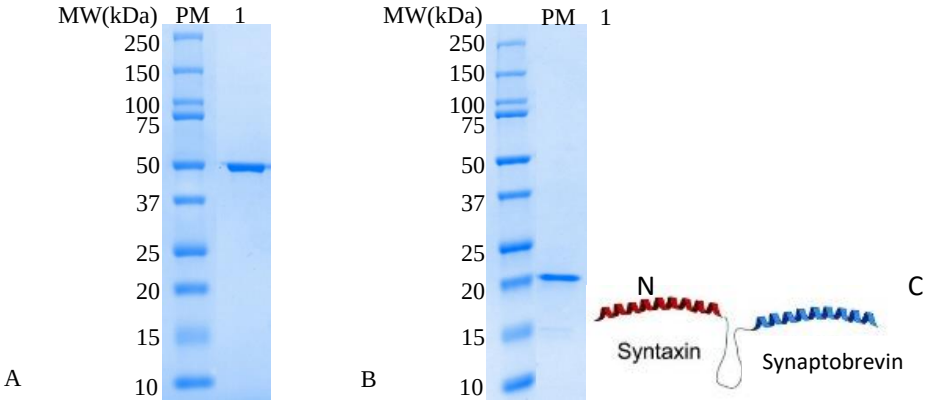

Figure 3. 8 ***SDS-PAGE of GST-SNAP25 and Nanolock.*** ***In both A and B, PM is the protein marker (BioRad, Precision Plus Protein™ Dual Color). Lane 1 of A is GST-SNAP25, lane 1 of B is Nanolock. The insert in panle B shows a schematic of the Nanolock design (Ferrari, Darios et al. 2010). MW is molecular weight.***

The calculated molecular weight of GST-SNAP25 and Nanolock were 49kDa and 17kDa respectively and their identity was confirmed by SDS-PAGE (Figure 3.8).

GST-SNAP25 and Nanolock were expected to form a SNARE complex which has a molecular weight of about 67kDa. In Figure 3.9, lane 2 showed that GST-SNAP25 was degraded which was visible by low molecular weight band, it was probably because of long time storage and refreeze, nevertheless, the partially-degraded GST-SNAP25 was still able to form a SNARE complex (lane 3) with Nanolock, as confirmed by the migration of the band corresponding to a molecular weight between 50kDa and 75kDa.

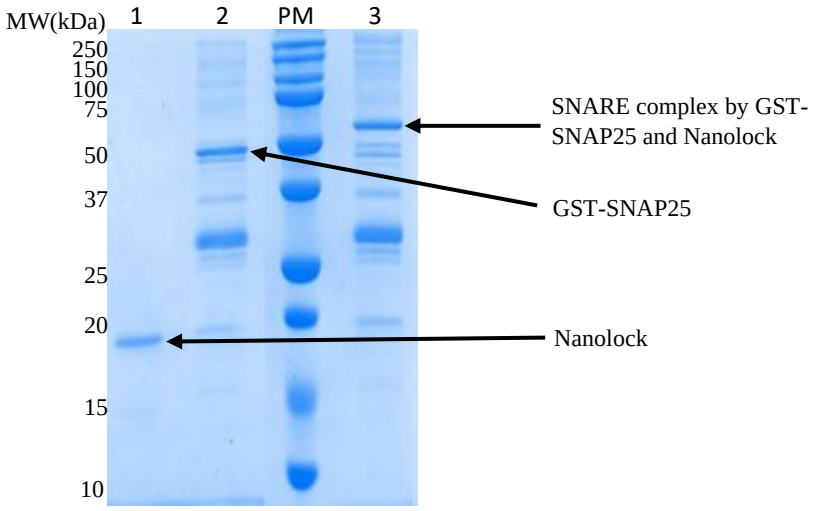

Figure 3. 9 ***SNARE complex assembled by GAT-SNAP25 and Nanolock. 1.*** *Nanolock. 2. GST-SNAP25, compare with the GST-SNAP25 of Figure 3.8, GST-SNAP25 of this experiment was partially degraded, however, the degraded GST-SNAP25 was still able to form SNARE complex with Nanolock in lane 3. The expected molecular weight of the complex is about 67kDa. PM is the protein marker (BioRad, Precision Plus Protein™ Dual Color). The according molecular weight (MW) of protein marker was labelled on the left.*

3.2.4 Synthesis and characterization of SpyCatcher/SpyTag Protein

SpyCatcher and SpyTag are a pair of proteins engineered from *Streptococcus pyogenes* (Spy) that are able to form isopeptide bonds (Figure 3.10) by simple mixing. This covalent peptide interaction is a simple and powerful tool for bioconjugation(Kang and Baker 2011). In this project, the recombinant SpyCatcher and SpyTag are used for the bioconjugation to GNPs, SpyTag has a molecular weight of 1.76kDa, which makes it difficult to purify from bacterial lysates. However, a GST fusion of SpyTag which has larger molecular weight was easily obtained and used as a proof-of-concept for conjugation of GST-SpyTag fusions to SpyCatcher. SpyCatcher and GST-SpyCatcher were also obtained, the second was designed to be adsorbed to GNPs through GST-gold interaction (**see 3.3.6**).

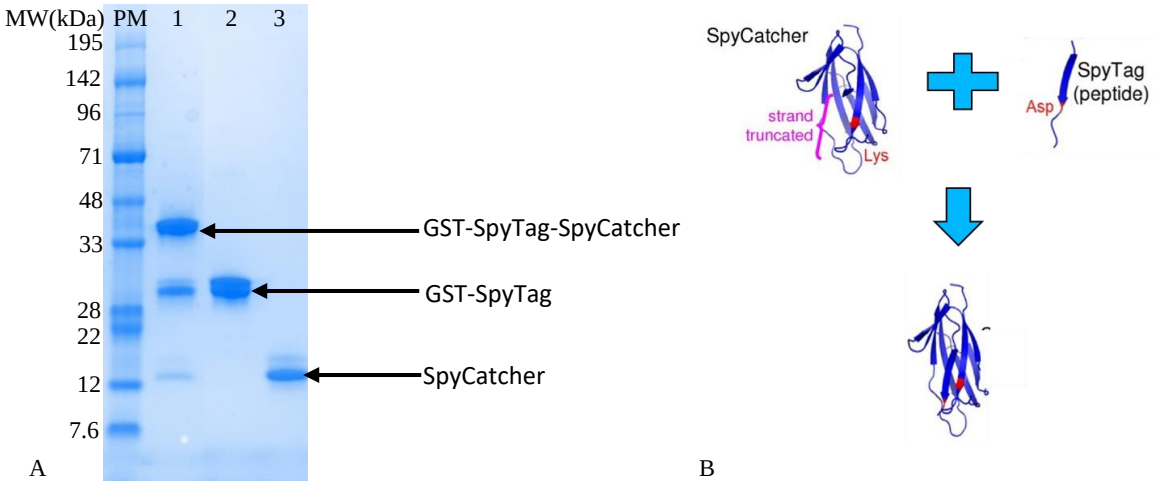

Figure 3. 10 ***Purified SpyCatcher and GST-SpyTag. A. 1. SpyCatcher and GST-SpyTag bound by isopeptide bonds, 2. GST-SpyTag, 3. SpyCatcher, PM is the RunBlue prestained dual colour protein marker. B. the formation of isopeptide bonds ((Zakeri, Fierer et al. 2012).***

The calculated molecular weights of SpyCatcher and GST-SpyTag are 12kDa and 28kDa respectively. The isopeptide bonds between SpyCatcher and GST-SpyTag should give a protein of about 40kDa. In the lane 3 of Figure 3.10, it seems that the molecular weight of SpyCatcher is bigger than 15kDa, this poor migration could because of non-fresh running buffer, or the SpyCatcher was still in a stretched status so that it run slower. The lane 1 of Figure 3.10 has a band around 40kDa, which indicated that SpyCatcher and GST-SpyTag were able to form isopeptide bonds.

3.2.5 Reduction of thiol groups for subsequent chemical conjugation

Cysteines were used to react some of the proteins described above with maleimide activated chemicals. However, the sulfhydryl is easily oxidized in the daily storage or can form disulphide bonds (S-S). Dithiothreitol (DTT), β-mercaptoethanol (β-ME), and Tris(2-Carboxyethyl)-Phosphine Hydrochloride (TCEP·HCl or TCEP) are all common sulfhydryl protective reducing agents. TCEP·HCl is stronger and more stable than DTT and β-ME(Konigsberg 1972). On the other hand, both of DTT and β-ME contain sulfhydryl which might introduce extra reaction with maleimide, therefore, TCEP·HCl was used as the reducing reagent in this project. The incubation time and dose of TCEP·HCl, were investigated to determine optimal conditions.

The calculated molecular weights of SNAP25C1, SynaptobrevinC1 and SyntaxinC1 are 24.5kDa, 7.28kDa and 8.97kDa respectively, and all of them have one cysteine. The minimum molecular weight of protein marker (BioRad, Precision Plus Protein^{TM} Dual Color) is 10kDa

which is slightly larger than SynaptobrevinC1 and SyntaxinC1. It is difficult to observe accurate position of SynaptobrevinC1 and SyntaxinC1 based on protein marker. Hence SNAP25C1 rather than the other two was used to determine the reduction time (Figure 3.11) and amount of TCEP (Figure 3.12) by estimating the intensity of the band at the expected size, versus the one of dimers due to disulphide bonds formation.

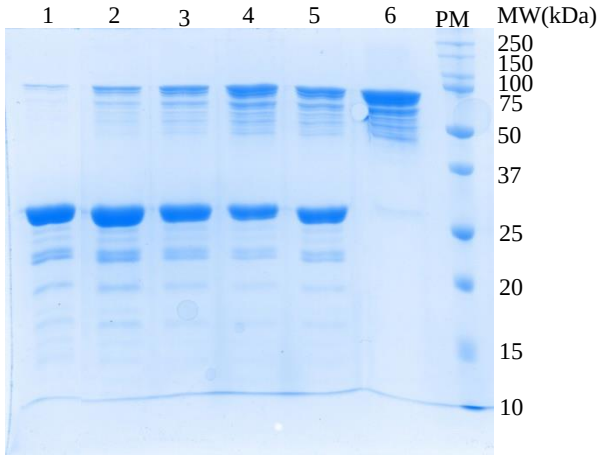

Figure 3. 11 ***Optimization of TCEP incubation time. The reduction lasted for 1. overnight, 2. 8 hours, 3. 5 hours, 4. 3 hours, 5. 1 hour, 6. 0 hour. PM is protein marker (BioRad, Precision Plus Protein™ Dual Color). 12% SDS-PAGE, 170V, 55 minutes. MW is molecular weight.***

In figure 3.11 the samples were prepared by SDS loading buffer without any reducing agent such as β-mercaptoethanol, therefore the disulfide bonds were only broken by 1mM TCEP was added prior to loading. Lane 6 shows non-reduced SNAP25C1, which is present only in the form of dimers (S-S bonds). Lane 1 shows the majority of SNAP25C1 was broken into monomers after overnight reduction by TCEP. Between 5 and 8 hours incubation, the majority of SNAP25C1 was reduced, but the reduction was not as good as overnight incubation. Between 1 and 3 hours reduction, approximately half SNAP25C1 was still dimerized. Therefore SNAP25C1, SynaptobrevinC1 and SyntaxinC1 were all reduced by TCEP overnight before performing the conjugation steps described below.

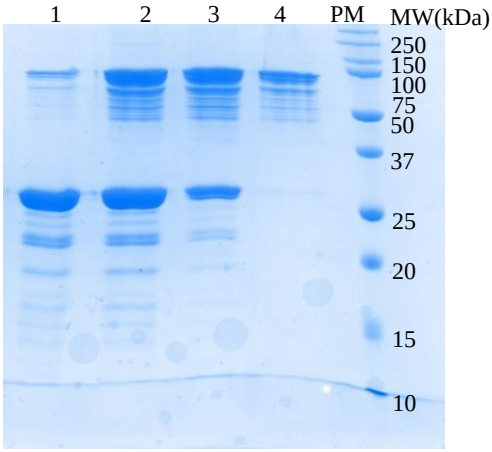

Figure 3. 12 ***Optimization of the amount of TCEP. The concentration of TCEP is 1. 1mM, 2. 0.5mM, 3. 0.1mM, 4. 0mM, PM is protein marker (BioRad, Precision Plus Protein™ Dual Color). 12% SDS-PAGE, 170V, 55 minutes, SDS loading buffer without β-mercaptoethanol. MW is molecular weight.***

SNAP25C1 was incubated overnight with different concentration of TCEP as shown in Figure 3.12. The majority of disulfide bonds were reduced by 1mM TCEP after an overnight incubation whereas lower concentrations of TCEP were not enough to reduce the disulfide bonds of SNAP25C1, therefore we used 1mM TCEP in subsequent experiments.

3.2.6 Cross-linking of SNARE Proteins

SNAREs were cross-linked to either maleimide-activated fluorophore Cy3 or BSA for gold nanoparticle assembly in section **3.5.** All the cysteine-containing proteins used in this section were reduced by 1mM TCEP overnight before the cross-linking reaction.

SNAP25C1 linked to maleimide-Cy3

Maleimide-Cy3 is a fluorescent molecule used for labelling proteins through maleimide at cysteine residues. In this project maleimide-Cy3 was combined with reduced SNAP25C1. Because of Cy3 fluorescence, the SDS-PAGE gel was imaged using UV illumination firstly (Figure 3.13A), and then it was stained by Instantblue (Figure 3.13B). The molecular weight of Cy3 is 791.0 Da, so that the difference of molecular weights between SNAP25C1 and SNAP25C1-Cy3 is negligible. Therefore, the bands around 25kDa (Figure 3.13) were considered compatible with both SNAP25C1-Cy3 and unconjugated SNAP25C1.

The synthesized SNAP25C1-Cy3 was purified by gel filtration to remove the excess maleimide-Cy3. SNAP25C1-Cy3 size is very close to SNAP25C1 so we were not able to separate them by gel filtration. With the aim to calculate the concentration of SNAP25C1-Cy3,

the absorbance of purified SNAP25C1-Cy3 was measured by Nanodrop (Thermo Scientific) from 250nm to 650nm. The absorbance value at 280nm and 550nm were 0.942 and 3.26 respectively. According to Equation 2.3 and 2.4, the concentration of SNAP25C1-Cy3 and SNAP25C1 were estimated as 20.5 μM and 24 μM respectively. Based on Equation 2.5, the concentration ratio of [Cy3]/[SNAP25C1] was calculated as 0.85, suggesting that 85% SNAP25C1 was labelled with Cy3.

SNAP25C1-Cy3 was incubated with SynaptobrevinC1 and SyntaxinC1 to confirm whether they were able to form a SNARE complex. The heated complex was disassembled and loaded as a control, hence, based on the protein marker, the bands around 25kDa and 10kDa of lane 2, Figure 3.13 were SNAP25C1-Cy3, SynaptobrevinC1 or SyntaxinC1. The non-heated complex (lane 3 of Figure 3.13) shown that the SNARE complex was visible under UV light and stained gel. However, the SynaptobrevinC1 or SyntaxinC1 might dimerize through disulphide bonds and dimers of SynaptobrevinC1 or SyntaxinC1 could form SNARE complexes, as evidenced by a double band near the size expected for the SNARE complex in lane 3, Figure 3.13.

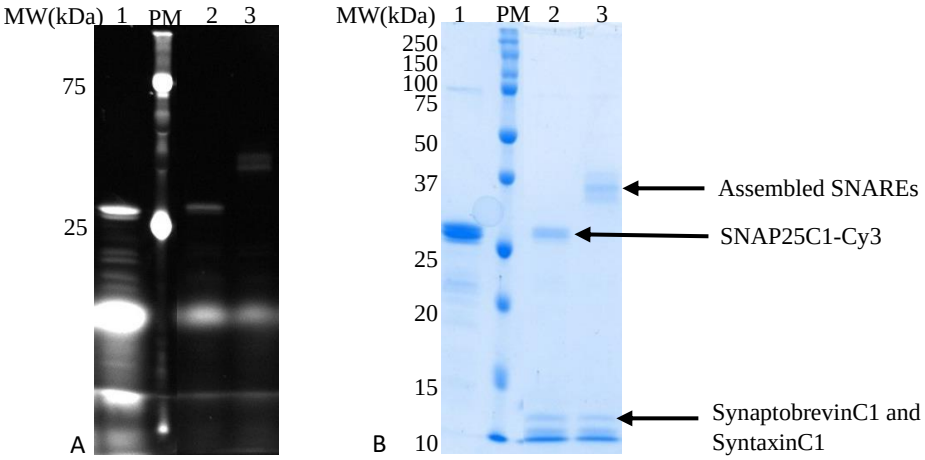

Figure 3. 13 ***SDS-PAGE of SNAP25C1-Cy3. (A) SDS-PAGE gel under UV light. (B) The same SDS-PAGE gel with A was stained with Instantblue. 1. SNAP25C1-Cy3 only 2. boiled complex: SNAP25C1-Cy3 assembled with Synaptobrevin -GSC and SyntaxinC1. 3:non-boiled complex. PM is the protein marker (BioRad, Precision Plus Protein^{TM} Dual Color). The molecular weight (MW) of fluorescent bonds (A) and protein marker (B) were labelled on the left.***

Figure 3.13 also suggests that SNAP25C1 was successfully linked to maleimide Cy3 as evidenced in lane 1 by the fluorescent band compatible with SNAP25 size. However, intense fluorescence at lower molecular weight suggests there is some excess of Cy3 that was not entirely removed after purification. As a consequence of this, we believe the conjugation efficiency is probably less than the estimated 85%.

Optimization of SNARE-BSA synthesis

SynaptobrevinC1 and SyntaxinC1 were combined with BSA through Sulfo-SMCC (sulfosuccininidyl 4-[N-maleimidomethyl]cyclohexane-1-carboxylate) which is a water soluble heterobifunctional crosslinker that contains N-hydroxysuccinimide (NHS) ester and maleimide groups that allow covalent conjugation of amine- and sulfhydryl- containing molecules(Lee and Hoover 1995). In this experiment, the first step was incubation of SynaptobrevinC1 or SyntaxinC1 with Sulfo-SMCC. Second, BSA was linked to activated SynaptobrevinC1 or SyntaxinC1. This reaction order was expected to achieve the right orientation of SNARE-BSA conjugates: BSA links to the C-terminal of SynaptobrevinC1 or SyntaxinC1. The C-terminal of SynaptobrevinC1 and SyntaxinC1 present one cysteine which is expected to react with the maleimide group of Sulfo-SMCC, whereas BSA was combined to activated SynaptobrevinC1 or SyntaxinC1 through NHS ester and one of the several amines. In this configuration, the N-terminal of SNAREs would be far apart from the BSA and the SNARE-BSA conjugates would possibly assemble into a SNARE complex, which in fact forms from the N-terminal of SNAREs to C-terminal (Fasshauer and Margittai 2004).

In order to find the best conditions to synthesize SNARE-BSA conjugates in the right orientation, the reaction of maleimide/sulfhydryl and NHS ester/amine were optimized independently, in terms of incubation time and amount of reactant. All the optimized conditions were listed in Table 3.2.

	optimization conditions			
Sulfo-SMCC concentration	**1mM**	5mM	10mM	
BSA concentration	10 μM	**30 μM**	40 μM	
NHS-ester incubation time	overnight	5 hours	**1 hour**	0.5 hour
maleimide incubation time	overnight	5 hours	1 hour	**0.5 hour**

Table 3. 2 ***The optimization conditions of SNARE-BSA conjugates. The best conditions were bold.***

Both SynapbrevinC1 and SyntaxinC1 were linked to BSA after activation in the same way, therefore, SyntaxinC1 was used as a model for optimization. Based on previous results (see section **3.2.5**), SyntaxinC1 was reduced by 1mM TCEP overnight before reacting with Sulfo-SMCC.

Although SyntaxinC1 was reduced by TCEP, sulfhydryl group could potentially oxidize again during Sulfo-SMCC reaction to form S-S bonds which would compete with maleimide reaction, and this would result in less SyntaxinC1-BSA conjugate. For this reason, maleimide reactions with or without TCEP were compared to assess whether it is essential to keep TCEP in reaction

or it is possible to remove it before the reaction. In both tests, TCEP was removed by desalting columns after the reaction between maleimide and cysteine happenes, at the same time of removal of Sulfo-SMCC excess. Therefore, there was no need to investigate whether TCEP might also affect the reaction between NHS ester and amine.

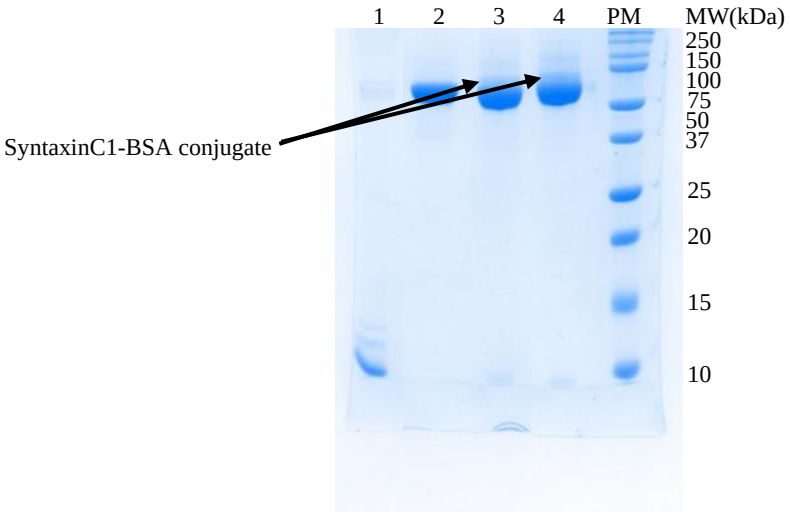

Figure 3. 14 ***Maleimide incubation with or without TCEP. 1. Reduced SyntaxinC1. 2. BSA. 3. SyntaxinC1-BSA (without TCEP). 4. SyntaxinC1-BSA (with TCEP). PM is Protein marker (BioRad, Precision Plus Protein^{TM} Dual Color). 12% SDS-PAGE, 170V, 55minutes. MW is molecular weight.***

SyntaxinC1-BSA conjugate is indicated by arrows in Figure 3.14. These are proteins with a molecular weight slightly above BSA and present at a lower concentration compared to unreacted BSA. Therefore they appear in the gel as a faint band slightly above BSA. Lane 3 (without TCEP) has slightly less conjugates than lane 4 (with TCEP), therefore, we concluded that it is beneficial, or at least not problematic, to keep TCEP in the maleimide reaction, which also removes one step from the conjugation flow-chart.

Sulfo-SMCC is a heterobifunctional crosslinker containing maleimide and NHS ester, and since SyntaxinC1 has one cysteine but several amine groups, it is potentially able to cross-link more than one Sulfo-SMCC molecule through reaction of maleimide/cysteine and amine/NHS-ester at the same time. Moreover, BSA has many amine groups that could be combined with several activated SyntaxinC1. Hence, the concentration of Sulfo-SMCC and BSA were optimized to avoid over-crosslinking. The results are shown in Figure 3.15 and Figure 3.16 respectively. Besides concentrations, also reaction times were carefully optimized. In fact, maleimide and NHS ester would be hydrolysed slowly in aqueous solution resulting in loss of reaction activity(Lee and Hoover 1995), therefore, the two parts of the crosslinker, maleimide

and NHS ester, should react before the hydrolytic degradation. The incubation time of each part of the crosslinking reaction was optimized and shown in Figure 3.17 and 3.18 respectively.

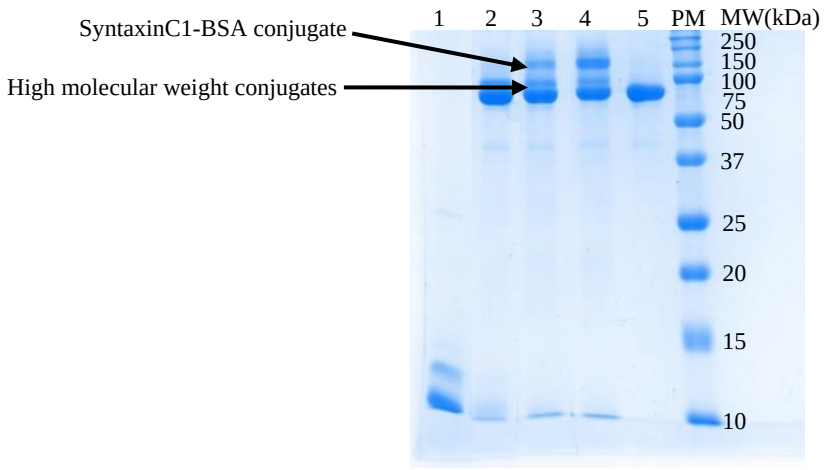

Figure 3. 15 ***Syntaxin-BSA was produced by different amount of Sulfo-SMCC. 1. Reduced SyntaxinC1. 2. SyntaxinC1-BSA (1mM Sulfo-SMCC). 3. SyntaxinC1-BSA (5mM Sulfo-SMCC). 4. SyntaxinC1-BSA (10mM Sulfo-SMCC). 5. BSA. PM is the Protein Marker (BioRad, Precision Plus Protein^{TM} Dual Color). 12% SDS-PAGE, 170V, 55minutes. MW is molecular weight.***

Figure 3.15 shows the optimization of Sulfo-SMCC concentration. 1mM Sulfo-SMCC reaction has the best yield of SyntaxinC1-BSA, whereas 5mM and 10mM Sulfo-SMCC reaction had less SyntaxinC1-BSA conjugates than 1mM and more high molecular weight conjugates. This is likely because the high concentration of Sulfo-SMCC yield over-crosslinking, consequently, one SyntaxinC1 was possibly combined with two BSA molecules thus originating the high molecular weight conjugates. The more Sulfo-SMCC added, the higher molecular weight conjugates were produced. From the results of figure 3.15 we determined that 1mM Sulfo-SMCC was the best concentration to be used in the crosslinking reaction.

Different concentrations of BSA (10 µM, 30 µM and 40 µM) were incubated with 30 µM SyntaxinC1-SMCC to find the best reaction conditions. In figure 3.16, 10 µM BSA reaction gave the least SyntaxinC1- BSA conjugates. 30 µM BSA and 40 µM BSA have nearly the same amount of SyntaxinC1- BSA conjugates. However, there are several high molecular weight conjugates in the 40 µM BSA reaction, possibly due to the over-crosslink between BSA and activated SyntaxinC1. We concluded that 30 µM BSA was the best compromise to be used in the reaction.

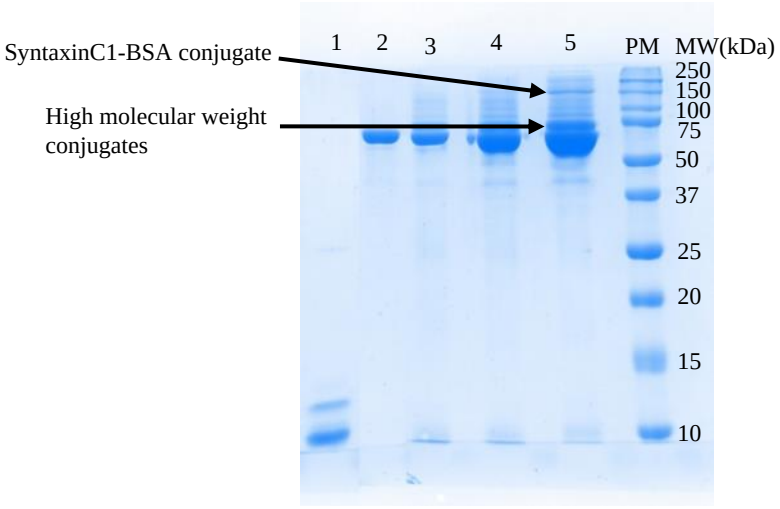

Figure 3. 16 ***Optimization of different amount of BSA. Lane 1. Reduced SyntaxinC1, lane 2. BSA, lane 3. 10mM BSA incubation, lane 4. 30mM BSA incubation, lane 5. 40mM BSA incubation. PM is the protein marker (BioRad, Precision Plus Protein^{TM} Dual Color). 12% SDS-PAGE, 170V, 55minutes. MW is molecular weight.***

Figure 3.17 shows the optimization of incubation time for SyntaxinC1 and Sulfo-SMCC reaction. 1 hour incubation and 5 hours incubation resulted in the same amount of conjugates, which is larger than the amount at 0.5 hour. The overnight incubation has the least amount, this is likely because Sulfo-SMCC have been hydrolyzed in aqueous buffer during overnight incubation. Therefore, 1 hour incubation was considered long enough for linking Sulfo-SMCC and SyntaxinC1.

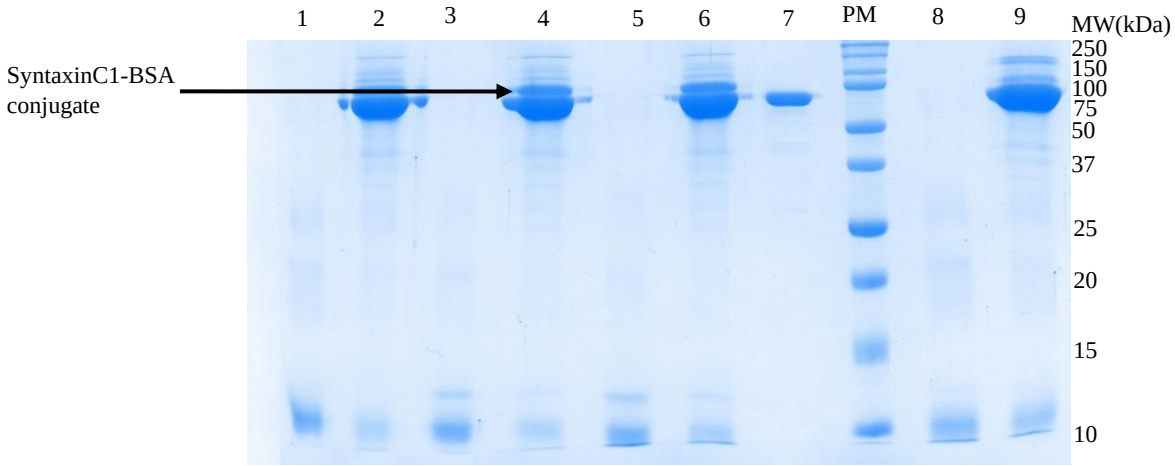

Figure 3. 17 ***Optimisation of the incubation time of the maleimide reaction. Lanes 1, 3, 5 and 8 are SyntaxinC1-Sulfo-SMCC which have been incubated for 0.5 hour, 1 hour, 5 hours and overnight respectively. Lanes 2, 4, 6 and 9 are SyntaxinC1-BSA conjugates made from lane 1, 3, 5 and 8 respectively. Lane 7 is BSA only. PM is the protein marker (BioRad, Precision Plus ProteinTM Dual Color). 12% SDS-PAGE, 170V, 55minutes. The molecular weight (MW) of protein marker was labelled on the right.***

Figure 3.18 shows the optimization of incubation time between activated SyntaxinC1 and BSA. The amount of conjugates is the same at different incubation times. It indicates that reaction

between SyntaxinC1-Sulfo-SMCC and BSA is very quick and efficient. Therefore we considered 0.5 hour incubation sufficient for the following experiments.

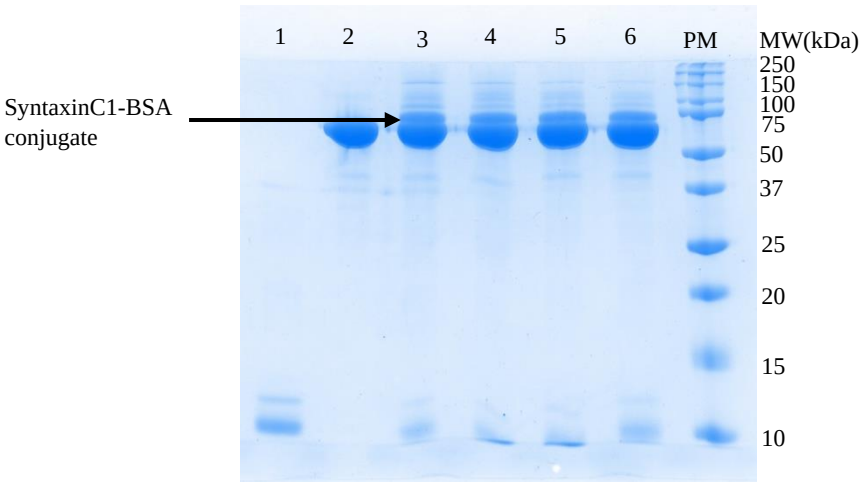

Figure 3. 18 ***Optimization of incubation time for NHS ester reaction. Lane 1. Reduced SyntaxinC, lane 2. BSA only, lane 3, lane 4, lane 5 and lane 6 are 0.5 hour, 1 hour, 5 hours and overnight incubation respectively, PM is protein marker(BioRad, Precision Plus Protein^{TM} Dual Color). 12% SDS-PAGE, 170V, 55minutes. MW is molecular weight.***

In summary, the best conditions for synthesizing BSA-SNARE conjugates were: 50 µM of SyntaxinC1 (or SynaptobrevinC1) mixed with 1mM Sulfo-SMCC for 1 hour incubation at room temperature. The excess Sulfo-SMCC was then removed by Zeba desalting columns. 30 µM of the mixture was then added to 30 µM BSA for 0.5 hour incubation at room temperature. In this condition, the reaction achieved the highest yield.

We then verified whether the crosslinking of SyntaxinC1 to BSA by Sulfo-SMCC was happening in the desired orientation, which is maleimide reaction with the cysteine on the C-terminal of SNAREs first and then NHS on any amino group of BSA. As it was described in the introduction, the quaternary structure of SNARE complex is formed from the N-terminal to C-terminal of SNARE proteins. Both for SynaptobrevinC1 and SyntaxinC1 the cysteine is at the end of C-terminal that was intended to link to BSA. The reason of this design is that we want to assemble together Syntaxin-BSA and Synaptobrevin-BSA in presence of SNAP25C1-Cy3 (see section **3.5**) and this would be facilitated if the BSA is at the C-terminal of the SNAREs, as this wouldn't interfere with the priming of the assembly.

The crosslinking reaction was performed at pH7.2 which is suitable for both NHS-ester and maleimide reaction. BSA has an active Cysteine (Cys-34) which is available to link to the maleimide group of Sulfo-SMCC. Therefore, the N-terminal amine groups of SynaptobrevinC1 or SyntaxinC1 could link to BSA through Sulfo-SMCC in the wrong orientation. In this

configuration, the SNARE-BSA might not be able to form SNARE complex because of steric hindrance.

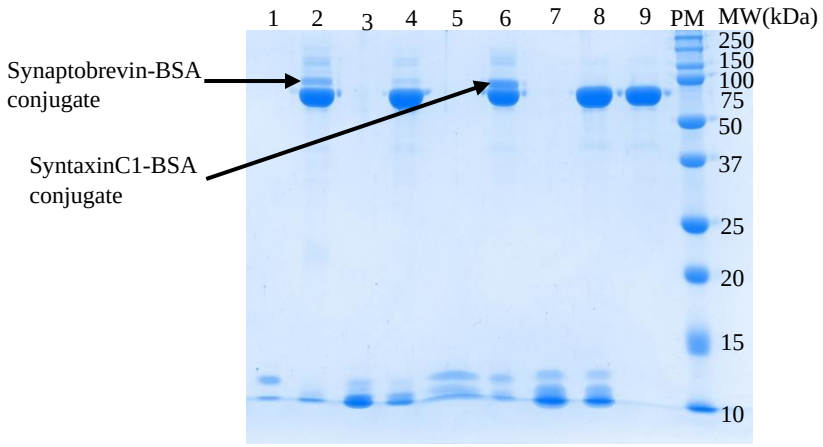

Figure 3. 19 ***The orientation of SNARE-BSA conjugates. 1. SynaptobrevinC1-Sulfo-SMCC. 2. SynaptobrevinC1-BSA. 3. Synaptobrevin-Sulfo-SMCC. 4. Synaptobrevin-BSA. 5. SyntaxinC1-Sulfo-SMCC. 6. SyntaxinC1-BSA. 7. Syntaxin-Sulfo-SMCC. 8. Syntaxin-BSA. 9. BSA. PM is the protein marke(BioRad, Precision Plus ProteinTM Dual Color)r. 12% SDS-PAGE, 170V, 55minutes. MW is molecular weight.***

We performed the conjugation to BSA using Synaptobrevin and Syntaxin without the cysteine residues and compared with the ones with a single cysteine. Lane 4 and lane 8 (Synaptobrevin and Syntaxin without SH groups) of Figure 3.19 show that there is a negligible (if any) amount of Synaptobrevin-BSA and Syntaxin-BSA compared to lanes 2 and 6. These results suggest that the amount of SNARE-BSA conjugates obtained by cross-linking of the NHS moiety to SNARE's amino groups is negligible compared to the maleimide-SH reactivity.

Also, it is known that a reaction between amine and maleimide can happen, but it is much slower than the reaction between sulfhydryl and maleimide, and it generally happens only at very high concentration of maleimide (100mM)(Phelps, Enemchukwu et al. 2012). This experiment, also confirms that this is unlikely to happen in our conditions as the synthesized SynaptobrevinC1-BSA and SyntaxinC1-BSA in lane 2 and lane 6 of Figure 3.19 show that the reaction between sulfhydryl and maleimide is quicker than NHS-ester and amine. In conclusion, we can say that SNARE-BSA conjugates were most likely assembled in the desired orientation, and could be therefore expected to be usable in subsequent assembly reactions (see section **3.5**).

3.3 Adsorption of protein on gold nanoparticles

Protein-GNPs conjugates are commonly used for biological applications, such as biosensor design, drug delivery and cancer therapy. Due to these promising applications based on the immobilization of proteins on to GNPs, many investigations have been reported on understanding the mechanism of protein adsorption on GNPs. However, the studies on the mechanism are still not comprehensive. In this section, the role of electrostatic interaction in GNPs/proteins adsorption was investigated by taking GST as an example. Also, a comparison of the adsorption of GNPs/GST with GNPs/NEM-GST was done to understand the role of thiols on GNPs/proteins interaction. We also demonstrated that proteins fused to GST are still able to accomplish their function after adsorption: GST-SNAP25 on GNPs could form a SNARE complex with Nanolock, and GST-SpyCatcher on GNPs could form isopeptide bonds with GST-SpyTag. These two binary protein systems could be potentially used to decorate and assemble GNPs in a highly modular way, which is the overarching theme of this work.

3.3.1 Equilibrium binding of GST to GNPs

The equilibrium binding of GST to GNPs was measured at different pH values (6.0, 6.5, 7.3, and 8.0) using dynamic light scattering (DLS) to investigate the effect of electrostatic force in GST-GNPs interaction. The affinity of binding was described in terms of affinity dissociation constant (K_D) and the maximum increase of particle hydrodynamic diameter (Δd_{MAX}) at high concentration of GST. This also gives an estimate of the maximum size of monolayer which formed on the surface of GNPs. Figure 3.20 A-D show plots of particle size increase (Δd) versus concentration of GST, drawn based on DLS measurements.

DLS data were fit to Equation 1.6 using nonlinear least-squares, and K_D and Δd_{MAX} were calculated. Figure 3.20 E shows the K_D and Δd_{MAX} at the four pH values. pH mildly affected the binding affinity of GST to GNPs. The binding has the highest Δd_{MAX} at pH6.5 (10.2nm), while at this pH, it has the lowest K_D (0.053 µM) suggesting that this is the pH, among those tested, at which GST binds more effectively. Opposite to this, at pH8.0, Δd_{MAX} has the lowest value (7.5nm) and the highest K_D (0.078 µM). This is likely due to better binding at pH close to the isoelectric point of the protein (pI of GST is 6.65 as calculated using bioinformatics tools available at http://web.expasy.org/protparam/) which minimizes the number of charges on the

protein and probably helps orientation and binding. This is discussed more in depth in section **3.3.3**.

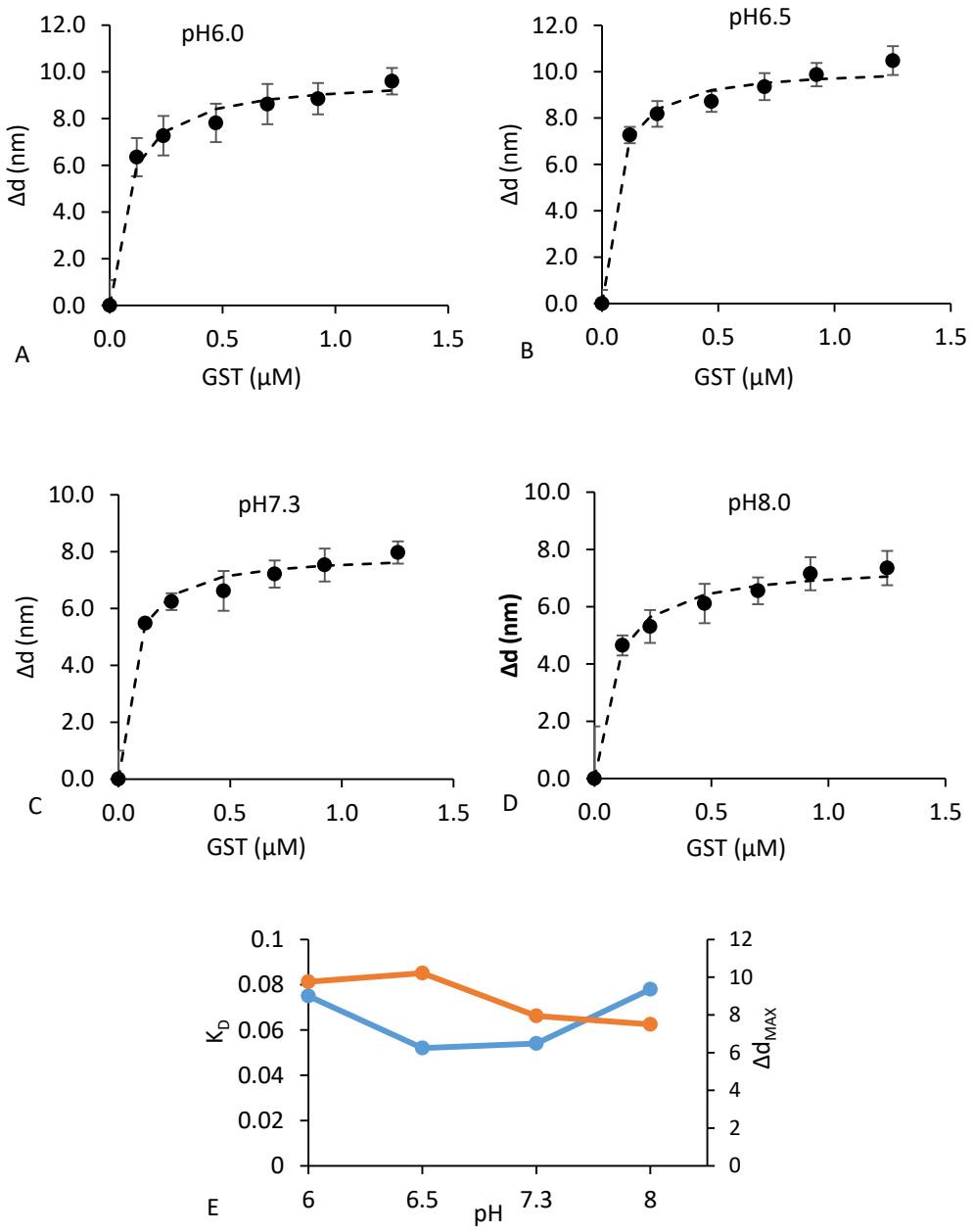

Figure 3. 20 ***DLS measurements of equilibrium binding of GST to GNPs. The data was fitted to the Hill equation at different values. (A) pH6.0. (B) pH6.5. (C) pH7.3. (D) pH8.0. Data points (black dots) are the average values of three replicate measurements fitted (dash line) to the Hill equation. The error bars represent the standard deviation of the three replicates. (E) K_D (blue line) and Δd_{MAX} (orange line) were calculated from Equation 1.6. The lowest K_D value corresponds to the best affinity binding of GST to GNPs. The largest Δd_{MAX} corresponds to the maximum amount of GST adsorbed to GNPs.***

3.3.2 Mapping surface charges on GST

The pH affects the distribution of charges on GST surface, furthermore, the charge may affect the affinity binding of GST to GNPs. Adaptive Poisson-Boltzmann Solver (APBS)(Konecny, Baker et al. 2012) was used to map the electrostatic surface potential of GST. The calculated potential was presented in different colours, blue is positive, and red is negative. In Figure 3.21, panels A, B, C and D show that pH6.0 and pH6.5 have excess of positive potential, while pH7.3 and pH8.0 have net negative potential. This is consistent with the calculated pI of 6.65 (http://web.expasy.org/protparam/), so net charges of GST at pH6.0 and pH6.5 below pI were positive whereas pH7.3 and pH8.0are above pI and therefore negative.

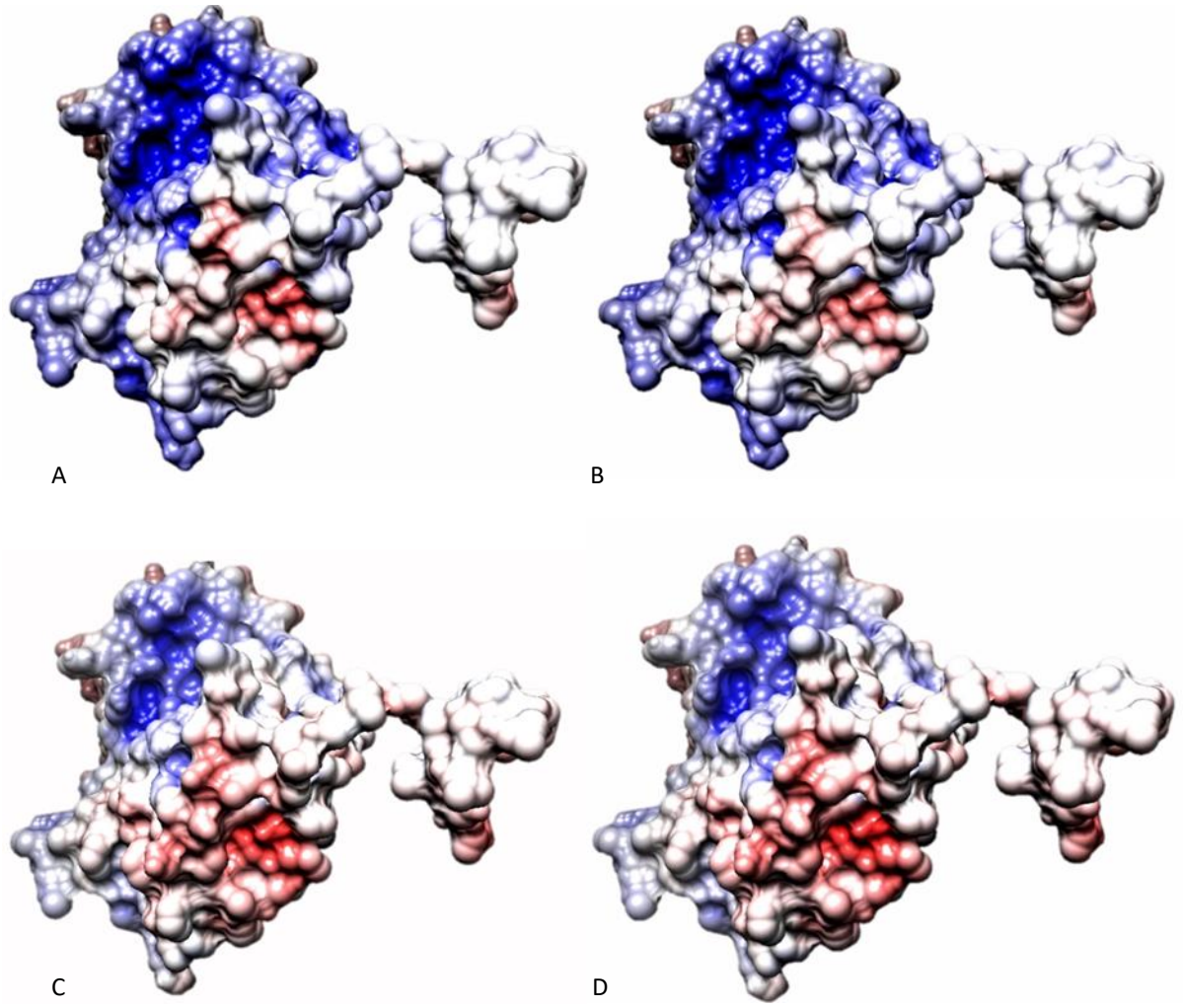

Figure 3. 21 ***Electrostatic surface potential distribution of GST (the protein data bank ID of GST is 1UA5) calculated using APBS and displayed by Chimera(Vitozzi, Lapierre et al. 2002) at (A) pH6.0, (B) pH6.5, (C) pH7.3, (D) pH8.0. The blue indicates positive surface potential and the red represents negative surface potential.***

GNPs surface has net negative charges due to citrate capping, likely contributing to GST adsorption onto GNPs by electrostatic force. Therefore, it can be deduced that GST with net

positive charges has higher affinity binding, which gives low K_D value and high Δd_{MAX}. Figure 3.21 showed that pH6.5 gives the lowest K_D (0.053µM) and highest Δd_{MAX} (10.218nm). At pH8.0, GST has maximum net negative charges tested and showed highest K_D (0.078µM) and lowest Δd_{MAX} (7.493nm). However, there were different observations at pH6.0 and pH7.3. At pH6.0, it was expected the most positive charge would give the lowest K_D and the highest Δd_{MAX}. However, at pH6.0 the K_D (0.075µM) is higher than pH6.5 (0.053µM) and pH7.3 (0.054µM). At pH7.3, the K_D (0.054µM) has the similar low level to pH6.5 (0.053µM). From the images of figure 3.21, the net positive charged GST (at pH6.0 and pH6.5) also has negative potential parts. The higher K_D at pH6.0 (0.075µM) suggests that there are persistent negative charged parts of GST that result in low binding affinity, While, positively charged parts at pH7.3 still contribute to good binding, consequently, the K_D (0.054µM) at pH7.3 was higher than expected based on net charge only. This is an indication that the distribution of the charges might be as important as the net charge. Nevertheless, the Δd_{MAX} at pH7.3 (7.945nm) is as low as pH8.0 (7.493nm) which suggests that there was a lower amount of GST adsorbed to GNPs. At pH6.0, although K_D is high, the Δd_{MAX} is up to 9.8nm. Conclusively, the affinity of electrostatic binding of GST to GNPs is described by both K_D and $\Delta d_{MAX,}$ and the binding seems more efficient at pH close to the pI. It is worth noting that the residues of GST directly adsorbed to GNPs surface do not necessarily have the same charge of the overall charge of GST, suggesting that the distribution of charges is important and would be worth exploring, for example using molecular dynamics simulations.

3.3.3 Zeta-potential measurement of GNPs-GST conjugates

The electrostatic surface potential mapping describes the charge distribution of GST at different pH values (pH6.0, pH6.5, pH7.3 and pH8.0). Based on charge distribution, we evaluated the effect of electrostatic force on equilibrium binding of GST to GNPs. However, this was not a direct evidence of the charge of GNPs-GST conjugates. The overall electrostatic potential of GNPs-GST conjugates at different pH values (pH6.0, pH6.5, pH7.3 and pH8.0) was measured by Zeta-potential. Figure 3.22 shows that both GNPs-GST conjugates and naked GNPs were negatively charged. The conjugates made at pH6.0 were the least negatively charged (-19.18mV), followed by pH6.5 (-23.55mV), then pH7.3 (-33.40mV), and pH8.0 had the highest negative charge (-39.28mV). However, the surface charges of GNPs-GST at any pH was less negative than the charges of GNPs only (approximately -40mV). The surface

charges of GNPs-GST at pH8.0 (-38.28mV) were nearly the same of naked GNPs (approximately -40mV).

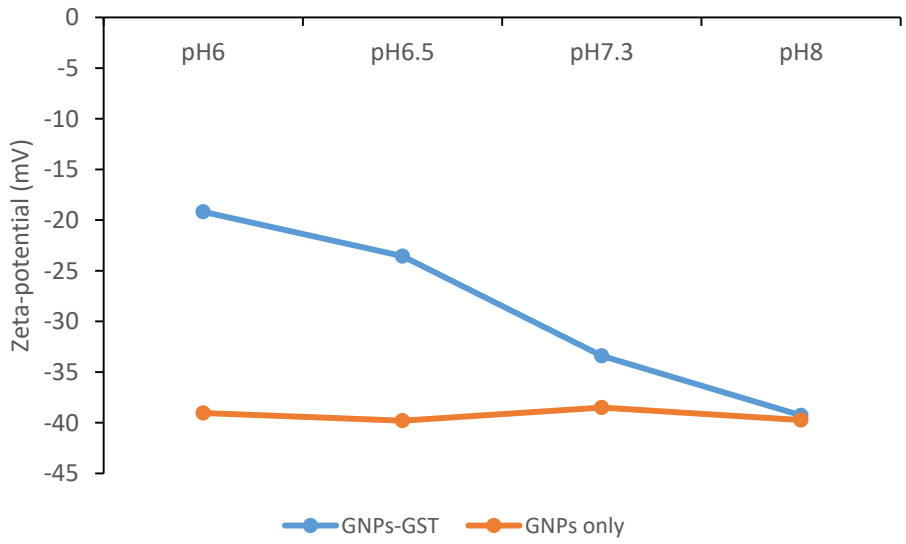

Figure 3. 22 ***Zeta-potential of GNPs-GST (blue) and GNPs only (orange) at different pH values (pH6.0, pH6.5, pH7.3 and pH8.0).***

The Zeta-potential data suggest that pH6.0 and pH6.5, which are below pI (6.65) and therefore positive charged, did counteract the negative charge from the surface of GNPs, but only partially. Moreover, the pH7.3 and pH8.0, which are above pI (6.65), only have a few of positive charges which result in negligible compensation of the negative charges of GNPs only, which are highly negative charged (low potential of the orange lane across all pH). These findings further explain the conclusion that GNPs-GST conjugates at pH6.5 have best affinity and most strong binding likely due to less electrostatic repulsion existing between GST and GNPs. By contrast, at pH8.0, the electrostatic repulsion that exist between GST and GNPs likely led to weaker binding.

The lowest K_D (0.053μM) and highest Δd_{MAX} (10.218nm) were found at pH6.5 likely as this is very close to the pI of GST (6.65), GST has an almost neutral overall charge which generates the lowest electrostatic repulsion between GST and GST-GNPs surface causing the strongest binding.

3.3.4 Binding kinetics of GST to GNPs

Based on the mapping of surface charges and measurements of Zeta-potential, it was concluded that the binding between GST and GNPs was driven by electrostatic interactions. However, these findings did not provide any information on rates of GNPs/GST binding.

In order to study this, the increased in size of GNPs-GST was measured at different time by DLS at the optimum pH6.5 and at different concentrations of GST (0.02 µM, 0.05 µM, 0.1 µM, 0.2 µM and 0.5 µM).

In Figure 3.23 (A- E) size increase (Δd) data versus time were plotted. The increase in size (black dots) was fitted to Equation 1.8 (dash line) and the kinetic constant of GST ($K_{[GST]}$) at different concentrations was calculated. The maximum Δd obtained at each concentration was also plotted versus the concentration of GST in Figure 3.23 (F) and the data fit to Hill equation as discussed above to confirm equilibrium binding data obtained previously. The resulting calculated K_D (dissociation constant) was 0.056 µM which is very close to the K_D (0.053 µM) of Figure 3.20 (B) obtained by equilibrium binding studies. However, based on Figure 3.23 (F), Δd_{MAX} was 7.6nm which is about 3nm less than the Δd_{MAX} of Figure 3.20 (B). The difference maybe from the different concentration range tested here which may give a less accurate estimate of the size at saturating concentration. In fact, in Figure 3.20 (B), the highest concentration of GST was 1.25 µM, whereas the highest GST concentration of Figure 3.23 (F) was only 0.5 µM. which might lead to inaccuracy while determining the Δd_{MAX} parameter, as the saturation of adsorption between GNPs and GST can be reached at concentrations higher than 0.5 µM. Nevertheless, the affinity and the reaction rate of the adsorption are not affected by concentration range.

Based on the measurements of Figure A-D, the $K_{[GST]}$ was plotted versus concentrations of GST in Figure 3.23 (G). The dataset in Figure E did not contribute to the calculation of $K_{[GST]}$ calculation as the association step has only few points, due to the fast adsorption at this concentration. According to Equation 2.6, Figure 3.23 (G) indicates that the association constant (K_{on}) of GST adsorption on GNPs was 0.0257 M^{-1} s^{-1}, and the dissociation constant (K_{off}) of the adsorption was 0.0023 s^{-1}.

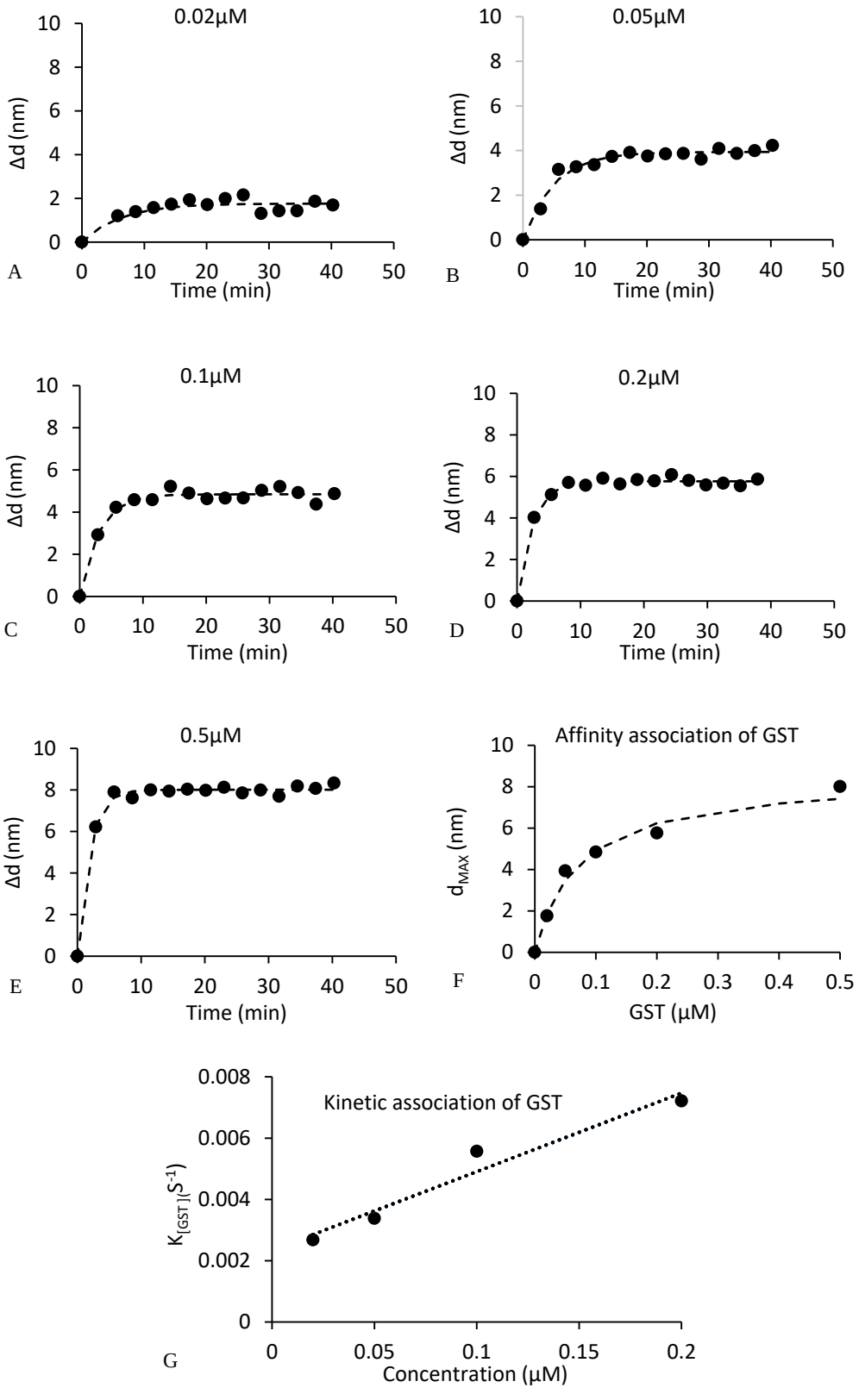

Figure 3. 23 ***GST binding kinetic (A-E). The increased size (∆d) was plotted against time at different concentration of GST from 0.02µM to 0.5µM. ∆d (black dots) was fitted (dash line) to Equation 1.8. (F) ∆d (black dots) was plotted against concentration and was fitted (dot line) to Equation1.6. The K_D and Δd_{MAX} were calculated as 0.056µM and 7.639nm. (G) $K_{[GST]}$ (black dots) was calculated from Figure 3.24(A-D) data and was fitted by Equation 2.6 (dot line). The equation of the linear trendline (y=0.0257x+0.0023) indicates that the K_{on} of the adsorption of GST to GNPs is 0.0257M^{-1} S^{-1}, and the K_{off} of the adsorption is 0.0023S^{-1}.***

3.3.5 Binding kinetics of NEM-GST to GNPs

It is known that gold and thiol can form Au-S covalent bond(Hurst, Lytton-Jean et al. 2006). Each GST protein molecule has 4 cysteines (each cysteine has one sulphydric group) that could bind to GNPs though Au-S covalent bonds. Therefore, GST might be able to bind to GNPs by physisorption (electrostatic force) as well as chemisorption (Au-S covalent bonds). In order to study the contribution of chemisorption between GNPs and GST, the sulphur groups of GST were blocked by *N*- Ethylmaleimide (NEM).

The availability of unreacted thiol groups of NEM-GST was quantified by Ellman's Reagent comparing its reactivity to a standard curve (Figure 3.24) obtained with L-cysteine, the adsorption was measured by UV-vis at 412nm.

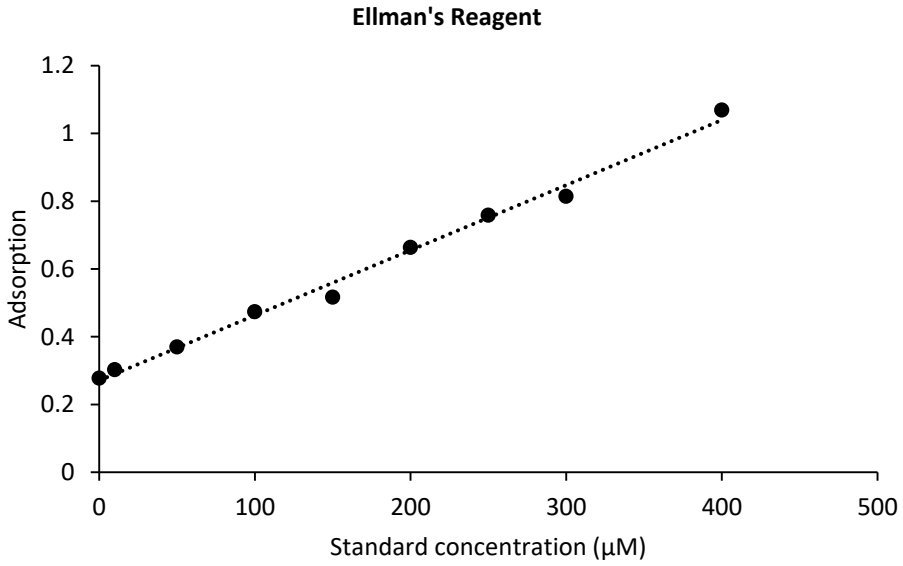

Figure 3. 24 ***The standard curve of Ellman's reagent. The adsorption value was fitted by linear trendline (the dot line, y=0.0019x+0.2712, R2=0.9925).***

The concentration of GST before and after NEM-blocking were measured by Nanodrop and were found to be 30.4 µM and 30.06 µM respectively. This indicated that GST was not lost during desalting to remove the excess NEM. The adsorption at Ellman's reagent wavelength of NEM-GST and GST were 0.2534 and 0.5098 respectively. Based on the standard curve (Figure 3.24), no thiol groups were available in NEM-GST, whereas the estimated thiol concentration of GST was 125.6 µM. Since each GST protein has 4 cysteines, this value would account for a GST concentration of 31.4 µM, which was very close to the Nanodrop-measured value of 30.4 µM.

The NEM-blocked GST (NEM-GST) was adsorbed onto GNPs at different concentration (0.02 µM, 0.05 µM, 0.1 µM, 0.2 µM and 0.5 µM) at pH6.5 and the increase in size of GNPs/NEM-GST conjugates were measured by DLS at different times, like in the previous section for unblocked GST. GNPs/NEM-GST binding data were plotted in Figure 3.25 (A-E). The increased sizes (black dots) were fitted to Equation 1.8 (dash line). K of NEM-GST at different concentration (0.02 µM, 0.05 µM, 0.1 µM, 0.2 µM and 0.5 µM) was calculated by Equation 1.8 and K_D (0.050µM) and Δd_{MAX} (6.2nm) of the adsorption between GNPs and NEM-GST were calculated from Figure 3.25 (F). K_D (0.050 µM) of GNPs/NEM-GST is slightly lower than K_D (0.056 µM) of GNPs/GST. Nevertheless, it could be considered close enough to conclude that SH groups do not contribute substantially to the binding affinity. The blocked cysteines on NEM-GST are not supposed to change the pI value or charge distribution either, as cysteines are hardly ionized at pH6.5 so a study of affinity at different pH was considered unnecessary. Δd_{MAX} (6.2nm) of GNPs/NEM-GST is 1.5nm less than Δd_{MAX} (7.6nm) of GNPs/GST which might be just due to an insufficient range of concentrations to determine this accurately.

In order to calculate the rate constant K consistently, the $K_{[NEM\text{-}GST]}$ was plotted against concentrations of NEM-GST (Figure 3.25 (G) according to Figure A-D. The fit of Figure 3.25 (G) indicates that the K_{on} of the adsorption between GNPs and NEM-GST was 0.0077 $M^{-1} \cdot S^{-1}$, and the K_{off} of the adsorption was 0.003 S^{-1}. K_{on} of GNPs/NEM-GST is lower than GNPs/GST and K_{off} of is only slightly lower. The results of K_{on} and K_{off} suggest that GST have a better binding rate to GNPs, therefore we can conclude that cysteines may play an important role in determining the binding rate or the binding affinity.

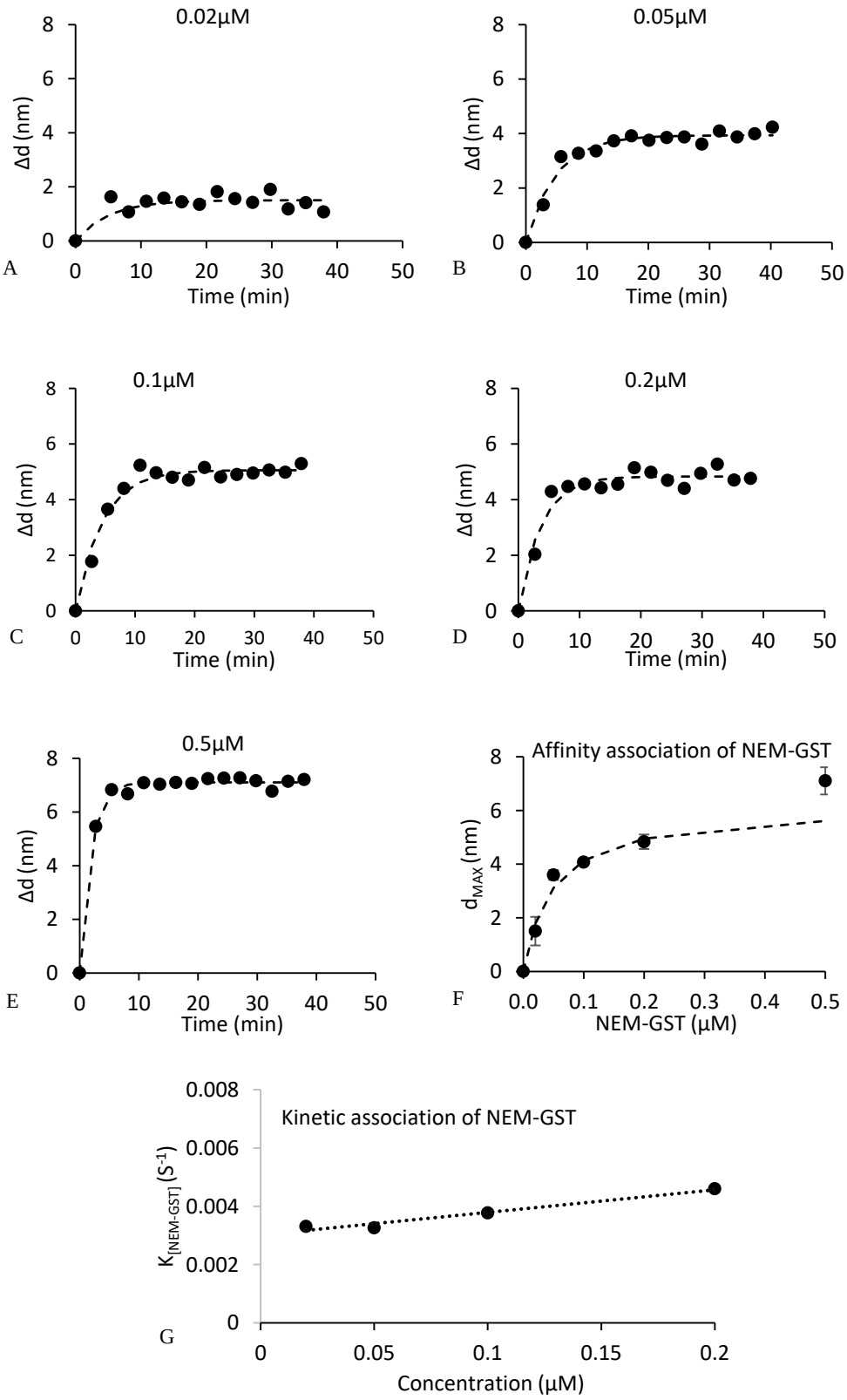

Figure 3. 25 ***NEM-GST binding kinetic (A-E). The increased size (Δd) against time was plotted at different concentration (0.02µM, 0.05 µM, 0.1 µM, 0.2 µM and 0.5 µM) of NEM-GST. The Δd (black dots) was fitted (dash line) to Equation 1.8. Δd (black dots) against concentration of NEM-GST was plotted (F) and was fitted (dash line) to Equation 1.6. The K_D and Δd_{MAX} of NEM-GST were calculated as 0.050µM and 6.161nm. (G) $K_{[NEM-GST]}$ (black dots)was calculated from Figure 3.26 (A-D) and was fitted to Equation 2.6 (dot line, y=0.0077x+0.003). The equation of (G) suggested that the Kon of NEM-GST is 0.0077M^{-1} S^{-1}, and the K_{off} is 0.003S^{-1}.***

3.3.6 Displacement of GST from gold nanoparticles by β-Mercaptoethanol

The comparison of K_D and K of GST and NEM-GST showed that the sulphydric groups do not contribute to the affinity or binding rate. However, the thiols might play a role in enhancing the long-term stability of binding between protein and GNPs as suggested in(Rosi, Giljohann et al. 2006) We observed that GNPs precipitate in presence of thiol reagent (Figure 3.26), such as dithiothreitol (DTT) and β-Mercaptoethanol (β-ME), unless the GNPs are covered with proteins through chemisorption (Au-S bonds) that prevent thiols' binding. GST is potentially able to bind to GNPs through thiols in the cysteine residues to form Au-S covalent bonds. By contrast, NEM-GST has no thiol available, so the only option for binding is physisorption (electrostatic interaction). Our hypothesis is that NEM-GST adsorbed onto GNPs could be displaced by β-ME and result in GNPs precipitation whereas GST could bind covalently and prevent particles precipitation.

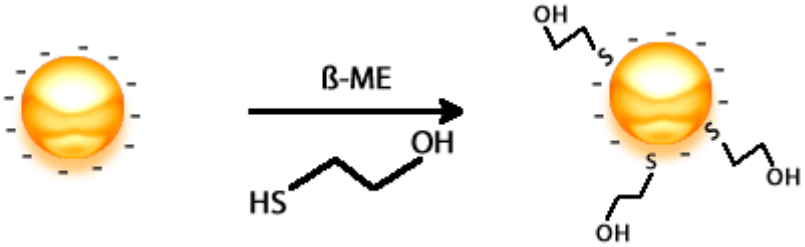

Figure 3. 26 ***GNPs tend to precipitate in the presence of β-Mercaptoethanol (β-ME).***

GST and NEM-GST were incubated with GNPs for different times and β-ME was added to GNPs/GST and GNPs/NEM-GST conjugates after the set time for an extra 20 minutes incubation. Then the absorbance at the Surface Plasmon Resonance (SPR) peak of GNPs/GST and GNPs/NEM-GST conjugates was measured. The size of GNPs/GST and GNPs/NEM-GST is about 47nm (Figure 3.20) which corresponds to a SPR peak around 530nm. The adsorption ratio of 530nm to 600nm ($Ab_{530nm/600nm}$) was used to indicate the stability of the colloid, as an increase of the absorbance at 600nm is observed following aggregation. In Figure 3.27 (A), GNPs/GST conjugates incubated for 0 min and 2mins had a low ratio value, which indicates that GNPs were completely aggregated. 5mins and 10mins incubation had higher values, indicating partial protein coverage, and therefore less aggregation. GNPs/GST incubated longer than 20mins showed peaks at 530nm and flat adsorption between 600nm-700nm, indicating that GNPs/GST conjugates were stable in the presence of 0.2mM β-ME but only after more than 20 minutes incubation.

We observed $Ab_{530nm/600nm} \approx 1$ for aggregated GNPs, whereas stable GNPs have $Ab_{530nm/600nm} \geq 2$. In Figure 3.27 (B), $Ab_{530nm/600nm}$ was plotted versus time of GST adsorption and the graph shows that GST needs 20min at least to bind covalently on GNPs surface thorough Au-S bonds. This experiment was conducted with 1.5 µM GST which is a concentration higher than the one used in adsorption rate estimation. According to the Kon calculated above the adsorption at this concentration should happen within the very few initial minutes but it is clear that the covalent binding takes longer, suggesting some rearrangement on the surface might be involved.

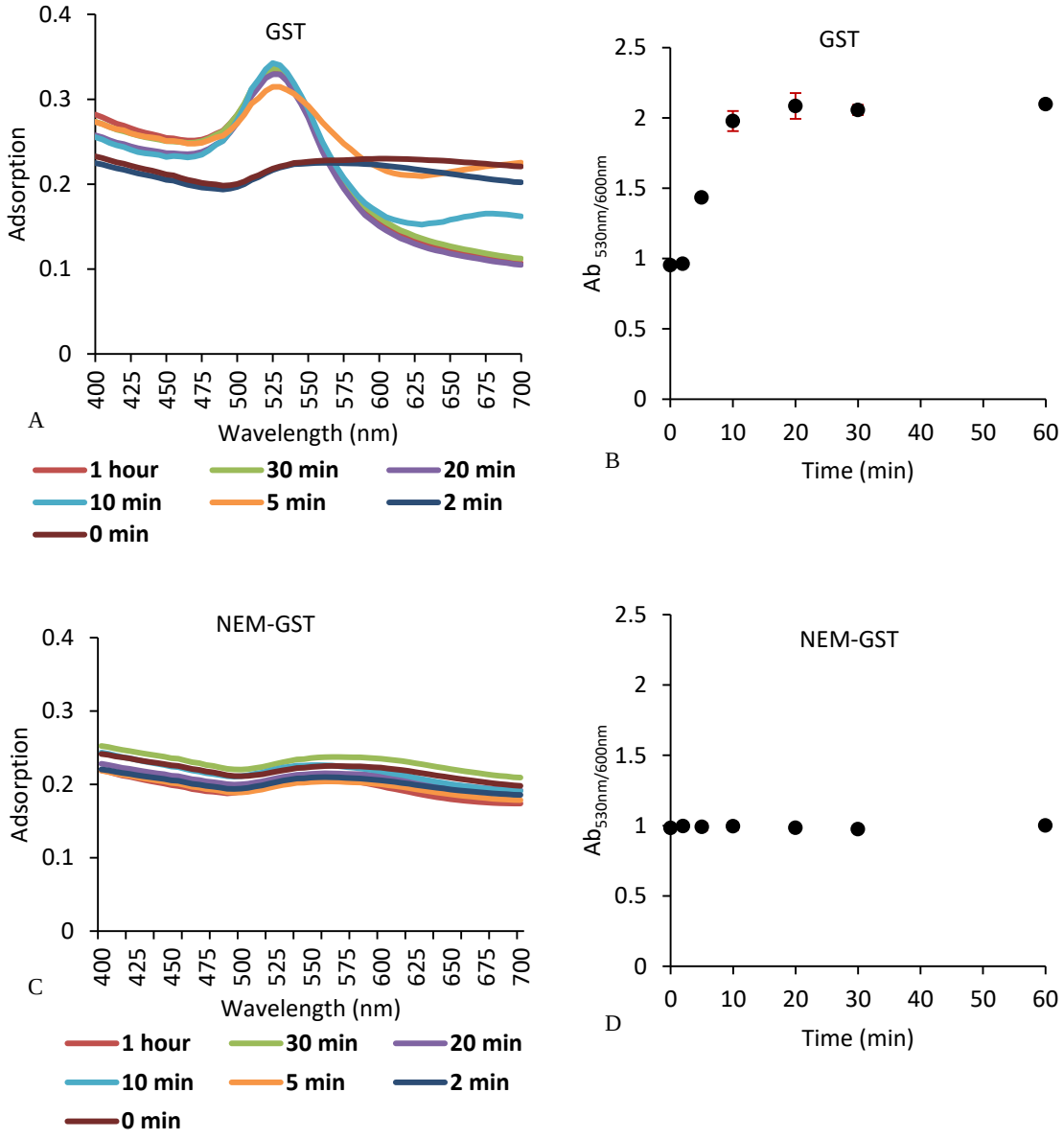

Figure 3. 27 ***Displacement of GST and NEM-GST by 0.2mM β-Mercaptoethanol (β-ME). (A, C). GNPs were incubated with GST or NEM-GST for different time, 0.2m β-ME was added to GNPs protein conjugates at the end of incubation the colloids were measured by UV-vis. (B) and (D) show the adsorption ratio of GST and NEM-GST colloids respectively.***

Figure 3.27 (C), and Figure 3.27 (D) represent the same experiment of Figure 3.27 (A-B) but performed using NEM-GST instead, and they shows disappearance of the SPR peak at any time, with $Ab_{530nm/600nm}$ ratios around 1. Figure 3.27 (C) and (D) suggest that NEM-GST was replaced by β-ME regardless of the incubation time, which indicates physisorption rather than chemisorption. The β-Mercaptoethanol assay showed that thiols are implicated in the long-term stable binding on GNPs surface.

Combining the conclusions of affinity binding, kinetics and β-Mercaptoethanol measurements, our data suggest that GST is adsorbed to GNPs in two steps. First, electrostatic force brings GST close to GNPs surface, the charge of GST dominates the binding rate and affinity. K_D and Δd_{MAX} values obtained at different pH showed that GST has higher binding to GNPs surface by less electrostatic repulsion. Also, the Zeta potential measurement are in agreement with the pH. The second step happens between thiols and gold. The thiols need a longer time, in the order of 20min to approach the GNPs surface (Figure 3.27(A) and (B)). This is because cysteine residues of GST might be initially away from the surface, therefore, the interaction between cysteine and GNPs could only occur after GST is close to GNPs surface due to electrostatic interaction.

3.3.7 Equilibrium binding of GST-SNAP25 and SNAP25 to GNPs

The binding kinetics of GST and NEM-GST to GNPs shows that the adsorption of GST to GNPs does not have higher affinity or quicker binding rate than NEM-GST, however, the ME displacement assay shows that cysteines can bind GNPs by Au-S bonds. These can be used as a site-oriented strategy for binding GST fusion proteins to GNPs if they do not have cysteine residues apart from those on GST.

In this part of the study we used GST-SNAP25, where all 4 cysteines of SNAP25 were mutated into alanines in this case. GST-SNAP25 was adsorb onto GNPs, supposedly by chemisorption between cysteines on GST and GNPs, so to form a stable protein corona surrounding GNPs. The rationale behind this configuration is that, as SNAP25 doesn't have any cysteine, at equilibrium it is expected to be exposed to the outside of the protein corona and be available to bind other SNARE proteins. Opposite to GST-SNAP25, SNAP25 has no cysteines, and was used as a control to support the hypothesis of GST-SNAP25 chemisorption. We also compared the affinity of GST-SNAP25 and SNAP25 to establish whether fusion to GST can enhance how efficiently a protein binds to GNPs.

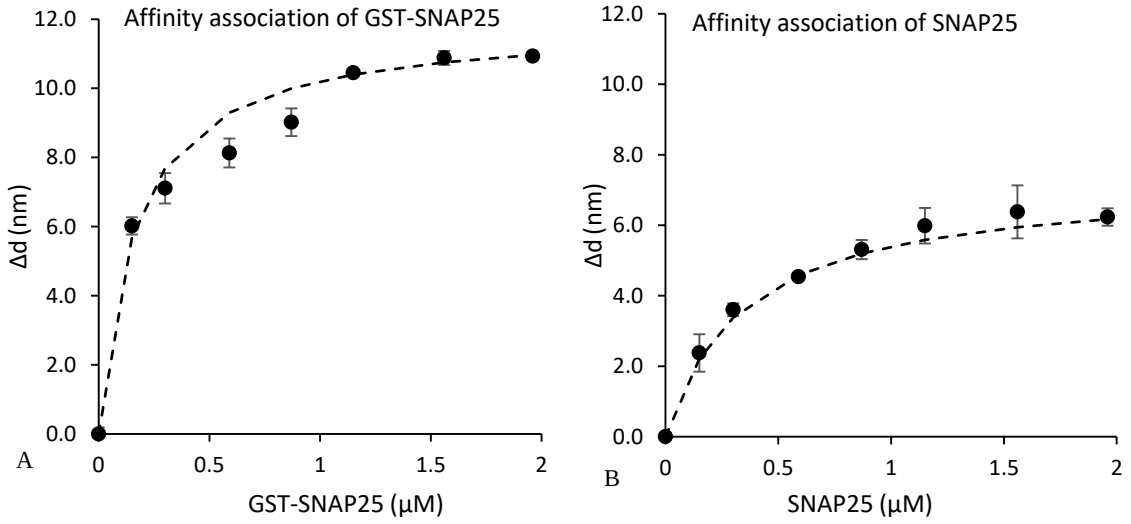

Figure 3. 28 ***The affinity measurement of GST-SNAP25 and SNAP25 binding onto GNPs. The increase in size (Δd) against concentration (0 μM, 0.15 μM, 0.30 μM, 0.59 μM, 0.87 μM, 1.15 μM, 1.56 μM and 1.96 μM) was plotted for GST-SNAP25 (A) and SNAP25 (B). The Δd data (black dots) were fitted (dash line) to Equation 1.6.***

The affinity associations of GST-SNAP25 and SNAP25 were obtained by plotting size (Δd) against GST concentration (Figure 3.28). According to Equation 1.6, the K_D of GST-SNAP25 and SNAP25 were 0.188μM and 0.343μM respectively and the Δd_{MAX} of GST-SNAP25 and SNAP25 were 9.5nm and 7.6nm respectively. The values are consistent with our previous observation that GST binds gold very effectively and here increased the affinity to GNPs of SNAP25 when fused to GST. The larger Δd_{MAX} observed for GST-SNAP25 is consistent with the larger size of the molecule (GST-SNAP25 molecular weight is about twice bigger than SNAP25).

Also, the pI of GST-SNAP25 is 5.09 which is higher than SNAP25 (4.66), therefore, GST-SNAP25 has less negative charges at pH7.2 which might also contribute better binding. Consequently, the K_D of adsorption of GST-SNAP25 (K_D =0.188 μM) to GNPs was lower than SNAP25 (K_D =0.343 μM).

GNPs/GST-SNAP25 conjugates (Figure 3.29) showed a clear peak at 530nm, and $Ab_{530nm/600nm}$ was 1.8. These results suggest that GST-SNAP25 binds to GNPs surface efficiently by chemisorption, so that β-Mercaptoethanol could not replace the Au-S covalent bond.

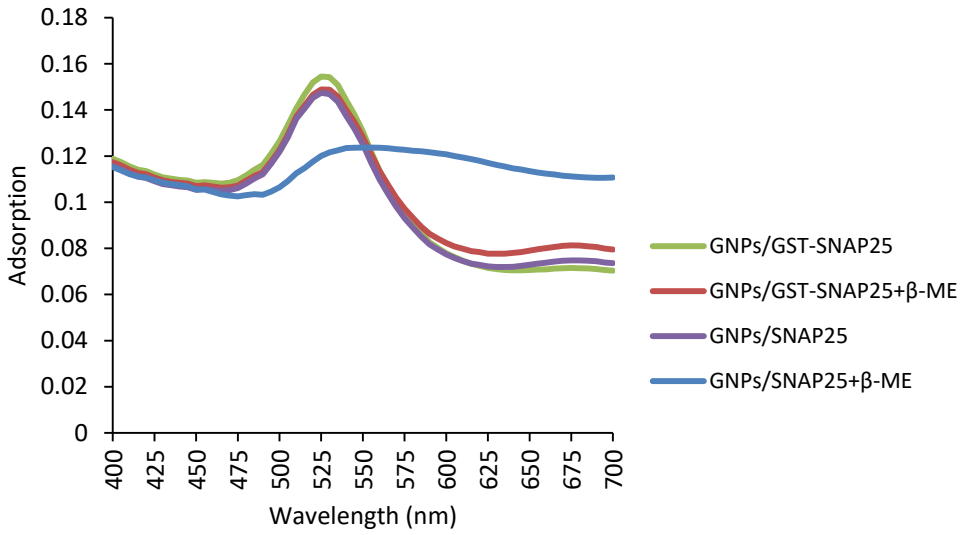

Figure 3. 29 ***Displacement of GST-SNAP25 and SNAP25 by 0.2mM β-Mercaptoethanol.***

By contrast, GNPs/SNAP25 did not show a SPR peak in Figure 3.29 upon incubation with β-Mercaptoethanol and the $Ab_{530nm/600nm}$ value was 0.99. This indicates only physisorption between SNAP25 and GNPs, resulting in the GNPs aggregation.

The β-Mercaptoethanol assay offers indication that GST-SNAP25 binding involves cysteines and it is most likely site-oriented. Therefore, GST-SNAP25 could be potentially able to form a SNARE complex, for example with Nanolock. This observation is the foundation of our work on modular assembly of proteins on GNPs reported in section **3.4.1**.

3.3.8 Equilibrium binding of GST-SpyCatcher and SpyCatcher to GNPs

SpyCatcher and SpyTag pair, similarly to SNAP25 and Nanolock, could be a powerful tool for gold nanoparticles modular assembly, but opposite to the SNAREs based system, this would offer covalent protein-protein binding through inter-molecular isopeptidic bonds. To assess the ability of GST-SpyCatcher fusion to efficiently bind to GNPs, we compared the binding affinity of GST-SpyCatcher and SpyCatcher to GNPs surface similarly to what we did for GST-SNAP25 and SNAP25. Also, β-Mercaptoethanol displacement experiment were used to prove the binding orientation between GNPs and GST-SpyCatcher.

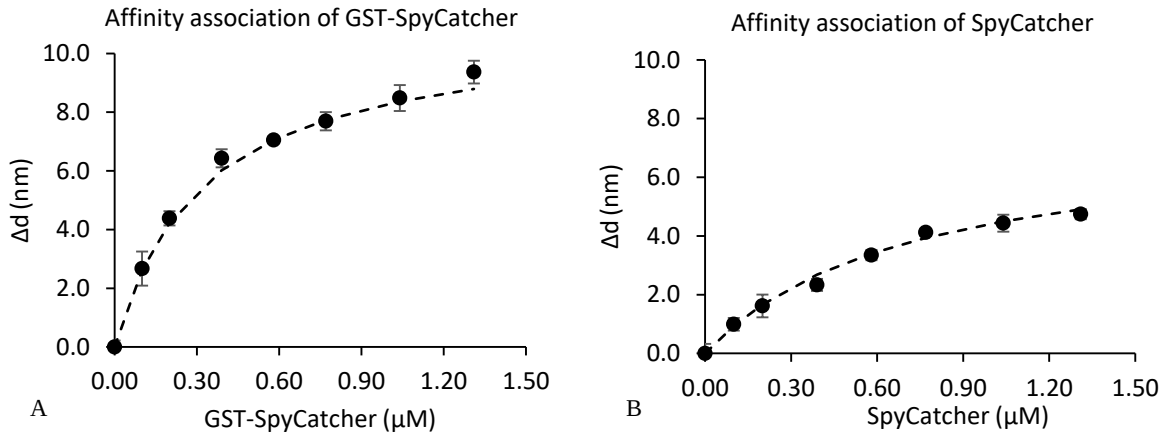

Figure 3. 30 ***The affinity measurement of GST-SpyCatcher and SpyCatcher. The increase in size (Δd) against concentration (0 μM, 0.15μM, 0.30μM, 0.59μM, 0.87μM, 1.15μM, 1.56μM and 1.96μM). Δd (black dots) was fitted (dash line) to Equation 1.6.***

From the data in Figure 3.30, the K_D and Δd_{MAX} of GST-SpyCatcher were 0.317μM and 10.9nm, whereas K_D and Δd_{MAX} of SpyCatcher were 0.713μM and 7.6nm respectively. Similarly to the case of GST-SNAP25/SNAP25, GST fusion improved the affinity of SpyCatcher to gold. The pI of GST-SpyCatcher and SpyCatcher are 5.17 and 4.39 respectively. The adsorption was undertook at pH7.2. Based on the finding of **3.3.1**, GST-SpyCatcher had less negative charges than SpyCatcher at pH7.2, probably contributing to provide a higher affinity at this pH because of lower electrostatic force to negative charged GNPs surface. Δd_{MAX} of GST-SpyCatcher was about 3.3nm bigger than SpyCatcher, most likely because GST-SpyCatcher has a bigger molecular weight than SpyCatcher.

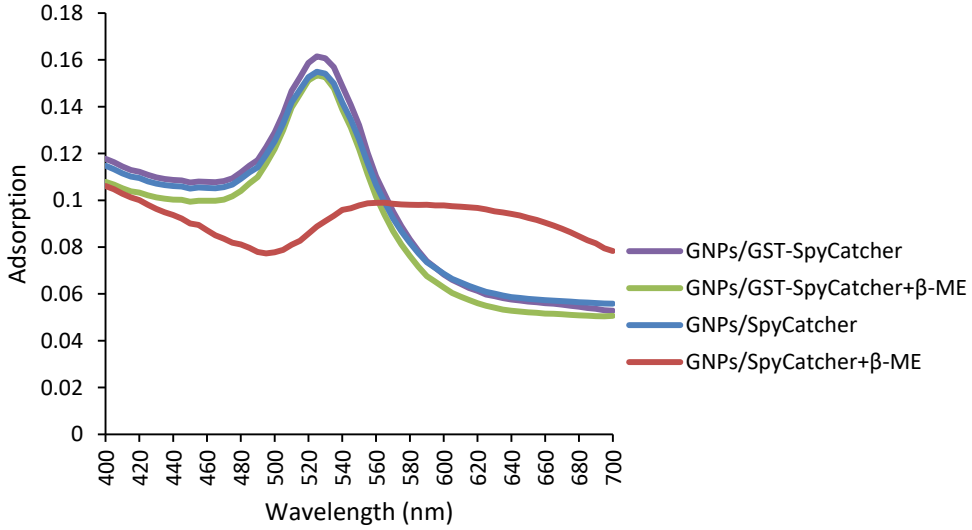

Figure 3. 31 ***Displacement of GST-SpyCatcher and SpyCatcher by 0.2mM β-Mercaptoethanol.***

In Figure 3.31, GNPs/GST-SpyCatcher shows clear SPR peaks with and without β-ME, and the $Ab_{530nm/600nm}$ value was 2.44. Instead, the peak of GNPs/SpyCatcher disappeared after adding β-ME, and the $Ab_{530nm/600nm}$ value was 0.91. The β-Mercaptoethanol displacement experiments (Figure 3.31) showed GST-SpyCatcher was stable on GNPs in presence of β-ME, on the contrary, SpyCatcher was replaced by β-ME and brought out the GNPs from the colloidal suspension. This experiment also suggests the possible site-oriented binding nature between GNPs and GST-SpyCatcher, as the only cysteines in GST-SpyCatcher are those on GST. The binding between GNPs/GST-SpyCatcher and SpyTag would be more likely to happen in this case. This strategy of modular assembly will be discussed in the following section **3.4.2**.

3.4 Modular assembly of proteins on gold nanoparticles

The previous findings proved that GST-SNAP25 and GST-SpyCatcher stably bind to GNPs surfaces through the cysteines of GST. This section shows evidence of the ability of these GST fusion proteins (GST-SNAP25 and GST-SpyCatcher) adsorbed onto GNPs to form complexes with their partner proteins, Nanolock and SpyTag respectively.

3.4.1 Binding of Nanolock to GST-SNAP25 coated GNPs

To determine the saturation concentration of GST-SNAP25 binding to GNPs and confirm the DLS measurements of section **3.3.7**, 40nm GNPs were titrated at 7 concentration of GST-SNAP25 (0.15 µM, 0.30 µM, 0.59 µM, 0.87 µM, 1.15 µM, 1.56 µM, and 1.96 µM) and their migration was observed on an agarose gel (lanes 1-7 of Figure 3.32). The higher the concentration of GST-SNAP25, the faster was the migration of GNPs/GST-SNAP25. As we already discussed (see section **3.3.7**), GST-SNAP25 (pI=5.08) is negatively charged at pH7.2, therefore, the higher concentration of adsorbed GST-SNAP25 contributed more negative charge to GNPs/GST-SNAP25 conjugates and determined faster migration. The experiment also suggested that the saturation concentration of GST-SNAP25 was around 1.56 µM (lane 6 of Figure 3.32) because there was no migration difference between lane 6 and lane7. This is consistent with the affinity association curve (Figure 3.28) of GST-SNAP25 that showed the Δd measured by DLS stop increasing from 1.56 µM. Conclusively, GST-SNAP25 was able to completely cover GNPs surface at a concentration of about 1.5 µM. The sample with GNPs

only was thoroughly precipitated because of high salt concentration of TBE and did not migrate (lane 8 of Figure 3.32).

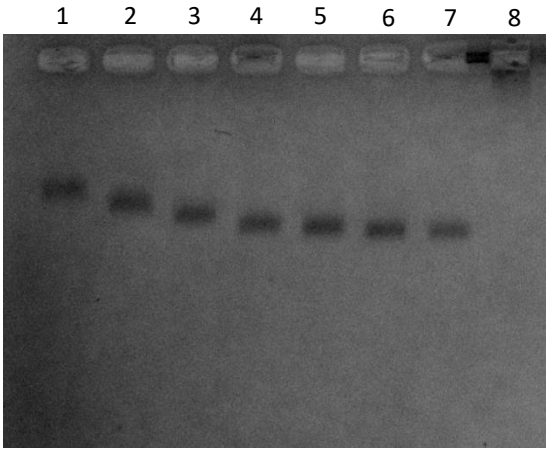

Figure 3. 32 ***Agarose gel of GNPs/GST-SNAP25. GST-SNAP25 adsorbed onto GNPs forms a monolayer at concentrations larger than 1.56μM. Migration in 0.8% agarose of GNPs with adsorbed GST-SNAP25 at 0.15, 0.30, 0.59, 0.87, 1.15, 1.56, 1.96 μM concentrations (lanes 1-7); lane 8 has GNPs with no GST-SNAP25 that are unstable in 0.5xTBE and therefore precipitated in the well.***

In order to verify the ability of GST-SNAP25 adsorbed on GNPs to bind its partner protein Nanolock, the GNPs/GST-SNAP25 conjugates were incubated with excess Nanolock for 1 hour. GST in place of GST-SNAP25 was used as a control. After incubation, the mixtures were washed by Buffer B for three times to remove the unbound Nanolock and the bound proteins were analysed by SDS-PAGE.

The Au-S were broken in SDS-PAGE loading buffer at 42 ℃(Li, Jin et al. 2002) for 10 hours, so all the proteins bound to GNPs, including those linked through GST, detached from GNPs. The mixture of GNPs and proteins was loaded into SDS-PAGE and the individual proteins were displayed in the gel.

GNPs-adsorbed GST (Figure 3.33A, lane1) and GST-SNAP25 (Figure 3.33A, lane2) were used as controls that represent the amount of capture proteins on the nanoparticles. Lanes 3 and 4 show the same particles upon incubation with Nanolock. Nanolock was captured by GST-SNAP25 GNPs as clearly shown in lane 4 but GST-only GNPs (lane 3) did not bind any Nanolock as expected. This results show that Nanolock specifically bind to GST-SNAP25 coated GNPs, most likely through the formation of a SNARE complex.

SNARE proteins coated GNPs were also verified by agarose gel electrophoresis similarly to figure 3.32. Opposite to SDS-PAGE, the SNARE complexes should be in near-native conditions in the agarose gel. We expected the particles would run into the gel resulting in different migration depending on different size/charge, possibly offering a way to compare

GNPs with GST-SNAP25 and Nanolock or GST-SNAP25 only. We found that GNPs/GST-SNAP25-Nanolock migrated less than GNPs/GST-SNAP25 as shown in lane 5 compared to lane 4 (Figure 3.33B). This is probably due to larger mass of the particle. However, the difference in migration was minimal and was not conclusive on its own, unless the results are considered together with SDS-PAGE evidence and DLS data (see below). No significant migration difference was observed between lane 2 and lane 3 (Figure 3.33B) where GST conjugated particles were incubated (lane 3) or not (lane 2) with Nanolock. This is consistent with what was observed on SDS-PAGE which showed GST was not able to interact with Nanolock.

GNPs-protein conjugates were analysed by DLS to determine whether the formation of the SNARE complex could be evidenced by a change of overall size of the particles. In Figure 3.33 (C), GNPs/GST-SNAP25 were incubated with Nanolock and the size increase compared to GNPs/GST-SNAP25 only. The size of GNPs/GST-SNAP25 (50.57nm) was around 8nm bigger than GNPs (42.60nm), and was around 2nm smaller than GNPs/GST-SNAP25-Nanolock (52.74nm). This 2nm change was likely due to the binding of Nanolock to GST-SNAP25. In Figure 3.33 (D), the size of naked GNPs (41.76nm) was about 7.5nm smaller than GNPs/GST (49.20nm) and nearly no change was observed in presence Nanolock (49.18nm). Figure 3.33 (D) suggested that, as expected, Nanolock did not bind to GST. The modest increment in hydrodynamic size upon SNARE complex formation is consistent with the fact that the SNARE complex is structurally a rod-shaped coiled-coil with all parallel helices. This structure is more rigid than the unstructured SNARE domains before assembly, but most likely not much longer along the major axis of the coiled-coil, therefore the SNARE complex formation is unlikely to result into a substantial increase of size of the particles.

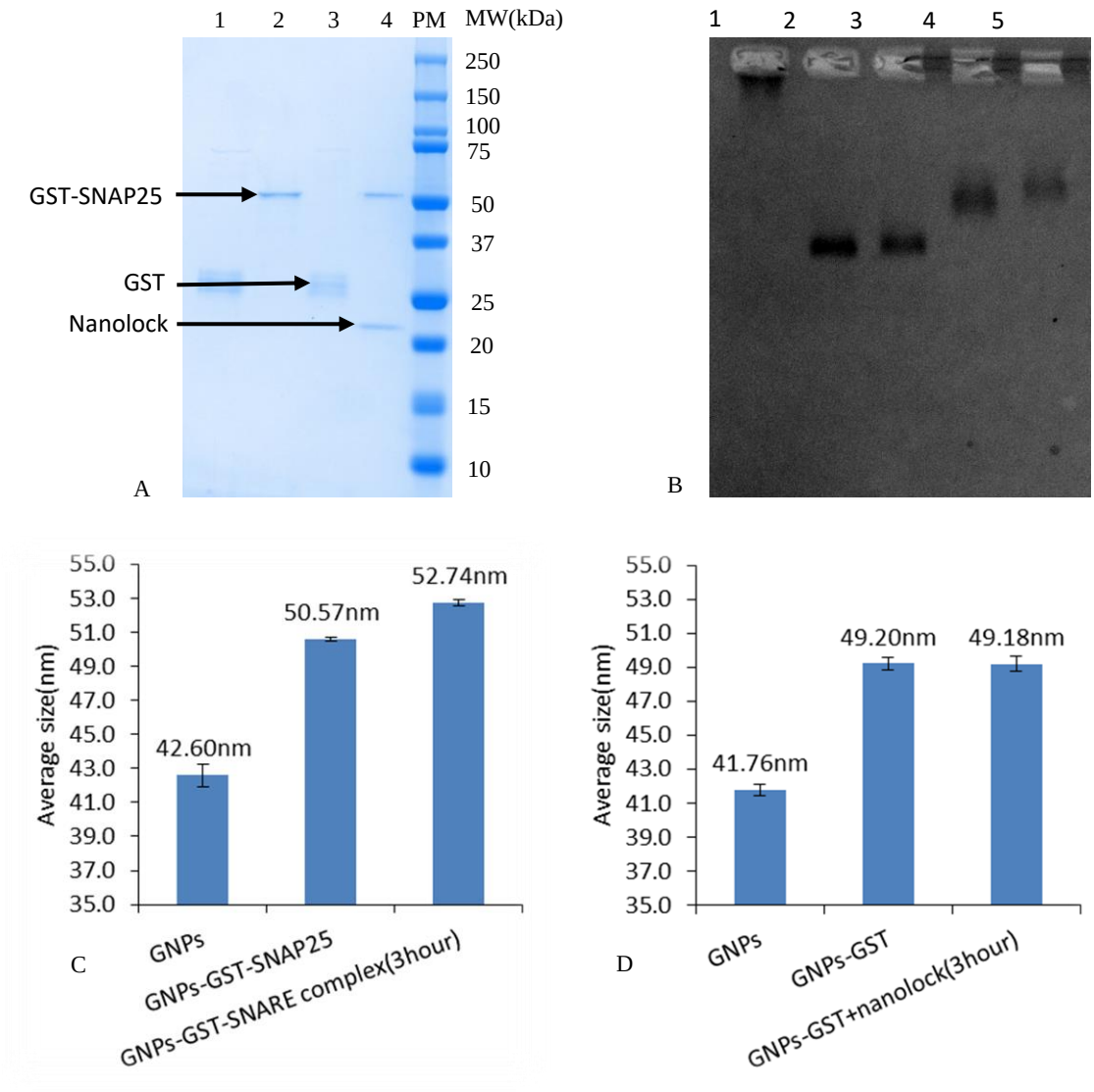

Figure 3. 33 ***SNARE complex assembled on GNPs surfaces. (A). GNPs protein conjugates were heated in SDS-PAGE gel loading buffer at 42 ℃ for 10 hours and then analysed by SDS-PAGE. Lane 1 is GNPs/GST, lane 2 is GNPs/GST-SNAP25, lane 3 is the mixture of GNPs/GST and Nanolock, lane 4 is the mixture of GNPs/GST-SNAP25 and Nanolock, PM is the protein marker (BioRad, Precision Plus Protein™ Dual Color). (B) GNPs protein conjugates were run in 0.8% agarose gel, lane 1 is naked GNPs, lane 2 is GNPs/GST, lane 3 is the mixture of GNPs/GST and Nanolock, lane 4 is GNPs/GST-SNAP25, lane 5 is the mixture of GNPs/GST-SNAP25 and Nanolock. (C) DLS analysis of the mixture of GNPs/GST-SNAP25 and Nanolock. (D) DLS analysis of the mixture of GNPs/GST and Nanolock. MW is molecular weight.***

From these results together, we can draw the conclusion that GST-SNAP25/Nanolock can be used to modularly adsorb proteins by simple mixing, for example a fusion of Nanolock to a protein of interest, would likely allow this to bind GNPs through the previously adsorbed GST-SNAP25 molecules.

3.4.2 Binding of NEM-GST-SpyTag to GST-SpyCatcher coated GNPs

The limitation of SNARE complex in bio-conjugation is that the coiled-coil, although only in harsh conditions, could disassemble. This feature might be useful in some circumstance (for

example could be exploited for some form of stimuli-responsive nanoparticle-mediated drug delivery), but in many other context a permanent conjugation is more desirable. SpyCatcher and SpyTag can form a covalent isopeptide bond, therefore providing a permanent link. Their reaction is fast, requires only simple mixing, and shows good specificity. Especially, it is robust in a range of experimental conditions: it could not be destroyed by low temperature or non-ionic detergents (Zakeri, Fierer et al. 2012). The isopeptide bond, opposite to SNARE complex, is also stable in boiling SDS buffer (see below). Based on these advantages, SpyCatcher and SpyTag could potentially allow a range of use in living cells (37 ℃) for drug delivery, or for pull-downs in cell lysate(Zakeri, Fierer et al. 2012).

In this study, GST-SpyCatcher was adsorbed onto GNPs, and was expected to form the isopeptide bond with NEM-GST-SpyTag by simple mixing. We used SpyTag fused to GST as the molecular weight shift in case of binding of SpyTag only would be otherwise too small to allow detection by DLS and SDS-PAGE. To prevent potential competition between GST-SpyTag and GST-SpyCatcher in GNPs binding, we used NEM-GST-SpyTag rather than GST-SpyTag, so to avoid presence of free cysteines linked to SpyTag and subsequent displacement of GST-SpyCatcher from the GNPs. As the isopeptide bond was expected to be formed between SpyCatcher and SpyTag, NEM-GST was used as a negative control to react with GST-SpyCatcher.

GST-SpyCatcher was incubated with NEM-GST-SpyTag (Figure 3.34 (A), lane 1) or NEM-GST (Figure 3.34 (A), lane 2) for 1 hour at room temperature in Buffer B to check whether the isopeptide bonds could form between GST-SpyCatcher and NEM-GST-SpyTag. Only lane 1 shown a sharp band between 50kDa and 75kDa. This suggested that GST-SpyCatcher formed an isopeptide bonds with NEM-GST-SpyTag but not with NEM-GST (lane 2).

GNP/GST-SpyCatcher were incubated with NEM-GST-SpyTag (Figure 3.34 (A), lane 3) and NEM-GST (Figure 3.34 (A), lane 4) respectively. The GNPs mixture was washed by Buffer B for three times to remove the unreacted proteins. As it was described in **3.4.1**, the Au-S bonds could be broken after a 10 hours incubation in SDS loading buffer at 42 ℃. Consequently, the GST fusion proteins were detached from GNPs. The mixture was loaded in SDS-PAGE. Lane 3 shown the complex, but there is only a band corresponding to GST-SpyCatcher in lane 4. This suggests that NEM-GST-SpyTag could form an isopeptide bond with GST-SpyCatcher on the GNPs surface, NEM-GST could not form a complex with GST-SpyCatcher, therefore, it was simply removed when washing by centrifugation.

The observation was also confirmed by DLS data. In Figure 3.34 (B), the size of GNPs/GST-SpyCatcher/NEM-GST-SpyTag was ~2nm bigger than GNPs/GST-SpyCatcher only. In contrast, the size of GNPs/GST-SpyCatcher had nearly no change (~0.5nm) after adding NEM-GST without the SpyTag (Figure 3.34C).

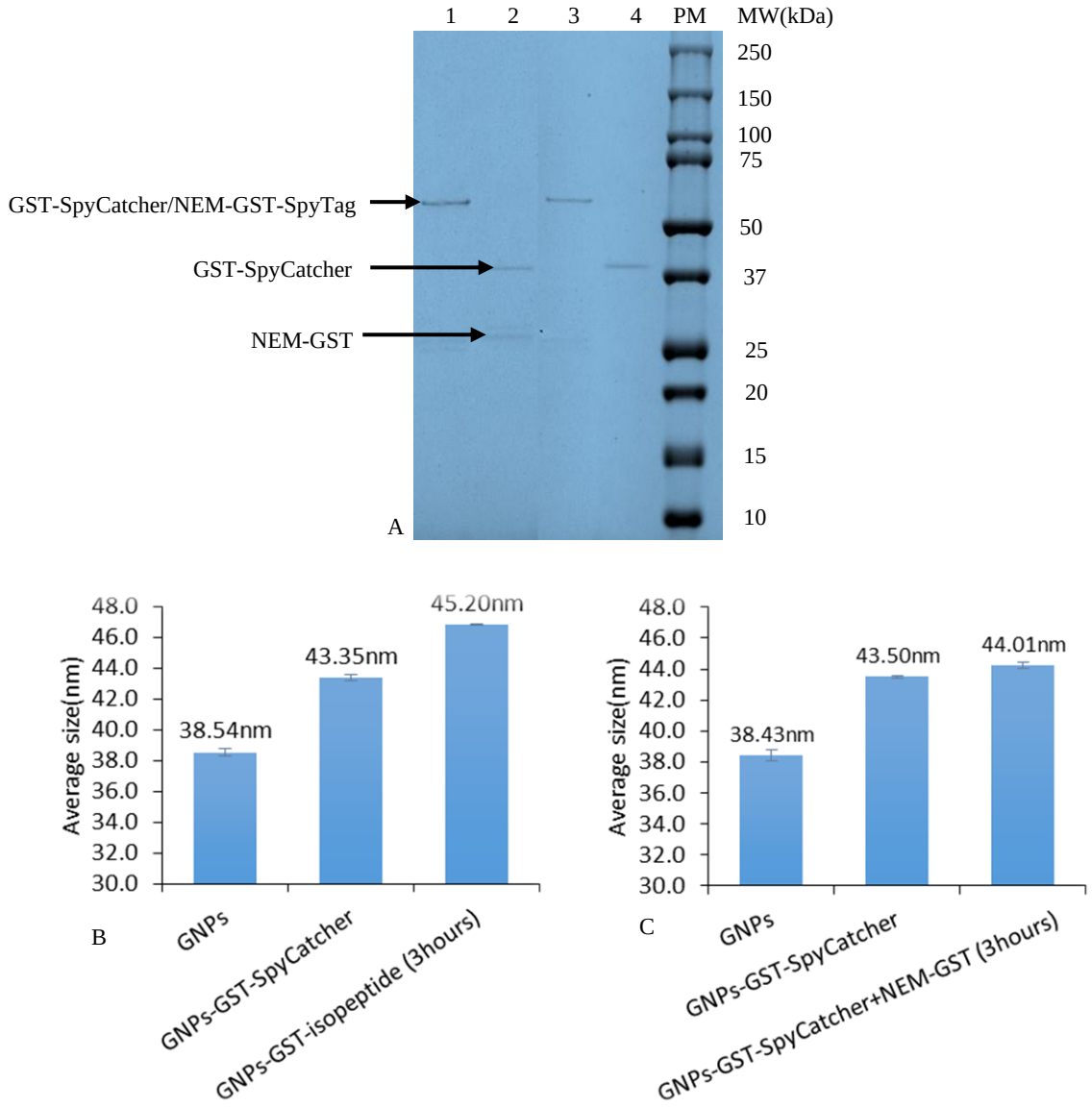

Figure 3. 34 ***Isopeptide bonds formed on GNPs surfaces. (A) 12% precast SDS-PAGE gel showing mixture of GST-SpyCatcher with NEM-GST-SpyTag (lane 1) or NEM-GST (lane 2). Lane 3: GNPs/GST-SpyCatcher mixed with NEM-GST-SpyTag. Lane 4: GNPs/GST-SpyCatcher and NEM-GST. PM is the protein marker (BioRad, Precision Plus Protein™ Dual Color). (B) DLS analysis of mixtures of GNPs/GST- SpyCatcher and NEM-GST-SpyTag. (C) DLS analysis of mixtures of GNPs/GST- SpyCatcher and NEM-GST. MW is molecular weight.***

In this section, we proved that GNPs/GST-SpyCatcher conjugates could bind and form isopeptide bonds with NEM-GST-SpyTag and potentially be used as an easy conjugation strategy for functionalization of GNPs with recombinant proteins tagged with SpyTag.

3.5 Assembly of gold nanoparticles dimers using SNARE-BSA conjugates

BSA was intended as an alternative to GST to efficiently adsorb SNAREs on GNPs. Similarly to GST, BSA could form a stable layer surrounding the particle and prevent SNAREs from collapsing on the gold surface, which would compromise their ability to form a complex. In this experiment, SNAP25C1-Cy3 was used to trigger the SNARE complex formation between GNPs/SyntaxinC1-BSA and GNPs/SynaptobrevinC1-BSA. In this case, the complex could be also visualized under UV light due to the Cy3 on SNAP25.In section **3.2.6**, we reported the best conditions to synthesize SNARE-BSA and SNAP25C1-Cy3.

In order to visualize the SNARE complex, SyntaxinC1-BSA, SynaptobrevinC1-BSA and SNAP25C1-Cy3 were mixed for a 1 hour incubation at room temperature and the heated (Figure 3.35, lane 1) and non-heated (Figure 3.35, lane 2) mixture were loaded on SDS-PAGE. The gel was observed under UV light first and then stained by InstantBlue. In Figure 3.35, the bands above 150kDa (lane 1) corresponds to a molecular weight compatible with the complex formed of SyntaxinC1-BSA (75.4kDa), SynaptobrevinC1-BSA (73.8kDa) and SNAP25C1-Cy3 (25.3kDa). However, there were considerable amounts of un-complexed SNAREs (SNAP25 is especially visible as it is very bright). This phenomenon may because BSA is much bigger than SyntaxinC1 and SynaptobrevinC1 resulting in the introduction of steric effects, so that the coiled-coil complex could not be completely formed or assemble in a form not stable in SDS and disassembled into individual SyntaxinC1-BSA, SynaptobrevinC1-BSA and SNAP25C1-Cy3. Nevertheless, SNARE-BSA and SNAP25C1-Cy3 were able to combine together to some extent, as evidenced by the high molecular weight band that disappears when boiling.

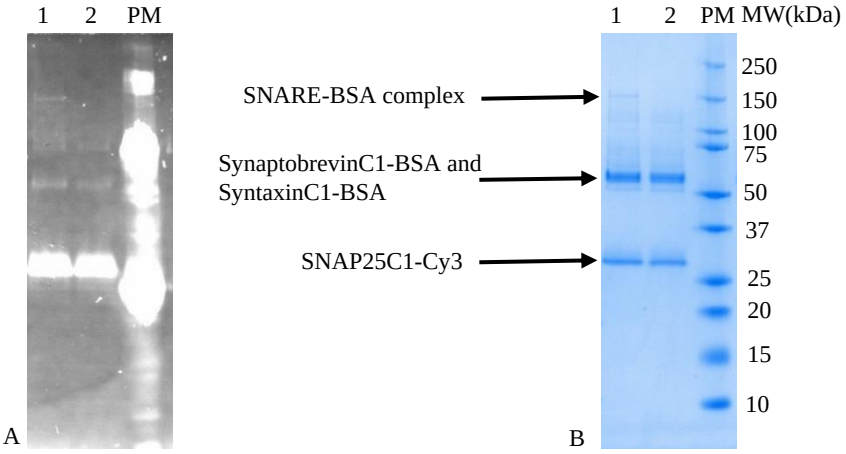

Figure 3. 35 ***The SNARE-BSA complex. (A) The SDS-PAGE gel under UV light. (B). The same SDS-PAGE gel of B was stained with Instantblue. 1. non-boiled complex: SNAP25C1-Cy3 assembled with SynaptbrevinC1-BSA and SyntaxinC1-BSA. 2. boiled complex. PM is the protein marker (BioRad, Precision Plus Protein^{TM} Dual Color). Precast SDS-PAGE gel, 170V, 55 minutes. MW is molecular weight.***

The two SNARE-BSA conjugates were adsorbed on different sizes of GNPs to verify whether SNAP25C1-Cy3 would trigger SNAREs to form a SNARE complex and bring the GNPs close. SyntaxinC1-BSA and SynaptobrevinC1-BSA were adsorbed onto 40nm GNPs and 20nm GNPs respectively and then mixed with SANP25C1-Cy3. The AFM image of Figure 3.36 (A) shows that a dimer was assembled with one small GNP (20nm) and one big GNP (40nm) as expected. The gray line was the specific profile of interest analyzed by Gwyddion (Figure 3.36 (B)). The Y axis of Figure 3.36 (B) was the step height, with the largest heights representing the diameter of GNPs. The distance between the peaks of the two particles (Figure 3.36 (B)) was calculated as 57nm, representative of the distance between the centre of the two spheres. The schematic (Figure 3.36 (C)) of our hypothetical particle dimer, formed by BSA-SNARE conjugates assembled together, shows that the theoretical distance should be 55nm. This is calculated from the radius of each gold nanoparticles (20nm and 10nm), two BSA molecules (each BSA has a hydrodynamic diameter in the order of 7nm, based on the structure at PDB ID 4F5S), and the size of SNARE complex which is about 11nm (calculated from PDB ID 1SFC). The difference between calculated and measured distance was only 2nm which we considered acceptable, especially as the SNARE complex was formed using a new bio-conjugation method that might give a looser structure than the one obtained for the original X-ray structure.

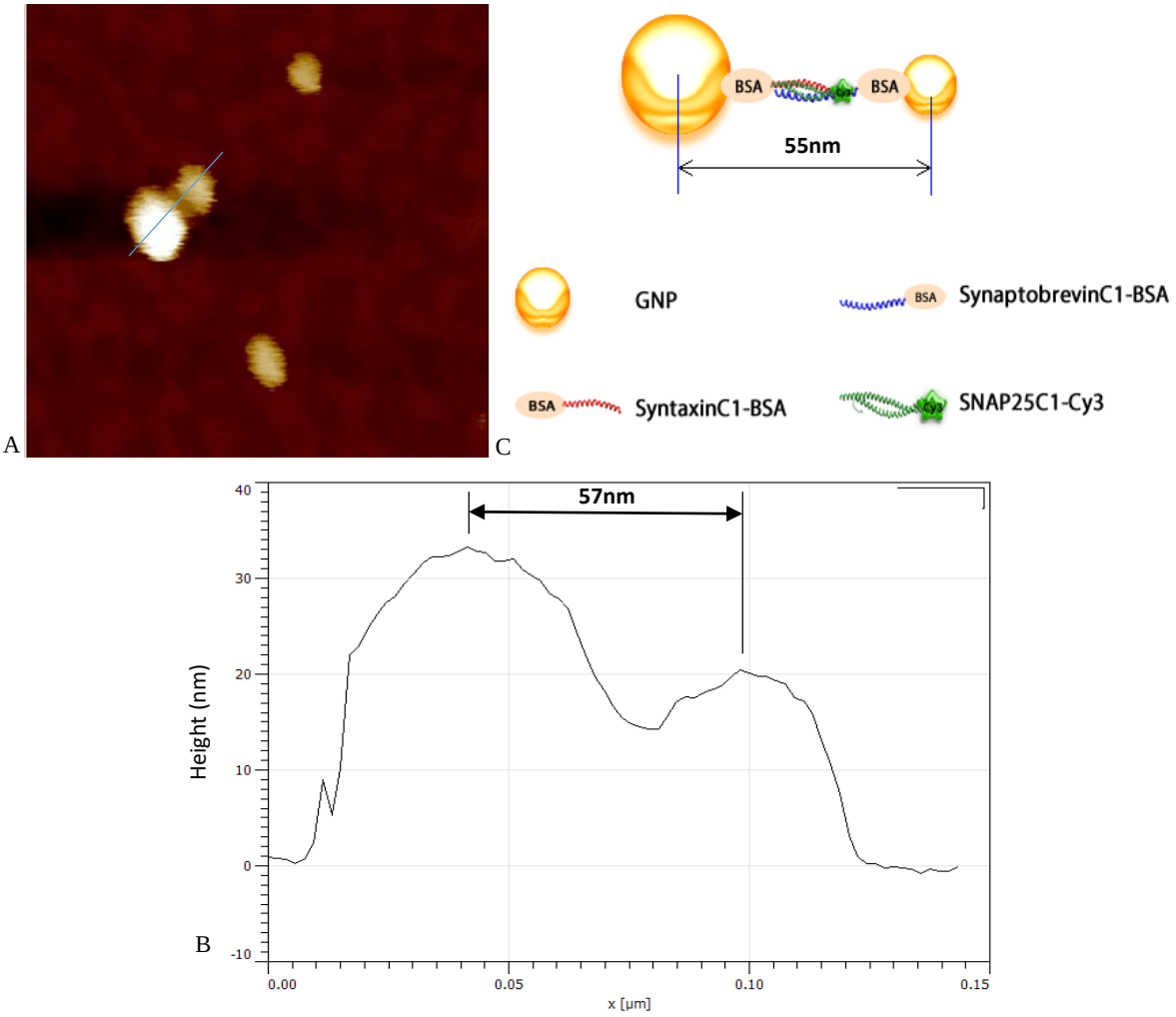

Figure 3. 36 ***Dimers assembled by GNPs and SNARE-BSA conjugates. (A) AFM image of dimer. (B) Particle distance analysis from Gwyddion software, Y axis is the height of GNPs, X axis is linear distance (C) The scheme of gold nanoparticle dimer assembled by SNARE-BSA and SNAP25C1-Cy3.***

The formation of GNPs dimer suggested that BSA played a role as interface protein which adsorb to GNPs surface and oriented SyntaxinC1 and SynaptobrevinC1 so they could form a SNARE complex with SNAP25C1-Cy3. The concept of the manufacturing of GNPs dimers by SNARE-BSA proteins was proved, however, there were only few dimers in the AFM images attempted. In order to obtain a better yield of dimers, it would be beneficial to optimized reaction conditions in the future, such as the concentration of SNARE-BSA and SNAP25C1-Cy3, the incubation time, and the incubation buffers. The poor yield observed might also reflect the sub-optimal stability also observed in SDS-PAGE of SNARE-BSA complex in Figure 3.35. We haven't attempted formation of dimers using GST-SNARE fusions, as the GST is at the N-terminal of the SNARE domain and it would likely interfere with the assembly, which is triggered at the very N-terminal. Nevertheless, it might be possible to use a similar approach to BSA-SNAREs by fusing GST at the C-terminal.

Chapter4. Conclusions and future work

We successfully synthesized two different sizes of gold nanoparticles by sodium citrate method. The data of atomic force microscope, nanoparticle tracking analysis, dynamic light scattering and ultraviolet-visible spectroscopy show that the GNPs distributions are homogeneous and the sizes as expected. We concluded that laboratory-made and commercial particles are equally suitable for conjugation experiments and we opted for the latter to guarantee consistency of the results.

Recombinant SNARE proteins with one single cysteine were cloned, synthesized and purified for their conjugation to BSA or fluorophores. Their ability to assemble in a coiled coil complex was proved, also in the case of BSA-SNAREs bound to GNPs. We believe that self-assembling metal nanoparticle dimers of this type could be used to develop a rapid Surface Enhanced Raman Scattering (SERS) sensor for single molecule detection. We used two different sizes of GNPs linked to either SyntaxinC1-BSA or SynaptobrevinC1-BSA to prove that the dimers assemble in the expected hierarchical way. Cy3 bound to SNAP25 is likely to be oriented inside the gap between the particles, which is the SERS hot spot. Cy3 could be used as a convenient analyte as it has a good Raman signal, but this would require an optimization of the assembly conditions, to increase the number of dimers obtained, as currently we estimated an efficiency of less than 10%, based on assembled particles versus individual particles in AFM images. In a final version of the sensor, a ligand binding molecule would replace Cy3 at the C-terminal of SNAP25 and the analyte would bind in the hot spot position when the system assembles. This would be the first particle dimers based sensor which works with an analyte in solution. In fact, all previous attempts to prove particle dimers based SERS sensors, were not using self-assembling systems, and the analyte had to be embedded into the dimer during synthesis(Lim, Jeon et al. 2010).

The study of GST adsorption onto GNPs lead to the understanding of the strong interaction that this protein has with gold and to indications on how the electrostatic forces and the thiols play a significant role in the mechanism of adsorption of proteins to GNPs. For the determination of thiols contribution we also developed a novel method based on SPR data measured in a simple β-Mercaptoethanol displacement assay. We confirmed previous observations(Rahman, Laurent et al. 2013) that adsorption of proteins with cysteines follows a two-steps model. In the first step, the electrostatic force brings the protein close to GNPs

surface. We estimated for the first time that, at the protein concentrations that are achievable on the NPs surface, the second step happens after approximately 20 minutes from initial binding of GST.

It was reported previously (Laera, Ceccone et al. 2011) that proteins are denatured on the GNPs surface. GST or BSA used as a sacrificial corona increase the distance between a protein of interest and the surface, and this could help preventing denaturation. In fact, we proved that in the case of SNARE proteins and SpyCatcher, GST- and BSA-mediated conjugation to GNPs preserved their function. Therefore, GST-SNAP25/Nanolock, GST-SpyCatcher/SpyTag and also BSA-SNAREs could be used in the synthesis of GNP-based biosensor by fusing a protein of interest (antibody or enzyme) to Nanolock, SpyTag or a SNARE. The discovery of GST as an ideal protein domain which has excellent affinity to gold, also opens the question whether other proteins could be tested or engineered to bind other materials used in biosensors or other applications, such as glass, polystyrene or carbon nanotubes. This work contributed to develop a number of methods that can be applied in this field of research, whenever a specific material would be available in the form of nanoparticles.

Acknowledgments

I would like to thank my supervisor Dr Enrico Ferrari for his ideas, help and supervision for the project. A huge hug for Sophina Christ and Juan Luis Gomez Gonzalez, the kind, patient and smiling girl who give me countless support during the difficulties. Thank you for the friendship of all lab mates. Thank everyone else in the Joseph Banks Laboratories for their help. Thank the University of Lincoln for my studentship, I could have money to do the research. Finally I thank my parents for all their love and support over the years, without which I would not be who I am today.

References

Albrecht-Buehler, G. (1977). "The phagokinetic tracks of 3T3 cells." Cell **11**(2): 395-404.

Alexander, K. D., et al. (2009). "A high‐throughput method for controlled hot‐spot fabrication in SERS‐active gold nanoparticle dimer arrays." Journal of Raman Spectroscopy **40**(12): 2171-2175.

Arduengo, M., et al. (2007). "The role of cell-free rabbit reticulocyte expression systems in functional proteomics." Cell-Free Expression. Austin, TX: Landes Bioscience **2007**: 1-18.

Aslam, M., et al. (2004). "Novel one-step synthesis of amine-stabilized aqueous colloidal gold nanoparticles." Journal of materials Chemistry **14**(12): 1795-1797.

Avvakumova, S., et al. (2014). "Biotechnological approaches toward nanoparticle biofunctionalization." Trends in biotechnology **32**(1): 11-20.

Bernkop-Schnürch, A., et al. (2004). "Thiolated chitosans: development and in vitro evaluation of a mucoadhesive, permeation enhancing oral drug delivery system." Journal of Controlled Release **94**(1): 177-186.

Bracher, A., et al. (2002). "X-ray structure of a neuronal complexin-SNARE complex from squid." Journal of Biological Chemistry **277**(29): 26517-26523.

Browne, D. T. and S. B. H. Kent (1975). "Formation of non-amidine products in the reaction of primary amines with imido esters." Biochemical and biophysical research communications **67**(1): 126-132.

Brust, M., et al. (1994). "Synthesis of thiol-derivatised gold nanoparticles in a two-phase liquid–liquid system." Journal of the Chemical Society, Chemical Communications(7): 801-802.

Cai, W., et al. (2008). "Applications of gold nanoparticles in cancer nanotechnology." Nanotechnology, science and applications **2008**(1).

Campion, A. and P. Kambhampati (1998). "Surface-enhanced Raman scattering." Chemical Society Reviews **27**(4): 241-250.

Cedervall, T., et al. (2007). "Detailed identification of plasma proteins adsorbed on copolymer nanoparticles." Angewandte Chemie International Edition **46**(30): 5754-5756.

Cedervall, T., et al. (2007). "Understanding the nanoparticle–protein corona using methods to quantify exchange rates and affinities of proteins for nanoparticles." Proceedings of the National Academy of Sciences **104**(7): 2050-2055.

Chang, H.-C., et al. (2005). "De novo folding of GFP fusion proteins: high efficiency in eukaryotes but not in bacteria." Journal of molecular biology **353**(2): 397-409.

Chapman, E. R., et al. (1994). "SNAP-25, a t-SNARE which binds to both syntaxin and synaptobrevin via domains that may form coiled coils." Journal of Biological Chemistry **269**(44): 27427-27432.

Chen, C., et al. (2009). "Kinetics and thermodynamics of DNA hybridization on gold nanoparticles." Nucleic acids research **37**(11): 3756-3765.

Clapp, A. R., et al. (2006). "Förster resonance energy transfer investigations using quantum‐dot fluorophores." ChemPhysChem **7**(1): 47-57.

Connor, E. E., et al. (2005). "Gold nanoparticles are taken up by human cells but do not cause acute cytotoxicity." Small **1**(3): 325-327.

El-Sayed, I. H., et al. (2005). "Surface plasmon resonance scattering and absorption of anti-EGFR antibody conjugated gold nanoparticles in cancer diagnostics: applications in oral cancer." Nano Letters **5**(5): 829-834.

El-Sayed, I. H., et al. (2006). "Selective laser photo-thermal therapy of epithelial carcinoma using anti-EGFR antibody conjugated gold nanoparticles." Cancer letters **239**(1): 129-135.

Fasshauer, D., et al. (2002). "SNARE assembly and disassembly exhibit a pronounced hysteresis." Nature Structural & Molecular Biology **9**(2): 144-151.

Fasshauer, D. and M. Margittai (2004). "A transient N-terminal interaction of SNAP-25 and syntaxin nucleates SNARE assembly." Journal of Biological Chemistry **279**(9): 7613-7621.

Fasshauer, D., et al. (1998). "Conserved structural features of the synaptic fusion complex: SNARE proteins reclassified as Q-and R-SNAREs." Proceedings of the National Academy of Sciences **95**(26): 15781-15786.

Felsenfeld, D. P., et al. (1996). "Ligand binding regulates the directed movement of beta1 integrins on fibroblasts." Nature **383**(6599): 438.

Ferrari, E., et al. (2010). "Binary polypeptide system for permanent and oriented protein immobilization." Journal of nanobiotechnology **8**(1): 9.

Filipe, V., et al. (2010). "Critical evaluation of Nanoparticle Tracking Analysis (NTA) by NanoSight for the measurement of nanoparticles and protein aggregates." Pharmaceutical research **27**(5): 796-810.

Fix, M., et al. (2004). "Imaging single membrane fusion events mediated by SNARE proteins." Proceedings of the National Academy of Sciences of the United States of America **101**(19): 7311-7316.

Frens, G. (1973). "Controlled nucleation for the regulation of the particle size in monodisperse gold suspensions." Nature **241**(105): 20-22.

Gessner, A., et al. (2003). "Functional groups on polystyrene model nanoparticles: influence on protein adsorption." Journal of Biomedical Materials Research Part A **65**(3): 319-326.

Ghosh, P., et al. (2008). "Gold nanoparticles in delivery applications." Advanced drug delivery reviews **60**(11): 1307-1315.

Ghosh, P. S., et al. (2008). "Efficient gene delivery vectors by tuning the surface charge density of amino acid-functionalized gold nanoparticles." ACS nano **2**(11): 2213-2218.

Gibert, S., et al. (2000). "Three-step chromatographic purification procedure for the production of a His-tag recombinant kinesin overexpressed in E. coli." Journal of Chromatography B: Biomedical Sciences and Applications **737**(1): 143-150.

Goldfarb, D. S., et al. (1986). "Synthetic peptides as nuclear localization signals."

Gole, A. and C. J. Murphy (2004). "Seed-mediated synthesis of gold nanorods: role of the size and nature of the seed." Chemistry of Materials **16**(19): 3633-3640.

Grobelny, J., et al. (2011). "Size measurement of nanoparticles using atomic force microscopy." Characterization of nanoparticles intended for drug delivery: 71-82.

Hagan, R. M., et al. (2010). "NMR spectroscopic and theoretical analysis of a spontaneously formed Lys–Asp isopeptide bond." Angewandte Chemie International Edition **49**(45): 8421-8425.

Hagihara, Y., et al. (2007). "Stabilization of an immunoglobulin fold domain by an engineered disulfide bond at the buried hydrophobic region." Journal of Biological Chemistry **282**(50): 36489-36495.

Haiss, W., et al. (2007). "Determination of size and concentration of gold nanoparticles from UV− Vis spectra." Analytical chemistry **79**(11): 4215-4221.

Hayat, M. A. (2012). Colloidal gold: principles, methods, and applications, Elsevier.

Hermanson, G. T. (1996). Bioconjugate Techniques Academic Press, san Diego, CA.

Hill, A. V. (1910). "The possible effects of the aggregation of the molecules of haemoglobin on its dissociation curves." J Physiol (Lond) **40**: 4-7.

Holzinger, M., et al. (2014). "Nanomaterials for biosensing applications: a review." Frontiers in chemistry **2**: 63.

Hostetler, M. J., et al. (1998). "Alkanethiolate gold cluster molecules with core diameters from 1.5 to 5.2 nm: core and monolayer properties as a function of core size." Langmuir **14**(1): 17-30.

Hou, Y., et al. (2012). "NaGdF4 nanoparticle-based molecular probes for magnetic resonance imaging of intraperitoneal tumor xenografts in vivo." ACS nano **7**(1): 330-338.

Huang, X., et al. (2006). "Cancer cell imaging and photothermal therapy in the near-infrared region by using gold nanorods." Journal of the American Chemical Society **128**(6): 2115-2120.

Hurst, S. J., et al. (2006). "Maximizing DNA loading on a range of gold nanoparticle sizes." Analytical chemistry **78**(24): 8313-8318.

Jahn, R. and D. Fasshauer (2012). "Molecular machines governing exocytosis of synaptic vesicles." Nature **490**(7419): 201.

Jahn, R. and R. H. Scheller (2006). "SNAREs—engines for membrane fusion." Nature reviews Molecular cell biology **7**(9): 631-643.

Kang, H. J. and E. N. Baker (2011). "Intramolecular isopeptide bonds: protein crosslinks built for stress?" Trends in biochemical sciences **36**(4): 229-237.

Kang, H. J., et al. (2007). "Stabilizing isopeptide bonds revealed in gram-positive bacterial pilus structure." science **318**(5856): 1625-1628.

Kawano, T., et al. (2006). "Stabilizing of plasmid DNA in vivo by PEG-modified cationic gold nanoparticles and the gene expression assisted with electrical pulses." Journal of Controlled Release **111**(3): 382-389.

Kemmer, G. and S. Keller (2010). "Nonlinear least-squares data fitting in Excel spreadsheets." Nature protocols **5**(2): 267-281.

Kim, C. K., et al. (2009). "Entrapment of hydrophobic drugs in nanoparticle monolayers with efficient release into cancer cells." Journal of the American Chemical Society **131**(4): 1360.

Konecny, R., et al. (2012). "iAPBS: a programming interface to the adaptive Poisson–Boltzmann solver." Computational science & discovery **5**(1): 015005.

Konigsberg, W. (1972). "[13] Reduction of disulfide bonds in proteins with dithiothreitol." Methods in enzymology **25**: 185-188.

Kumar, A., et al. (2012). "Gold nanoparticles functionalized with therapeutic and targeted peptides for cancer treatment." Biomaterials **33**(4): 1180-1189.

Laera, S., et al. (2011). "Measuring protein structure and stability of protein–nanoparticle systems with synchrotron radiation circular dichroism." Nano Letters **11**(10): 4480-4484.

Lee, J. H. and T. R. Hoover (1995). "Protein crosslinking studies suggest that Rhizobium meliloti C4-dicarboxylic acid transport protein D, a sigma 54-dependent transcriptional activator, interacts with sigma 54 and the beta subunit of RNA polymerase." Proceedings of the National Academy of Sciences **92**(21): 9702-9706.

Lee, J. S., et al. (2007). "Colorimetric detection of mercuric ion (Hg2+) in aqueous media using DNA - functionalized gold nanoparticles." Angewandte Chemie International Edition **46**(22): 4093-4096.

Lee, S. H., et al. (2008). "Amine-functionalized gold nanoparticles as non-cytotoxic and efficient intracellular siRNA delivery carriers." International journal of pharmaceutics **364**(1): 94-101.

Lévy, R., et al. (2004). "Rational and combinatorial design of peptide capping ligands for gold nanoparticles." Journal of the American Chemical Society **126**(32): 10076-10084.

Li, Z., et al. (2002). "Multiple thiol-anchor capped DNA–gold nanoparticle conjugates." Nucleic acids research **30**(7): 1558-1562.

Lim, D.-K., et al. (2010). "Nanogap-engineerable Raman-active nanodumbbells for single-molecule detection." Nature materials **9**(1): 60-67.

Lindman, S., et al. (2007). "Systematic investigation of the thermodynamics of HSA adsorption to N-iso-propylacrylamide/N-tert-butylacrylamide copolymer nanoparticles. Effects of particle size and hydrophobicity." Nano Letters **7**(4): 914-920.

Lomant, A. J. and G. Fairbanks (1976). "Chemical probes of extended biological structures: synthesis and properties of the cleavable protein cross-linking reagent [35S] dithiobis (succinimidyl propionate)." Journal of molecular biology **104**(1): 243-261.

Lundqvist, M., et al. (2008). "Nanoparticle size and surface properties determine the protein corona with possible implications for biological impacts." Proceedings of the National Academy of Sciences **105**(38): 14265-14270.

Lynch, I. and K. A. Dawson (2008). "Protein-nanoparticle interactions." Nano today **3**(1): 40-47.

Mahon, E., et al. (2012). "Designing the nanoparticle–biomolecule interface for “targeting and therapeutic delivery”." Journal of Controlled Release **161**(2): 164-174.

Majzik, A., et al. (2010). "Functionalization of gold nanoparticles with amino acid, β-amyloid peptides and fragment." Colloids and Surfaces B: Biointerfaces **81**(1): 235-241.

McNaught, A. D. and A. D. McNaught (1997). Compendium of chemical terminology, Blackwell Science Oxford.

Mirkin, C. A., et al. (1996). "A DNA-based method for rationally assembling nanoparticles into macroscopic materials." Nature **382**(6592): 607.

Miyake, Y., et al. (2006). "MercuryII-mediated formation of thymine− HgII− thymine base pairs in DNA duplexes." Journal of the American Chemical Society **128**(7): 2172-2173.

Monopoli, M. P., et al. (2011). "Physical− chemical aspects of protein corona: relevance to in vitro and in vivo biological impacts of nanoparticles." Journal of the American Chemical Society **133**(8): 2525-2534.

Niazov, T., et al. (2004). "DNAzyme-functionalized Au nanoparticles for the amplified detection of DNA or telomerase activity." Nano Letters **4**(9): 1683-1687.

Nie, S. and S. R. Emory (1997). "Probing single molecules and single nanoparticles by surface-enhanced Raman scattering." science **275**(5303): 1102-1106.

Niidome, T., et al. (2004). "Preparation of primary amine-modified gold nanoparticles and their transfection ability into cultivated cells." Chemical Communications(17): 1978-1979.

Oke, M., et al. (2010). "The Scottish structural proteomics facility: targets, methods and outputs." Journal of structural and functional genomics **11**(2): 167-180.

Owens, D. E. and N. A. Peppas (2006). "Opsonization, biodistribution, and pharmacokinetics of polymeric nanoparticles." International journal of pharmaceutics **307**(1): 93-102.

Partis, M., et al. (1983). "Cross-linking of protein by ω-maleimido alkanoylN-hydroxysuccinimido esters." Journal of Protein Chemistry **2**(3): 263-277.

Patel, P. C., et al. (2008). "Peptide antisense nanoparticles." Proceedings of the National Academy of Sciences **105**(45): 17222-17226.

Phelps, E. A., et al. (2012). "Maleimide cross‐linked bioactive peg hydrogel exhibits improved reaction kinetics and cross‐linking for cell encapsulation and in situ delivery." Advanced Materials **24**(1): 64-70.

Poirier, M. A., et al. (1998). "Protease Resistance of Syntaxin· SNAP-25· VAMP Complexes IMPLICATIONS FOR ASSEMBLY AND STRUCTURE." Journal of Biological Chemistry **273**(18): 11370-11377.

Rahman, M., et al. (2013). Nanoparticle and protein corona. Protein-nanoparticle interactions, Springer**:** 21-44.

Raschke, G., et al. (2003). "Biomolecular recognition based on single gold nanoparticle light scattering." Nano lett **3**(7): 935-938.

Rosano, G. L. and E. A. Ceccarelli (2014). "Recombinant protein expression in Escherichia coli: advances and challenges." Recombinant protein expression in microbial systems **7**.

Rosi, N. L., et al. (2006). "Oligonucleotide-modified gold nanoparticles for intracellular gene regulation." science **312**(5776): 1027-1030.

Rouhana, L. L., et al. (2007). "Aggregation-resistant water-soluble gold nanoparticles." Langmuir **23**(26): 12799-12801.

Seferos, D. S., et al. (2007). "Nano-flares: probes for transfection and mRNA detection in living cells." Journal of the American Chemical Society **129**(50): 15477-15479.

Sener, G., et al. (2013). "Lysine-promoted colorimetric response of gold nanoparticles: a simple assay for ultrasensitive mercury (II) detection." Analytical chemistry **86**(1): 514-520.

Slocik, J. M. and R. R. Naik (2006). "Biologically programmed synthesis of bimetallic nanostructures." Advanced Materials **18**(15): 1988-1992.

Slocik, J. M., et al. (2005). "Viral templates for gold nanoparticle synthesis." Journal of materials Chemistry **15**(7): 749-753.

Slocik, J. M., et al. (2005). "Synthesis of gold nanoparticles using multifunctional peptides." Small **1**(11): 1048-1052.

Slocik, J. M., et al. (2008). "Colorimetric response of peptide‐functionalized gold nanoparticles to metal ions." Small **4**(5): 548-551.

Sokolov, K., et al. (2003). "Real-time vital optical imaging of precancer using anti-epidermal growth factor receptor antibodies conjugated to gold nanoparticles." Cancer research **63**(9): 1999-2004.

Sørensen, J. B., et al. (2006). "Sequential N‐to C‐terminal SNARE complex assembly drives priming and fusion of secretory vesicles." The EMBO journal **25**(5): 955-966.

Sperling, R. A., et al. (2008). "Biological applications of gold nanoparticles." Chemical Society Reviews **37**(9): 1896-1908.

Sun, L., et al. (2008). "Functional gold nanoparticle− peptide complexes as cell-targeting agents." Langmuir **24**(18): 10293-10297.

Thomas, K. G., et al. (2004). "Uniaxial plasmon coupling through longitudinal self-assembly of gold nanorods." The Journal of Physical Chemistry B **108**(35): 13066-13068.

Torcello-Gómez, A., et al. (2011). "Adsorption of antibody onto Pluronic F68-covered nanoparticles: link with surface properties." Soft Matter **7**(18): 8450-8461.

Torri-Tarelli, F., et al. (1985). "Temporal coincidence between synaptic vesicle fusion and quantal secretion of acetylcholine." The Journal of cell biology **101**(4): 1386-1399.

Treuel, L., et al. (2014). "Impact of protein modification on the protein corona on nanoparticles and nanoparticle–cell interactions." ACS nano **8**(1): 503-513.

Tu, Y., et al. (2012). "Fluorescence quenching of gold nanoparticles integrating with a conformation-switched hairpin oligonucleotide probe for microRNA detection." Chemical Communications **48**(87): 10718-10720.

Turkevich, J., et al. (1951). "A study of the nucleation and growth processes in the synthesis of colloidal gold." Discussions of the Faraday Society **11**: 55-75.

Vitozzi, S., et al. (2002). "Autoantibody detection in type 2 autoimmune hepatitis using a chimera recombinant protein." Journal of immunological methods **262**(1): 103-110.

Voet, D. and J. G. Voet (1995). "Nucleotide metabolism." New York: John Wiley & Sons: 795-828.

Vroman, L., et al. (1980). "Interaction of high molecular weight kininogen, factor XII, and fibrinogen in plasma at interfaces." Blood **55**(1): 156-159.

Waage, P. and C. M. Guldberg (1964). Forhandlinger: Videnskabs-SELSKABET i CHRISTIANA, 1864, 35.

Walkey, C. D. and W. C. W. Chan (2012). "Understanding and controlling the interaction of nanomaterials with proteins in a physiological environment." Chemical Society Reviews **41**(7): 2780-2799.

Wangoo, N., et al. (2008). "Synthesis and capping of water-dispersed gold nanoparticles by an amino acid: bioconjugation and binding studies." Journal of colloid and interface science **323**(2): 247-254.

Weerapreeyakul, N., et al. (2000). "Stability of bioreductive drug delivery systems containing melphalan is influenced by conformational constraint and electronic properties of substituents." Bioorganic & medicinal chemistry letters **10**(21): 2391-2395.

Yang, L., et al. (2009). "Single chain epidermal growth factor receptor antibody conjugated nanoparticles for in vivo tumor targeting and imaging." Small **5**(2): 235-243.

Yu, C. and J. Irudayaraj (2007). "Multiplex biosensor using gold nanorods." Analytical chemistry **79**(2): 572-579.

Zakeri, B., et al. (2012). "Peptide tag forming a rapid covalent bond to a protein, through engineering a bacterial adhesin." Proceedings of the National Academy of Sciences **109**(12): E690-E697.

Zhao, D., et al. (2007). "Adaption of Au Nanoparticles and CdTe Quantum Dots in DNA Detection** Supported by the Natural Science Foundation of Tianjin (Nos. 06TXTJJC14400, 07JCYBJC15900) and Young Teacher Foundation of Tianjin Polytechnic University (No. 029624)." Chinese Journal of Chemical Engineering **15**(6): 791-794.

Zhou, X., et al. (2008). "The effect of conjugation to gold nanoparticles on the ability of low molecular weight chitosan to transfer DNA vaccine." Biomaterials **29**(1): 111-117.